Kerr-lens mode locked lasers based on Yb^{3+}-doped materials

Masaki Tokurakawa

The University of Electro-Communications
Graduate School of Electro-Communications
Department of Applied Physics and Chemistry
Institute for Laser Science
Tokyo, Japan

Doctor of Engineering

March 2010

Kerr-lens mode locked lasers based on Yb^{3+}-doped materials

Masaki Tokurakawa

MAIN-SUPERVISOR: Prof. Ken-ichi Ueda
CO-SUPERVISOR: Assoc. Prof. Ken'ichi Nakagawa

APPROVED BY SUPERVISORY COMMITTEE:
CHAIRPERSON: Prof. Ken-ichi Ueda
MEMBER: Prof. Hitoki Yoneda
MEMBER: Prof. Kazuko Shimizu
MEMBER: Prof. Mitsuo Takeda
MEMBER: Prof. Watanabe Masayoshi
MEMBER: Assoc. Prof. Masayuki Katsuragawa

Yb 添加媒質を用いたカーレンズモード同期レーザーの開発

戸倉川　正樹

Abstract (Japanese)

本論文では Yb^{3+}添加媒質を用いた超短パルスレーザー光源の開発を行った。Yb^{3+}添加媒質を用いた超短パルスレーザー光源は、他の超短パルスレーザー光源と比べて多くの利点を有する。Yb^{3+}イオンは市販の高出力 InGaAs 系レーザーダイオード (LD) による直接励起が可能であり、容易に高効率な励起用高出力光源が得られる。また量子欠損が 10%以下と非常に小さく、さらに量子効率も 1 に近い値を得ることができ、発熱の少ない高効率、高出力なレーザー動作が可能となる。Yb^{3+}添加媒質の分光特性や熱機械特性はそのホスト媒質によって強く影響を受け、現在までに多くの Yb^{3+}添加媒質が研究開発されている。近年、不均一広がりによる広い利得帯域幅を有する Yb^{3+}添加媒質と高い Q 値を持った共振器を用いることにより、サブ 60fs 幅の超短パルス発生の報告がなされている。しかしながらそのような Yb^{3+}添加媒質（例えばガラス材料や disordered material）は熱特性や機械特性に欠点を有することが多く、高出力動作は制限されてしまう。さらに、短パルスを得る為に共振器の取り出し鏡の反射率を出力最適化条件の値よりも高くし、共振器全体の Q 値を高めている場合が多く、一般的に出力は 100mW 以下、光光変換効率も 10%以下と制限されていた。

本論文では安価な LD による直接励起、熱特性および機械特性に優れた一層の高出力化に対応できる利得媒質(主として Yb^{3+}：Re_2O_3、Re＝Y,Lu,Sc)の利用という条件の下、カーレンズモード同期、複合利得媒質モード同期レーザーなどの技術を利用することにより、上記問題を克服した高効率、高出力サブ 100fsYb^{3+}添加超短パルスレーザー光源の開発を行った。

はじめに Z 型の非点収差補正共振器を構築し、半導体可飽和体ミラー（SESAM）を用いた SESAM モード同期レーザー実験をおこなった。分散補償には SF10 プリズム対を用い、実験的にパルス幅が最短となる最適な分散補償長を選択した。このとき得られた最短パルス幅はマルチパルス発振への移行により制限され、200fs 程度であった。次により短いパルス幅を得るためにカーレンズモード同期共振器を構築した。カーレンズ効果により深い変調を与えることにより、最適な取り出し効率の共振器から超短パルス光を得る事を可能とし、高効率に 80 fs 以下のパルス幅で 1 W 以上の平均出力を得ることに成功した。このとき broad-stripe LD (BLD) 励起という条件のもとカーレンズ効果による利得変調効果が最大となるように、連続発振時の共振器状態が BLD の fast axis 方向においてのみ不安定状態に近くなるよう設計した。さらに一層の短パルス化を進めるために異種の Yb^{3+}添加利得媒質を同一共振器内で用い、人工的な不均一幅広がりにより実行的な利得帯域幅を広げた複合利得媒質カーレンズモード同期レーザーの開発を行い、53 fs のパルス幅で 1 W 以上の平均出

力を得ることに成功した。また上述の共振器内でのカーレンズ効果によるビーム径変化の計算を行い、カーレンズ効果の大きさ及び共振器条件依存性を数値的に評価した。次に利得媒質の飽和競合効果に基づいて、超短パルス発振時に CW 発振成分を抑制する為に必要とされる共振器内損失変化量、およびビーム径変化量の必要条件に関する計算を行い、上述のカーレンズ効果の重要性を数値的に再提示した。今後の展望として、上記計算をもとに更なる高出力化についての考察をおこなった。また我々の研究室はここ数年来新しいレーザー媒質形態としてセラミック媒質を提唱してきており、本論文においても種々のセラミック媒質および単結晶媒質を用い、セラミック媒質が超短パルスレーザー光源において単結晶と同様に利用可能であることを実証した。

Kerr-lens mode locked lasers based on Yb^{3+}-doped materials

Masaki Tokurakawa

Abstract

In this thesis, ultrashort pulse lasers based on Yb^{3+}-doped materials have been developed. Yb^{3+}-doped mode-locked lasers have several advantages over other mode-locked lasers in a high power operation. They can be directly pumped by a high power InGaAs laser diode. The unique energy-level scheme of Yb^{3+} ion leads to very small quantum defects (<10%) and high quantum efficiency (~1), and thus highly efficient high power laser operations under less heat loads are possible. The mechanical and thermal properties of Yb^{3+}-doped materials depend on their host materials, and therefore various kinds of Yb^{3+}-doped materials have been studied. Recently, sub 60-fs mode-locked laser operations based on Yb^{3+}-doped crystals having inhomogeneous broadened gain bandwidths and high *Q* cavities have been reported, but such crystals tend to show poor thermal properties, poor mechanical properties and/or anisotropy structure so that high power laser operation is difficult with them. In addition, their high Q cavities tend to be not suitable for highly efficient laser operations, because their output coupling efficiencies tend to be lower than optimized values for highly efficient laser operation. In general cases, the efficiency and output power were limited to less than 10 % and 100 mW, respectively.
In this thesis, direct LD pumped highly efficient high power ultrashort pulse lasers based on the techniques of Kerr-lens mode locking and multi-gain media oscillator have been developed. For power scalability, gain media having good thermal and mechanical properties such as Yb:sesquioxide materials were used.
In case of the SESAM mode locking, the available pulse durations were limited to be ~200 fs by a transition to multi-pulsed operations. To achieve much short pulse duration, the Kerr-lens mode-locked laser cavity was constructed. The fast and large gain modulation of Kerr lens enables ultrashort pulse operation with cavities having proper output coupling efficiencies. To achieve large soft aperture Kerr-lens effect with

broad-stripe LD (BLD) pumping, the cavity was aligned nearly unstable at fast axis of pumping BLD. Generations of sub 80-fs pulses with above 1-W average powers have been successfully achieved with the help pf Kerr-lens effect. Additionally the ultrashort pulse operation based on a multi-gain media oscillator has been also demonstrated to achieve further short pulse duration by an artificially broadened gain bandwidth. From the oscillator, pulses as short as 53 fs with above 1-W average power have been obtained. The influence of the Kerr-lens effect inside the cavity and its dependence on cavity state was numerically estimated. The necessary equations ultrashort-pulsed laser operations were calculated based on competition of gain saturation effect and the importance of Kerr-lens effect was explained. The power scalability is also discussed based on above calculations for future works. The usability of ceramic gain media in the femtosecond laser operation was also proved in this thesis.

Contents

Introduction 1
References 10
Chapter 1. Fundamental of laser operations 14
1.1 Efficiency of Yb^{3+}-doped laser operation 15
1.2 Rate equations 16
1.3 Multi-mode laser operation 21
1.4 Mode-locked pulses 23
1.5 Dispersion compensation 25
1.6 High power laser operation 27
References 30
Chapter 2. Ultrashort pulse laser operation 31
2.1 Active mode locking 31
2.2 Passive mode locking 32
2.3 SESAM mode locking 35
2.4 Kerr-lens mode locking 38
References 43
Chapter 3. Properties of Yb^{3+}-doped gain materials 45
3.1 Properties of Yb^{3+} ions 45
3.2 Ceramic materials 49
3.3 Sesquioxide materials 51
3.4 Yb^{3+}:$\{YGd_2\}[Sc_2](Al_2Ga)O_{12}$ ceramic material 56
3.5 Previous results of SESAM mode-locked Yb^{3+}-doped sesquioxide lasers 58
3.6 Multi-gain media oscillator 62
References 65
Chapter 4. Cavity design 68
4.1 Kerr-lens effect 69
4.2 Astigmatisms of gain medium and spherical mirror 71
4.3 Kerr-lens mode-locking with a broad-stripe LD pumping 73
4.4 Calculation of laser mode radius inside the cavity 75
References 81
Chapter 5. Experiments of mode-locked lasers 82
5.1 Yb^{3+}:Sc_2O_3 ceramic SESAM mode-locked laser 83
5.2 Yb^{3+}:Sc_2O_3 ceramic Kerr-lens mode-locked laser 87
5.3 Yb^{3+}:Lu_2O_3 and Y_2O_3 ceramic Kerr-lens mode-locked laser 91

5.4 Yb^{3+}:Sc_2O_3 and Yb^{3+}:Y_2O_3 ceramic multi-gain media KLM laser 95
5.4 Yb^{3+}:Sc_2O_3 and Yb^{3+}:Lu_2O_3 single crystal Kerr-lens mode-locked lasers..... 99
5.5 Yb^{3+}:{YGd_2}[Sc_2](Al_2Ga)O_{12} ceramic laser 105
5.5 Yb^{3+}:$Y_3Al_5O_{12}$ ceramic laser 109
References.....111
Chapter 6. Estimation of the gain bandwidth limitation of pulse duration.....112
6.1 Rate equations for mode-locked laser operation.....113
6.2 Calculation of output power 119
References..... 120
Chapter 7. Summary and outlook..... 121
Future Works..... 123
References..... 126

List of figures

Fig. 0.1. Average power versus pulse duration. 7
Fig. 1.1. Schematic picture of four-level laser scheme. 16
Fig. 1.2. Transverse mode of the cavity and gaussian gain profile. 21
Fig. 1.3. Effect of spatial-hole-burning. 22
Fig. 1.4. Ultrashort pulses in time domain and frequency domain. 23
Fig. 1.5. Transform-limited pulse and up chirp pulse. 24
Fig. 1.6. Frequency depending optical pass of prism and grating pairs. 26
Fig. 2.1. Schematic picture of active pulsed mode-locked laser cavity. 31
Fig. 2.2. Schematic picture of solitonlike mode locked laser cavity. 32
Fig. 2.3. Temporal dependence of gain, loss and pulse shape in short pulse operation. 33
Fig. 2.4. Schematic picture of SESAM. 35
Fig. 2.5. Fluence depending reflectance of SESAM. 36
Fig. 2.6. Pictures of CW mode locking and Q switch mode locking. 36
Fig. 2.7. Schematic pictures of Kerr-lens mode locking. 38
Fig. 2.8. Scamatic picture of laser mode profiles in soft aperture KLM. 40
Fig. 3.1. Energy levels of Nd:YAG and Yb:YAG. 46
Fig. 3.2. Fluorescence spectra of Yb:sesquioxides ceramics and crystals. 52
Fig. 3.3. Emission and absorption cross section of Yb:Y_2O_3 (1.8 at.%, 1.5 mm). 53
Fig. 3.4. Absorption cross section of Yb:Y_2O_3 (10 at.%, 2mm). 53
Fig. 3.5. Emission and absorption cross section of Yb:Sc_2O_3 ceramic and crystal. 54
Fig. 3.6. Emission and absorption cross section of Yb:Lu_2O_3 ceramic and crystal. 54
Fig. 3.7. Structure of $(YGd_2)Sc_2(Al_2Ga)O_{12}$ ceramic. 56
Fig. 3.8. Emission and absorption cross section of Yb:YAG. 57
Fig. 3.9. Absorption and emission spectrum of Yb$(YGd_2)Sc_2(Al_2Ga)O_{12}$. 57
Fig. 3.10. AC trace and spectrum of the 188 fs mode-locked pulses. 58
Fig. 3.11. Schematic picture of multi-pulsing. 59
Fig. 3.12. Spectra and AC traces of Yb^{3+}:Y_2O_3 ceramic laser. 60
Fig. 3.13. Spectra and AC traces of Yb^{3+}:Sc_2O_3 ceramic laser. 61
Fig. 3.14. Schematic picture of multi-gain media. 62
Fig. 3.15. Estimated effective cross-sections of the multi-gain-media. 64
Fig. 4.1. Picture of Z-shaped astigmatically compensated cavity 68
Fig. 4.2. Model cavity used in the calculation. 69
Fig. 4.3. Flow chart of calculation of the cavity state. 70
Fig. 4.4. Astigmatism of spherical lens. 71

Fig. 4.5. Astigmatisms of bulk material. 72
Fig. 4.6. Schematic picture of pump beam shaping elements. 74
Fig. 4.7. Calculated stability curves of the mode-locked cavity. 75
Fig. 4.8. Calculated laser beam radii with and without the KL effect (i). 76
Fig. 4.9. Calculated laser beam radii with and without the KL effect (ii). 77
Fig. 4.10. Two-dimensional map of soft aperture KL effect (single pulse). 78
Fig. 4.11. Calculated laser beam radii with and without the KL effect (iii). 79
Fig. 4.12. Two-dimensional map of soft aperture KL effect (double pulse). 80
Fig. 4.13. Two-dimensional map of multi-pulse suppression of KL effect. 80
Fig. 5.1. Experimental Setup of SESAM mode-locked Yb^{3+}:Sc_2O_3 laser. 83
Fig. 5.2. Output power property of SESAM mode-locked laser (i). 84
Fig. 5.3. AC traces of SESAM mode-locked Yb^{3+}:Sc_2O_3 laser (i). 84
Fig. 5.4. Output power property of SESAM mode-locked laser (ii). 85
Fig. 5.5. AC traces of SESAM mode-locked Yb^{3+}:Sc_2O_3 laser (ii). 85
Fig. 5.6. Spectra of pulses with different center wavelength. 86
Fig. 5.7. Experimental setup of Yb^{3+}:Sc_2O_3 Kerr-lens mode locking. 87
Fig. 5.8. Autocorrelation trace and spectra of 92 fs pulses. 88
Fig. 5.9. Pulse train of 92 fs pulses. 88
Fig. 5.10. Measured laser mode profiles. 88
Fig. 5.11. Measured beam radiuses. 89
Fig. 5.12. Output power property of the Kerr-lens mode-locked laser. 89
Fig. 5.13. Autocorrelation trace and spectra of 90 fs pulses. 90
Fig. 5.14. Setup of Yb^{3+}:Lu_2O_3 ceramic Kerr-lens mode-locked laser. 91
Fig. 5.15. Measured laser mode profiles of Yb^{3+}:Lu_2O_3 laser. 92
Fig. 5.16. Autocorrelation trace and spectrum of 65 fs pulses. 93
Fig. 5.17. Output power property of Yb^{3+}:Lu_2O_3 laser. 94
Fig. 5.18. Autocorrelation trace (a) and spectra (b) of 68 fs pulses. 94
Fig. 5.19. Setup of multi-gain media Kerr-lens mode-locked laser. 95
Fig. 5.20. Measured laser mode profiles. 96
Fig. 5.21. Autocorrelation trace and spectrum of 66 fs pulses. 97
Fig. 5.22. Autocorrelation trace and spectrum of 53 fs pulses. 97
Fig. 5.23. Spectra of the 53-fs pulses and gain media. 98
Fig. 5.24. Setup of the Kerr-lens mode-locked laser based on single crystal. 98
Fig. 5.25. Average power versus the incident pump power. 100
Fig. 5.26. AC trace and spectrum of the Yb^{3+}:Sc_2O_3 mode-locked laser. 101
Fig. 5.27. Mode profiles of the laser outputs. 101

Fig. 5.28. AC traces and spectra of 64 fs pulses and 68 fs pulses. 102
Fig. 5.29. Average power versus the incident pump power. 103
Fig. 5.30. Measured long-term mode-locking stability. 103
Fig. 5.31. Autocorrelation trace and spectrum of 71 fs pulses. 104
Fig. 5.32. Experimental setup of KLM Yb^{3+}:$(YGd_2)Sc_2(GaAl_2)O_{12}$ laser. 105
Fig. 5.33. Output power property of KLM Yb^{3+}:$(YGd_2)Sc_2(GaAl_2)O_{12}$ laser. 106
Fig. 5.34 AC trace and spectrum of the Yb^{3+}:$(YGd_2)Sc_2(GaAl_2)O_{12.}$ 107
Fig. 5.35. Mode profiles of the laser outputs. 107
Fig. 5.36. Spectra of mode-locked pulses. 108
Fig. 5.37. Setup of Yb^{3+}:$Y_3Al_5O_{12}$ Kerr-lens mode locked laser. 109
Fig. 5.38. Autocorrelation trace and spectrum of 128 fs pulses. 110
Fig. 5.39. Mode profiles of the laser outputs. 110
Fig. 6.1. Schematic picture of a mode-locked ring resonator. 112
Fig. 6.2. Spectrum of pulses from Yb^{3+}:Lu_2O_3 with narrow component. 113
Fig. 6.3. Spectrum of pulses from Yb^{3+}:Sc_2O_3 with narrow component. 114
Fig. 6.4. Schematic picture of soft aperture Kerr-lens effect. 116
Fig. 6.5. Necessary condition for suppressing parasitic component. 118
Fig. 6.6. Calculated output power properties vs. incident pump power. 119
Fig. 7.1. Schematic picture of our thin-disk laser cavity. 123
Fig. 7.2. Calculated laser beam radii with thin-disk laser cavity. 124

List of tables

Table 0. 1. Comparison of Yb^{3+}-doped laser and Ti:Al_2O_3 laser. 4
Table 0. 2. Performances of Yb^{3+}-doped femtosecond lasers. 6
Table 1. 1. Relation ships between pulse shape and K constant. 25
Table 1. 2. Limitation factors for high power laser operation. 27
Table 3. 1. Comparison of Nd:YAG and Yb:YAG.. 47
Table 3. 2. Properties of remarkable materials are shown. 48
Table 3. 3. Comparison of fracture toughness. 50
Table 3. 4. Properties of Yb-doped sesquioxide materials. 55
Table 3. 5. Comparison of multi-gain medium and disorder material. 61
Table 4. 1. Comparison of mode matching factors in different cavity states. 77
Table 7.1. Properties of Yb doped Kerr-lens mode locked laser 122

Introduction

Since the first laser operation based on flash lamp pumped ruby crystal had been reported in 1960 by Maiman [1], the laser technologies have been developing day by day and lasers have became indispensable tools not only in laboratory but also in our daily life. The word “LASER” coined from “Light Amplification by Stimulated Emission of Radiation”. The principal of stimulated emission was reported in 1916 by Einstein and the possibility of optical maser was reported in 1958 by Schawlow and Townes [2]. The stimulated emission provides a phase-coherent amplification, which enables amplified light to possess the same phase, same propagation direction, same polarization and same spectral property as signal light. As a result of them, the laser light enables many applications due to its special properties: wavelength order spatial resolution (~10^{-8} m), ultrashort time resolution (10^{-15} s), ultrahigh intense electrical field (>10^{15} W/cm^2), precise frequency (10^{-14} Hz/Hz$^{1/2}$) and so on. The optical spectral analysis with laser light source also gives us important information. Today huge kinds of gain media in several kinds of material states such as single crystal, glass, gas, metal vapor, dye solution, glass fiber, semiconductor and ceramic have been developed and the nonlinear wavelength conversion systems have also been developed. The laser wavelength range from soft-X ray to sub-millimeter is available. In the research field, the laser-light sources are used in biomedical, photochemistry, astrology, geology, nuclear fusion, laser cooling, metrology and so on. In the industrial field, the laser sources are used in lithography, material processing, laser detection and ranging system, optical coherent tomography, microscopy and so on. Moreover, the laser sources are used in our daily life, optical communication system, optical data-storage system, scanner, laser-TV and so on. In case of the ultrashort pulse laser, pulses as short as 5 fs have been obtained directly from a Kerr-lens mode-locked Ti^{3+}:Al_2O_3 laser [3]. 5 fs pulses with

multi-mJ energy level were also achieved by a parametric chirped-pulse amplifier system [4]. Furthermore, ultrashort pulse generation with sub-femtosecond pulse duration by high-harmonic generation [5] as well as ultrahigh peak power pulses above 10^{15} W peak intensity with low repetition rate by chirped-pulse amplifier system [6] are also available. As can be seen above, ultrashort pulse laser technology has been strongly investigated and developed very well. Today, applications of ultrashort pulse lasers in industrial field, particularly in material processing (extremely high precision and negligible mechanical shock and thermal damage, 3-dimensional processing for transparent materials, inducing a nanostructure on material surface and so on) are well known and being strongly investigated. However, their applications are still limited only in laboratories, because of extremely expensive photon cost of ultrashort pulse lasers. They are too expensive to use in industrial fields even though they have great potentials. Such high photon cost is generally caused by their requirements of expensive pump source, a large number of optical components, cooling system and its low electrical-to-optical efficiency. Furthermore, they are not only the problem in industrial filed but also in the scientific field, because they also tend to cause the limitation of the power scalability of ultrashort pulse lasers. The development of cost effective highly efficient power scalable ultrashort pulse lasers is key to open the doors of new high power femtosecond laser physics and many industrial applications. Development of ultrashort pulse laser source satisfying above demands is the purpose of this thesis.

There are many types of mode locked lasers: dye lasers, solid-state lasers, fiber lasers, semiconductor lasers and so on. Dye solutions are one of the desirable gain media for obtaining ultrashort pulses, because they have large emission cross section and cover broad wavelength range. Ultrashort pulses as short as 27 fs was obtained from dye solution [7]. Dye lasers opened the door of sub 100-fs ultrafast sciences and were also the most widely used tunable laser. They, however, have several difficulties for handling. The dye solutions generally have toxicity and easy to decay. Due to such decay the dye solutions have to be changed in a short period and a critical realignment is also required by it. Additionally, for the sub 100-fs short pulse operation, choice of the gain dye solutions and saturable

absorber dye solutions are limited and therefore the available wavelengths are also limited to be around 620 nm. Due to the above problem, easy handling tunable ultrashort pulse laser source was desired.

The appearance of ultrashort pulse lasers based on $Ti^{3+}:Al_2O_3$ strongly accelerated ultrafast physics such as high filed laser physics, ultrafast time-resolved measurement, optical comb application and so on. $Ti^{3+}:Al_2O_3$ has extremely broad vibronic fluorescence bandwidth with a spectral bandwidth of ~ 180 nm (Full width at half maximum (FWHM)) and 10^{-19} cm^2 order emission cross section [8]. It has 4-level laser scheme and does not suffer excited state absorption. The tuning range of cw laser operation is between 670-1070 nm. In 1991 Spence reported 60-fs pulse generation based on Kerr-lens mode-locked (KLM) $Ti^{3+}:Al_2O_3$ laser (first Kerr-lens mode locking) [9]. Today, as short as 5-fs pulse duration has been obtained directly from a cavity [3]. Besides favorable spectral properties, $Ti^{3+}:Al_2O_3$ also possess several advantage such as a high thermal conductivity, chemical inertness and strong mechanical toughness. $Ti^{3+}:Al_2O_3$ has a broad absorption band with the center wavelength position at 490 nm. It generally is pumped by an argon ion laser, cooper-vapor laser or Second Harmonic Generation of Nd^{3+}-doped lasers [10,11]. Such laser pumping leads to some advantage and disadvantage. The former is caused by high beam quality of pump laser light, which is suitable for a stable laser operation and soft aperture KLM operation [12]. The later is low electrical-to-optical efficiency, expensive photon cost. Such pump laser sources are very expensive and available pump power also tends to be limited. The center wavelength of the pump laser is around 490 nm and the center wavelength of $Ti^{3+}:Al_2O_3$ fluorescence is 780 nm so that the quantum defect is about 30 %. Therefore, above 30 % of the total pump power is converted to heat loads and therefore large cooling system is also required for the $Ti^{3+}:Al_2O_3$ laser itself. The large heat loads also restrict the high average power laser operation. For a highly efficient high average power laser operation, the direct laser diode (LD) pumped system is desirable. Very recently direct LD pumped $Ti^{3+}:Al_2O_3$ laser based on a GaN blue LD pumping has been reported[13]. However, their performance is still limited. Although $Ti^{3+}:Al_2O_3$ is still desirable gain media for tunable and ultrashort pulsed laser operations, direct LD pumped highly efficient ultrashort pulse lasers are desired particularly for industrial applications.

Cr^{3+}-ion doped lasers are very interesting candidate for an ultrashort pulse generation. They have broad tuning range of 780-920 nm in Cr^{3+}:$LiSrAlF_6$ and 720-840 nm in Cr^{3+}:$LiCaAlF_6$ [14]. They can be pumped by an AlGaInP red LD and pulses as short as 10 fs and 14 fs were obtained from Cr^{3+}:$LiCaAlF_6$ [15] and Cr^{3+}:$LiSrAlF_6$ [16], respectively. Although they are very interesting candidates for a LD pumped cost effective ultrashort pulse laser in low average power region, high average power operation is very difficult. Because, they suffer thermally induced quenching effect [17] and the available pump power from AlGaInP red LD is also limited so far.

Recently, Yb^{3+}-doped crystalline materials have been particularly recognized as great candidates for a highly efficient high power femtosecond laser system. Their absorption bands occurring around the wavelength of 940 nm and 980 nm enable direct pumping by a InGaAs LD. Thanks to the dramatic improvement of LDs in the past decade, today above 12-W average power high brightness single emitter broad-strip LD, above 1-KW average power fiber coupled LD and bulk LD array are commercially available. Their performances are still being improved rapidly and cost is also reducing. Yb^{3+} ions have broad emission band near the wavelength of 1-μm range that enable femtosecond laser operation. In

Table 0.1. Comparison of Yb^{3+}-doped laser and Ti:Al_2O_3 laser

Material	Yb^{3+}-doped	Ti^{3+}:Al_2O_3
Pulse duration	Sub 100 fs	Sub 10 fs
Opt-to-opt efficiency at gain material	>80% possible (CW) ~50% (sub ps)	<20%
Available wavelength	1010~1100 nm	620~1020 nm
Quantum defect	<10%	~30%
Pump power for a 100 W output power	>120 W (CW)	>500 W
Electro-opt efficiency	>40 % possible (CW)	<5%
Comalially available pump power from one module pump source	<1 kW	<100 W
Heat loads for a 100 W out put power	>12 W (CW)	>150 W
Cost	High	Very high

addition, the unique energy-level scheme of Yb^{3+} ion ($^2F_{5/2} \leftrightarrow {}^2F_{7/2}$ inter-manifold transition) leads to very small quantum defects and avoids undesirable processes such as excited-state absorption, cross relaxation and concentration quenching, and thus they suffer less heat loads (<10%) [18, 19] (See table 0.1). In case of the continuous wave (cw) laser operation, optical-to-optical efficiency above 70% is available. Their relatively long lifetimes (~ ms) are also suitable for femtosecond pulse amplifier operations. On the other hand, their quasi-three-level (some times called quasi-four-level) laser scheme leads to reabsorption loss [20]. The reabsorption loss can be reduced by several ways such as high intensity pumping, using low Yb^{3+}-ion doped material, cooling a gain medium and applying a thin-disk laser concept [21]. Comparison with $Ti^{3+}:Al_2O_3$ the gain bandwidth of Yb^{3+} ions are narrow and therefore generation of sub 100-fs pulses has some difficulties and generation of sub 10-fs pulses is impossible so far. Since the spectroscopic properties, thermal and mechanical properties of Yb^{3+}-doped materials strongly depend on their host materials, seeking for the Yb^{3+}-doped gain material having ideal properties has been very important subject and femtosecond laser operations based on various kinds of Yb^{3+}-doped crystalline materials (*e.g.* garnets, tungstates, fluorides, vanadates, borates, oxyorthosilicates and sesquioxides) have been reported in a past decade [22,23,24,25,26,27,28,29]. Yb^{3+}-doped glasses both of balk and fiber were also used for ultrashort pulse generation [30,31,32]. By a proper choice of the host materials, they can stand up to be pumped by high-brightness and high-power LDs and can be applied for high power laser operations. Yb^{3+}-doped glass materials have amorphous structures, which lead inhomogeneous broadened fluorescence spectra. Their gain bandwidths are broad enough for generating sub-100 fs pulses and the first sub 100 fs pulse operation based on Yb^{3+}-ion doped solid-state material was done by glass materials with semiconductor saturable absorber mirror [33, 34]. The glass materials are also used for a high pulse energy laser amplifier system with large beam aperture sizes, because of their size scalability. Their amorphous structures, however, decline their thermal conductivities so that they tend to suffer large heat loads and make serious limitation of average power scalability. On the other hand, crystalline materials have higher thermal conductivities than glass materials and therefore they are more

suitable for high average power laser operations. Yb^{3+}:$Y_3Al_{12}O_5$ (Yb:YAG) is the most popular gain material for high power solid-state laser operation due to its high thermal conductivity and strong mechanical toughness. The first femtosecond laser operation based on Yb:YAG was reported in 1995 [35]. The FWHM of its fluorescence spectral bandwidth at 1030 nm peak is about 9 nm, which corresponds to transform-limited pulse duration of 124 fs with an assumption of $sech^2$ pulse shape. The obtained pulse duration, however, was limited to be 340 fs. The first sub 100 fs pulsed laser operation based on Yb^{3+}-ion doped crystalline material was obtained by a KLM oscillator with Yb^{3+}:$KY(WO_4)_2$ (Yb:KYW) tungstate material [24], which has broader gain bandwidth and larger emission cross section than those of Yb:YAG. Today sub 100-fs pulses can be obtained by several kinds of Yb^{3+}-doped crystalline materials [36,37,38,39,40,41,42,43]. In case of the high power laser operation, however, they tend to suffer some problems caused by their lower thermal conductivity and weaker mechanical toughness than those of Yb:YAG, and/or their anisotropy structure [44]. The optical-to-optical efficiency and available output powers were also limited to be less than 10 % and around 100 mW (see table 0.2 and Fig. 0.1). The reason of such low efficiencies and average powers are existence

Table 0.2. Performances of Yb^{3+}-doped femtosecond lasers

Material	P_{out} (mW)	Δt (fs)	P_{p_Max} (W)	Method	Pump source	Year	Ref.
$KY(WO_4)_2$	120	71	3.2	KLM	two LD	2001	23
$Sr_3Y(BO_3)_3$	80	69	3.6	SESAM	two LD	2002	37
$SrY_4(SiO_4)_3O$	156	70	4	SESAM	LD	2004	38
YVO_4	54	61	0.4	KLM	FCLD	2005	39
$KLu(WO_4)_2$	70	81	3	SESAM	Ti:Al_2O_3	2005	40
$LuVO_4$	85	58	1.8	SESAM	Ti:Al_2O_3	2006	41
$CaGdAlO_4$	520	68	15	SESAM	FCLD	2007	25
YVO_4	1000	80	3.5	KLM	TLD	2007	26
$LaSc_3(BO_3)_4$	73	58	1.8	SESAM	Ti:Al_2O_3	2007	28
$NaY(WO_4)_2$	91	53	1.36	SESAM	Ti:Al_2O_3	2007	42
CaF_2	380	99	4.5	SESAM	FCLD	2009	43
$Y_3Al_{12}O_5$	151	100	4.7	KLM	FCLD	2008	44

SESAM: Semiconductor saturable absorber mirror

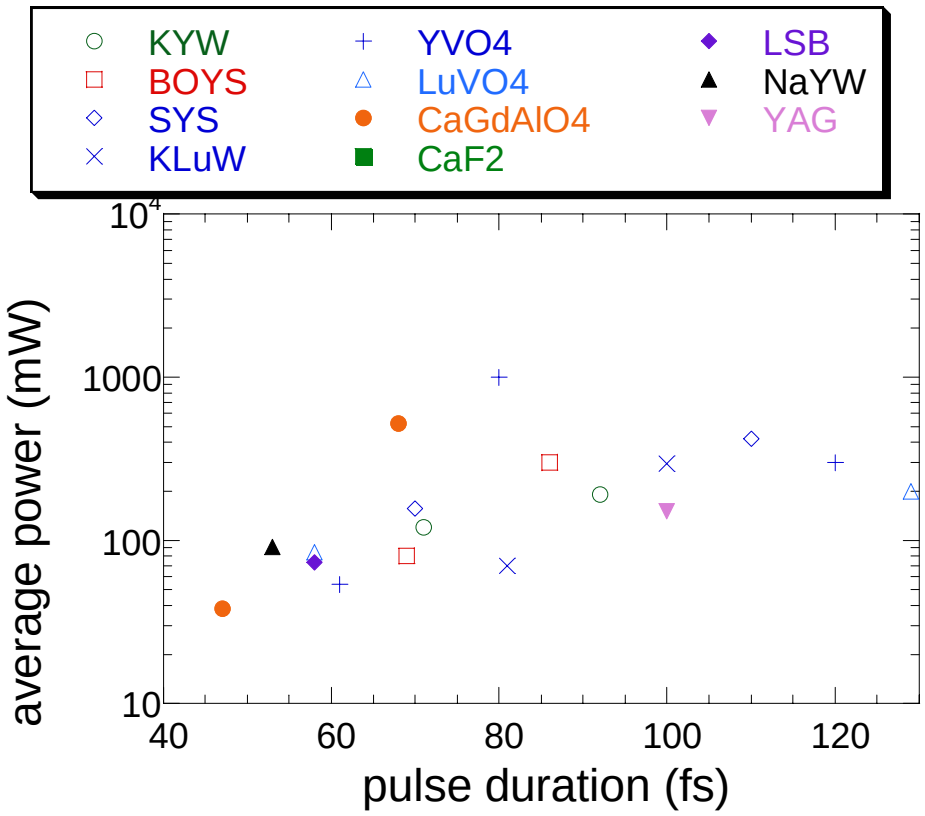

Fig. 0.1. Average power versus pulse duration.

of reabsorption losses and construction of high *Q* cavity (cavity with low output coupling efficiencies). Although such high *Q* cavity is suitable for generating ultrashort pulses, it tends to decrease their average powers and efficiencies. Because, mode-locked lasers tend to have slightly large cavity losses (caused by dispersion compensation elements and saturable absorber), which make requirement of slightly large output coupling efficiency for achieving highly efficient laser operations. Generation of sub-100 fs pulses with high average power and high efficiency is one of the purposes of this thesis. The keys for achieving the purpose are using low reabsorption loss material, suitable output coupling efficiency, large self phase modulation (SPM) and large modulation depth of saturable absorber. In the thesis, generations of sub 100 fs pulses above 1W average power with high optical-to-optical efficiency based on Kerr-lens mode locking is described.

Consideration of power scalability for above 10~100 W with ultrashort

pulse duration is also very important purpose of this thesis. For high power laser operation thin-disk laser concept is desirable [45]. It enables high intensity pumping, low Yb^{3+}-ion doping level, efficient heat removing and large beam aperture size. Today cw laser operation above 1-kW average power, sub-ps SESAM mode-locked laser operations with nearly 100-W average power and pulse energy beyond 20-μJ level based on thin-disk Yb:YAG have been reported [46,47]. The average power of 22 W with the pulse duration of 240 fs based on Yb:KYW [48] was also obtained. Average power up to 400 W with sub-700 fs pulse duration has been also achieved based on a Yb:YAG slab amplifier system [49]. TW peak power amplifier system at low repetition rate based on Yb^{3+}:CaF_2 [50] and the amplifier system with multi-mJ pulse energy with sub-200 fs pulse duration at high repetition rate based on the cryogenic cooled Yb^{3+}:CaF_2 [51] have also been reported. In this thesis, the possibility of ultrashort pulse operation based on KLM thin-disk laser is shown.

For a further high power laser operations, polycrystalline ceramic materials are very interesting, because ceramic materials have some interesting advantages. First they have better size scalability than single crystals. The available output power is proportional to laser beam area unless their intensity reaches self-focusing limitation. Comparison with fiber based ultrashort pulse laser, the scalability of laser beam apertures size is big advantage of bulk based laser system [52]. Second the ceramic technology is suitable for fabricating some unique materials such as sesquioxides (Re_2O_3, Re = Sc, Y or Lu) having high melting points and $\{YGd_2\}[Sc_2](Al_2Ga)O_{12}$ having partially disordered crystalline stricture. They show good thermal and mechanical properties and broad gain bandwidth. Third the ceramic materials have superior mechanical toughness. In case of the YAG ceramic, it has five times higher fracture toughness than that of YAG single crystal. In this thesis we used ceramic materials in mode-locked laser operations with high intensity pumping and experimentally proved that the ceramic materials can be used for mode-locked laser operation without any problems caused by its polycrystalline material structure.

In chapter 1 the fundamental of laser operation is written. Especially the quasi-3 level cw laser operation is analyzed by a point and 2-dimensional rate equations including gain and absorption saturation effects. Brief

introduction of short pulse laser operation and a limitation factor of high power laser operation are also written. In chapter 2 the fundamental of ultrashort pulse laser operation is written. Especially deference of slow and fast saturable absorber mode locking, SESAM mode locking, hard and soft aperture KLM are written. In chapter 3 general properties of Yb^{3+}-doped materials are shown. The measured spectroscopic properties of Yb^{3+}-doped materials used in this thesis are also shown. The problem of our previous Yb^{3+}-doped femtosecond laser experiment and the idea of multi-gain media oscillator are also written. In chapter 4 the calculation of the cavity based on ABCD matrix is described. Especially influence of the Kerr-lens effect on the cavity and the dependence of induced Kerr-lens effect on cavity state are shown. In chapter 5, KLM laser experiments with various gain materials are described. In chapter 6, gain bandwidth limitation of short pulse duration is estimated based on 3-dimensional rate equations. Influences of a linear cavity loss and Yb^{3+}-ion doping level on the limitation of pulse duration are also shown. In chapter 7 summary and outlook of this thesis are written.

References

[1] H. MAIMAN. “Stimulated optical radiation in ruby”. Nature **187**, 493 (1960).
[2] A. L. Schawlow and C. H. Townes, “Infrared and Optical Masers,” Physical Review, **112**, 1940-1949 (1958).
[3] R. Ell, U. Morgner, F. X. KÃÂrtner, J. G. Fujimoto, E. P. Ippen, V. Scheuer, G. Angelow, T. Tschudi, M. J. Lederer, A. Boiko, and B. Luther-Davies, “Generation of 5-fs pulses and octave-spanning spectra directly from a Ti:sapphire laser,” Opt. Lett. **26**, 373-375 (2001).
[4] S. Adachi, N. Ishii, T. Kanai, A. Kosuge, J. Itatani, Y. Kobayashi, D. Yoshitomi, K. Torizuka, and S. Watanabe, “5-fs, multi-mJ, CEP-locked parametric chirped-pulse amplifier pumped by a 450-nm source at 1 kHz,” Optics Express, **16**, 14341-14352 (2008)
[5] M. Hentschel, R. Kienberger, Ch. Spielmann, G. A. Reider, N. Milosevic, T. Brabec, P. Corkum, U. Heinzmann, M. Drescher, and F. Krausz, Nature **414**, 509 (2001).
[6] M. D. Perry, D. Pennington, B. C. Stuart, G. Tietbohl, J. A. Britten, C. Brown, S. Herman, B. Golick, M. Kartz, J. Miller, H. T. Powell, M. Vergino, and V. Yanovsky, “Petawatt laser pulses,” Opt. Lett. **24**, 160-162 (1999)
[7] J. A. Valdmanis, R. L. Fork, and J. P. Gordon, “Generation of optical pulses as short as 27 femtoseconds directly from a laser balancing self-phase modulation, group-velocity dispersion, saturable absorption, and saturable gain,” Opt. Lett. **10**, 131-133 (1985).
[8] P. F. Moulton, “Spectroscopic and laser characteristics of Ti:Al_2O_3,” J. Opt. Soc. Am. B **3**, 125-133 (1986)
[9] D. E. SPENCE, P. N. KEAN, W. SIBBETT. “60 fs pulse generation from a selfmode-locked Ti:sapphire laser,” Opt. Lett. **16,** 42 (1991).
[10] S. G. Bartoshevich, V. D. Burlakov, V. V. Zuev, N. P. Nazarenko, A. N. Mal’tsev, and G. A. Skripko, “Source of tunable radiation based on Ti^{3+}:Al_2O_3 crystals pumped by a copper-vapor laser,” Appl. Opt. **31**, 7575-7580 (1992)
[11] K. Takehisa and A. Miki, “Method for pumping a Ti:sapphire laser with a stable resonator copper vapor laser,” Appl. Opt. **31**, 2734-2737 (1992)
[12] T. Brabec, Ch. Spielmann, P. F. Curley, and F. Krausz, “Kerr lens mode locking,” Opt. Lett. **17**, 1292-1294 (1992).
[13] A. J. Maclean, P. Roth, G. J. Valentine, A. J. Kemp, and D. Burns, “Direct Diode Laser Pumping of a Ti:Sapphire Laser,” in *Advanced Solid-State Photonics*, OSA Technical Digest Series (CD) (Optical Society of America, 2009), paper WE2.
[14] D. Kopf, K.J. Weingarten, G. Zhang, M. Moser, M.A. Emanuel, R.J. Beach, J. A. Skidmore and U. Keller, “High-average-power diode-pumped femtosecond Cr:LiSAF lasers,” Appl. Phys. B **65**, 235-243, (1997).
[15] P. Wagenblast, R. Ell, U. Morgner, F. Grawert, and F. X. Kärtner, “Diode-pumped 10-fs Cr^{3+}:LiCAF laser,” Opt. Lett. **28**, 1713-1715 (2003)
[16] I. T. Sorokina, E. Sorokin, E. Wintner, A. Cassanho, H. P. Jenssen, and R. Szipöcs, “14-fs pulse generation in Kerr-lens mode-locked prismless Cr:LiSGaF and Cr:LiSAF lasers: observation of pulse self-frequency shift,” Opt. Lett. **22**, 1716-1718 (1997)
[17] M. Stalder, M. Bass, and B. H. T. Chai, “Thermal quenching of fluorescence in

chromium-doped fluoride laser crystals," J. Opt. Soc. Am. B **9**, 2271-2273 (1992)
[18] T. Y. Fan "Heat generation in Nd:YAG and Yb:YAG," IEEE J. of Quantum Electronics **29**, 1457-1459 (1993).
[19] W. F. Krupke, "Ytterbium solid-state lasers-the first decade," IEEE J. Sel. Top. Quantum Electron. **6**, 1287-1296 (2000).
[20] H. M. Pask, R. J. Carman, D. C. Hanna, A. C. Tropper, C. J. Mackechnie, P. R. Barber, and J. M. Dawes, "Ytterbium-Doped Silica Fiber Lasers: VersatileSources for the 1-1.2 pm Region" IEEE J. Sel. Topics Quantum Electron. **1,** 2 (1995).
[21] A. Giesen and J. Speiser "Fifteen Years of Work on Thin-Disk Lasers: Results and Scaling Laws," IEEE JSTQE **13**, 598-609 (2007).
[22] J. Saikawa, Y. Sato, and T. Taira, "Passive mode locking of a mixed garnet Yb:$Y_3ScAl_4O_{12}$ ceramic laser," Appl. Phys. Lett. **85**, 5845 (2004).
[23] H. Liu, J. Nees, and G. Mourou, "Diode-pumped Kerr-lens mode-locked Yb:$KY(WO_4)_2$ laser," Opt. Lett. **26**, 1723-1725 (2001)
[24] F. Druon, D. N. Papadopoulos, J. Boudeile, M. Hanna, P. Georges, A. Benayad, P. Camy, J. L. Doualan, V Ménard, and R. Moncorgé, "Mode-locked operation of a diode-pumped femtosecond Yb:SrF_2 laser," Opt. Lett. **34**, 2354-2356 (2009)
[25] J. Boudeile, F. Druon, M. Hanna, P. Georges, Y. Zaouter, E. Cormier, J. Petit, P. Goldner, and B. Viana, "Continuous-wave and femtosecond laser operation of Yb:$CaGdAlO_4$ under high-power diode pumping," Opt. Lett. **32**, 1962-1964 (2007).
[26] A. A. Lagatsky, V. E. Kiselb, F. Baina, C. T. A. Browna, N. V. Kuleshovb, and W. Sibbetta," Advances in femtosecond lasers having enhanced efficiencies," Proc. of SPIE **6731**, 673103, (2007).
[27] F. Thibault, D. Pelenc, F. Druon, Y. Zaouter, M. Jacquemet, and P. Georges, "Efficient diode-pumped Yb^{3+}:Y_2SiO_5 and Yb^{3+}:Lu_2SiO_5 high-power femtosecond laser operation," Opt. Lett. **31**, 1555-1557 (2006).
[28] S. Rivier, A. Schmidt, C. Kränkel, R. Peters, K. Petermann, G. Huber, M. Zorn, M. Weyers, A. Klehr, G. Erbert, V. Petrov, and U. Griebner, "Ultrashort pulse Yb:$LaSc_3(BO_3)_4$ mode-locked oscillator," Opt. Express **15**, 15539-15544 (2007).
[29] U. Griebner, V. Petrov, K. Petermann, and V. Peters, "Passively mode-locked Yb:Lu_2O_3 laser," Opt. Express **12**, 3125-3130 (2004).
[30] V. Petrov, U. Griebner, D. Ehrt, and W. Seeber, "Femtosecond self mode locking of Yb:fluoride phosphate glass laser," Opt. Lett. **22**, 408-410 (1997)
[31] A. Chong, W. H. Renninger, and F. W. Wise, "All-normal-dispersion femtosecond fiber laser with pulse energy above 20nJ," Opt. Lett. **32**, 2408-2410 (2007)
[32] Xiangyu Zhou, Dai Yoshitomi, Yohei Kobayashi, and Kenji Torizuka, "Generation of 28-fs pulses from a mode-locked ytterbium fiber oscillator," Opt. Express **16**, 7055-7059 (2008)
[33] C. Hönninger, F. Morier-Genoud, M. Moser, U. Keller, L. R. Brovelli, and C. Harder, "Efficient and tunable diode-pumped femtosecond Yb:glass lasers," Opt. Lett. **23**, 126-128 (1998)
[34] U. Keller, K. J. Weingarten, F. X. Kartner, D. Kopf, B. Braun, I. D. Jung, R. Fluck, C. Honninger, N. Matuschek, and J. Aus der Au, "Semiconductor Saturable Absorber Mirrors (SESAM's) for Femtosecond to Nanosecond Pulse Generation in Solid-State Lasers," IEEE J. Sel. Top. Quantum Electron. **2,** 435 (1996).
[35] C. Hönninger, G. Zhang, U. Keller, and A. Giesen, "Femtosecond Yb:YAG laser

using semiconductor saturable absorbers," Opt. Lett. **20**, 2402-2404 (1995)
[36] F. Druon, S. Chénais, P. Raybaut, F. Balembois, P. Georges, R. Gaumé, G. Aka, B. Viana, S. Mohr, and D. Kopf, "Diode-pumped Yb:$Sr_3Y(BO_3)_3$ femtosecond laser," Opt. Lett. **27**, 197-199 (2002)
[37] F. Druon, F. Balembois, and P. Georges, "Ultra-short-pulsed and highly-efficient diode-pumped Yb:SYS mode-locked oscillators," Optics Express **12**, 5005-5012 (2004)
[38] A. A. Lagatsky, A. R. Sarmani, C. T. A. Brown, W. Sibbett, V. E. Kisel, A. G. Selivanov, I. A. Denisov, A. E. Troshin, K. V. Yumashev, N. V. Kuleshov, V. N. Matrosov, T. A. Matrosova, and M. I. Kupchenko, "Yb^{3+}-doped YVO_4 crystal for efficient Kerr-lens mode locking in solid-state lasers," Opt. Lett. **30**, 3234-3236 (2005)
[39] U. Griebner, S. Rivier, V. Petrov, M. Zorn, G. Erbert, M. Weyers, X. Mateos, M. Aguiló, J. Massons, and F. Díaz, "Passively mode-locked Yb:$KLu(WO_4)_2$ oscillators," Opt. Express **13**, 3465-3470 (2005).
[40] S. Rivier, X. Mateos, J. Liu, V. Petrov, U. Griebner, M. Zorn, M. Weyers, H. Zhang, J. Wang, and M. Jiang, "Passively mode-locked Yb:$LuVO_4$ oscillator," Opt. Express **14**, 11668-11671 (2006).
[41] A. García-Cortés, J. M. Cano-Torres, M. D. Serrano, C. Cascales, C. Zaldo, S. Rivier, X. Mateos, U. Griebner and V. Petrov, "Spectroscopy and Lasing of Yb-Doped $NaY(WO_4)_2$:Tunable and Femtosecond Mode-Locked Laser Operation," IEEE J. Quantum Electron. **43**, 758-764 (2007)
[42] F. Friebel, F. Druon, J. Boudeile, D. N. Papadopoulos, M. Hanna, P. Georges, P. Camy, J. L. Doualan, A. Benayad, R. Moncorgé, C. Cassagne, and G. Boudebs, "Diode-pumped 99 fs Yb:CaF_2 oscillator," Opt. Lett. **34**, 1474-1476 (2009)
[43] S. Uemura and K.Torizuka, "Kerr-Lens Mode-Locked Diode-Pumped Yb:YAG Laser with the Transverse Mode Passively Stabilized," Appl. Phys. Express **1,** 012007 (2008)
[44] S. V. Marchese, C. R. E. Baer, R. Peters, C. Kränkel, A. G. Engqvist, M. Golling, D. J. H. C. Maas, K. Petermann, T. Südmeyer, G. Huber, and U. Keller, "Efficient femtosecond high power Yb:Lu_2O_3 thin disk laser," Opt. Express **15**, 16966-16971 (2007).
[45] T. Südmeyer, C. Kränkel, C.R.E. Baer, O.H. Heckl, C.J. Saraceno, M. Golling, R. Peters, K. Petermann, G. Huber and U. Keller, "High-power ultrafast thin disk laser oscillators and their potential for sub-100-femtosecond pulse generation," Appl Phys B **97** 281-295 (2009)
[46] F. Brunner, E. Innerhofer, S. V. Marchese, T. Südmeyer, R. Paschotta, T. Usami, H. Ito, S. Kurimura, K. Kitamura, G. Arisholm, and U. Keller, "Powerful red-green-blue laser source pumped with a mode-locked thin disk laser," Opt. Lett. **29**, 1921-1923 (2004).
[47] J. Neuhaus, D. Bauer, J. Zhang, A. Killi, J. Kleinbauer, M. Kumkar, S. Weiler, M. Guina, D.H. Sutter, and T. Dekorsy, "Subpicosecond thin-disk laser oscillator with pulse energies of up to 25.9 microjoules by use of an active multipass geometry," Opt. Express **16**, 20530-20539 (2008)
[48] F. Brunner, T. Südmeyer, E. Innerhofer, F. Morier-Genoud, R. Paschotta, V. E. Kisel, V. G. Shcherbitsky, N. V. Kuleshov, J. Gao, K. Contag, A. Giesen, and U. Keller, "240-fs pulses with 22-W average power from a mode-locked thin-disk Yb:$KY(WO_4)_2$ laser," Opt. Lett. **27**, 1162-1164 (2002).

[49] P. Russbueldt, T. Mans, G. Rotarius, J. Weitenberg, H. D. Hoffmann, and R. Poprawe, “400W Yb:YAG Innoslab fs-Amplifier,” Opt. Express **17**, 12230-12245 (2009)
[50] M. Siebold, M. Hornung, R. Boedefeld, S. Podleska, S. Klingebiel, C. Wandt, F. Krausz, S. Karsch, R. Uecker, A. Jochmann, J. Hein, and M. C. Kaluza, “Terawatt diode-pumped Yb:CaF_2 laser,” Opt. Lett. **33**, 2770-2772 (2008).
[51] A. Pugžlys, G. Andriukaitis, A. Baltuška, L. Su, J. Xu, H. Li, R. Li, W. J. Lai, P. B. Phua, A. Marcinkevičius, M. E. Fermann, L. Giniūnas, R. Danielius, and S. Ališauskas, "Multi-mJ, 200-fs, cw-pumped, cryogenically cooled, Yb,Na:CaF_2 amplifier," Opt. Lett. **34**, 2075-2077 (2009).
[52] G. Chang, M. Rever, V. Smirnov, L. Glebov, and A. Galvanauskas, “Femtosecond Yb-fiber chirped-pulse-amplification system based on chirped-volume Bragg gratings,” Opt. Lett. **34**, 2952-2954 (2009).

Chapter 1. Fundamental of laser operations

Lasers are based on amplification by stimulated emission. The amplification effect can be achieved by a population inversion inside a gain material. To achieve laser operation, we make a cavity, which worked as optical resonator and spatial mode (spatial frequencies, wave vectors) selector. It generally consists of several elements: gain material, pump source and mirrors for a continuous wave (CW) laser operation. An additional loss or gain modulator is used for a mode-locked laser operation. At the threshold pump power, the cavity's total gain per one round-trip including loss becomes 1 and the laser operation starts with the most suitable mode for the cavity condition. The most suitable means that the mode has lowest threshold. Above the threshold pump power, the laser modes, which can most strongly consume the population inversion of the gain material and can suppress other modes, become stable. If we would like to obtain some special laser operations such as tunable laser operation, ultrashort pulse laser operation and single longitudinal mode operation, we should make each operation mode most stable for the cavity.

The fundamental of the Yb^{3+}-doped laser operation, which is important to understand this thesis, is briefly written in this chapter. Especially, rate equations including saturation effect (gain and absorption) are very important to understand and design an Yb^{3+}-doped laser system.

The contents can be applied to other active ion doped laser system with slight modification.

1.1 Efficiency of Yb^{3+}-doped laser operation

The laser extraction efficiency η_e against the absorbed pump power inside the cavity can be described below [1]

$$\eta_e = \frac{\lambda_p}{\lambda_l} \cdot \eta_p \cdot \eta_s \qquad 1.1,$$

where λ_p and λ_l are pumping and lasing wavelength, respectively. λ_p/λ_l is a ratio of lasing photon energy and pumping photon energy. The value $1-\lambda_p/\lambda_l$ is called quantum defect. η_p is pumping quantum efficiency, which means a ratio of pumped ion number and absorbed photon number. η_s is stimulated emission quantum efficiency, which means a ratio of stimulately emitted photon number and pumped ion number. In this thesis we call the product of η_p and η_s quantum efficiency. With above parameters heat conversion efficiency η_h, which means the portion of heat generation during the laser operation, can be written below

$$\eta_h = 1 - \eta_p \left(\frac{\lambda_p}{\lambda_l} \cdot \eta_s + \frac{\lambda_p}{\lambda_f} \cdot (1 - \eta_s) \cdot \eta_f \right) \qquad 1.2,$$

where λ_f is an averaged wavelength of spontaneous emission and η_f is spontaneous emission quantum efficiency, which means a ratio of spontaneously emitted photon number per residual pumped ion number. Generally, the value $\eta_e = \lambda_p/\lambda_l$ gives a theoretical limitation value of extraction efficiency (in case of the $\eta_p=\eta_s=1$) except for the special case of $\eta_p > 1$, which can be seen in Tm-Ho lasers [2]. The real laser efficiency η_l can be obtained by multiplying an output coupling efficiency T and internal loss L of the cavity. In addition the quantum efficiencies η_p and η_s are

function of the total loss $T+L$ so that the η_l can be written as

$$\eta_l = \frac{\lambda_p}{\lambda_l} \cdot \eta_p(T,L) \cdot \eta_s(T,L) \cdot \frac{T}{T+L} \qquad 1.3.$$

The keys to achieve highly efficient laser operation are small quantum defect, high quantum efficiency, low internal loss and high (suitable) output coupling efficiency. The last three parameters have a reciprocal relationship and we have to optimize them. The relationship can be more deeply described by rate equations.

1.2 Rate equations

Yb^{3+} ions are main active ions used in this thesis and therefore we solve here rate equations for quasi-three-level laser scheme of Yb^{3+} ions.
The important physical parameters intrinsically depending on the gain materials for describing a laser operation are absorption and emission cross sections $\sigma_a(\lambda)$, $\sigma_e(\lambda)$ and upper state lifetime τ. In case of the quasi-three-level laser scheme of Yb^{3+} ions (Fig.1.1), we can effectively consider it as 2 level laser scheme by assuming very fast nonradiative relaxations from states 4 to 3 and 2 to 1 (in case of the Yb^{3+} ion generally it

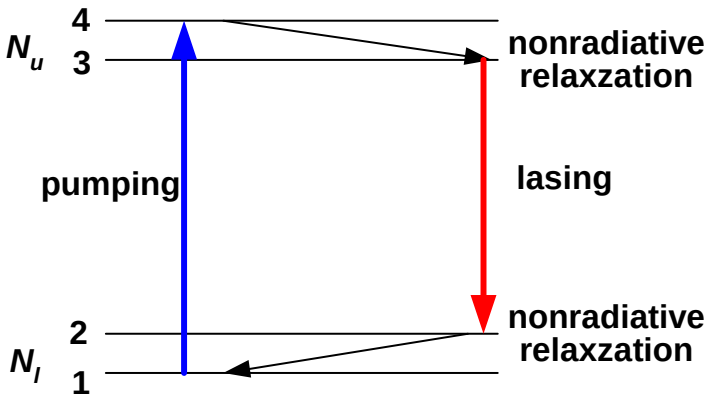

Fig. 1. 1. Schematic picture of four-level laser scheme.

has ~ ps order nonradiative decay time) and using emission and absorption cross section values taking account for thermally distributed population in their inter manifolds. The point rate equations can be written below [3,4,5]

$$N = N_u + N_l \qquad 1.4,$$

$$\frac{dN_u}{dt} = I_p\sigma_a(\lambda_p)N_l - I_p\sigma_e(\lambda_p)N_u - I_l\sigma_e(\lambda_e)N_u + I_l\sigma_a(\lambda_e)N_l - \frac{N_u}{\tau} \qquad 1.5,$$

$$\frac{dI_l}{dt} = I_l\sigma_e(\lambda_e)N_u - I_l\sigma_a(\lambda_e)N_l - (T+L)I_l \qquad 1.6,$$

$$\frac{dI_p}{dz} = I_p\sigma_e(\lambda_p)N_u - I_p\sigma_a(\lambda_p)N_l \qquad 1.7,$$

$$\frac{dI_p}{dz} = -\frac{N_u}{\tau} - I_l\sigma_e(\lambda_e)N_u + I_l\sigma_a(\lambda_e)N_l \qquad 1.8,$$

where N is total Yb^{3+}-ion number, N_u and N_l are upper state and lower state Yb^{3+} ion number. I_p and I_l are pumping and lasing intra-cavity photon number. T and L are output coupling efficiency and internal loss coefficient of the cavity. λ_p and λ_e are the lasing and pumping wavelengths. In case of the stationary state, the equations 1.5 and 1.6 become = 0, and then threshold upper state ion number N_u^{th} (eq. 1.9 from eqs. 1.4 and 1.5) and laser extraction efficiency η_e (eq. 1.10 from eqs. 1.4 and 1.5) can be written below

$$N_u^{th} = \frac{\sigma_a(\lambda_e)\cdot N + T + L}{\sigma_e(\lambda_e) + \sigma_a(\lambda_e)} \qquad 1.9,$$

$$\eta_e = \frac{I_l h\nu_l}{I_p h\nu_p} = \frac{\lambda_p}{\lambda_l}\frac{\sigma_e(\lambda_e)N_u^{th} - \sigma_a(\lambda_e)N + \sigma_a(\lambda_e)N_u^{th} + N_u^{th}/\tau}{\sigma_a(\lambda_p)N - \sigma_a(\lambda_p)N_u^{th} - \sigma_e(\lambda_p)N_u^{th}} \quad 1.\ 10,$$

the right side of the eq. 1.10 is the product of λ_p/λ_l and quantum efficiency. The eqs. 1.9 and 1.10 show the dependence of the extraction efficiency η_e on T and L.

From the eqs. 1.7 and 1.8, we can obtain the equation 1.11 below

$$\frac{dI_p}{dz}(1 + \frac{I_p}{I_{ps}}) = -NI_p\left[\sigma_a(\lambda_p) - \frac{I_l\sigma_a(\lambda_e)}{I_{ps}}\right] \quad 1.\ 11,$$

where I_{ps} is saturation pump fluence and can be written below

$$I_{ps}(I_l) = \frac{1/\tau + I_l\{\sigma_e(\lambda_e) + \sigma_a(\lambda_e)\}}{\{\sigma_a(\lambda_p) + \sigma_e(\lambda_p)\}} \quad 1.\ 12,$$

and then small signal absorption α_0 is written below

$$\alpha_0 = -N\left(\frac{I_{ps}}{I_p + I_{ps}}\right)\left[\sigma_a(\lambda_p) - \frac{I_l\sigma_a(\lambda_e)}{I_{ps}}\right] \quad 1.\ 13,$$

the saturation effect of the pumping laser absorption strongly depends on the lasing intra cavity photon number I_l. The eqs. 1.11-1.13 are very important to estimate correct absorbed pump power and pumped ion density profile inside the gain material.

From eqs. 1.4 and 1.5, the threshold upper state ion number N_u^{th} and lower state ion number N_l^{th} can also be considered as a function of I_p and I_l.

$$N_u^{th}(I_p, I_l) = \frac{I_p\sigma_a(\lambda_p)N + I_l\sigma_a(\lambda_e)N}{I_p\left(\sigma_a(\lambda_p) + \sigma_e(\lambda_p)\right) + 1/\tau + I_l\left(\sigma_e(\lambda_e) + \sigma_a(\lambda_e)\right)} \quad 1.\ 14,$$

$$N_l^{th}(I_p, I_l) = \frac{I_p\sigma_e(\lambda_p)N + I_l\sigma_e(\lambda_e)N + 1/\tau N}{I_p\left(\sigma_a(\lambda_p) + \sigma_e(\lambda_p)\right) + 1/\tau + I_l\left(\sigma_e(\lambda_e) + \sigma_a(\lambda_e)\right)} \quad 1.\ 15,$$

The laser operation mode, which has the lowest N_u^{th} become most stable. From eqs. 1.14 and 1.15, the gain g and small signal gain g_0 are described as a function of I_p and I_l

$$g(I_p, I_l) = \frac{\sigma_e(\lambda_e)\left(I_p\sigma_a(\lambda_p)N + I_l\sigma_a(\lambda_e)N\right)}{I_p\left(\sigma_a(\lambda_p) + \sigma_e(\lambda_p)\right) + 1/\tau + I_l\left(\sigma_e(\lambda_e) + \sigma_a(\lambda_e)\right)} - \frac{\sigma_a(\lambda_e)\left(I_p\sigma_e(\lambda_p)N + I_l\sigma_e(\lambda_e)N + 1/\tau N\right)}{I_p\left(\sigma_a(\lambda_p) + \sigma_e(\lambda_p)\right) + 1/\tau + I_l\left(\sigma_e(\lambda_e) + \sigma_a(\lambda_e)\right)} \quad 1.\ 16,$$

$$g_0(I_p, 0) = \frac{I_p\sigma_e(\lambda_e)\sigma_a(\lambda_p)N}{I_p\sigma_a(\lambda_p) + I_p\sigma_e(\lambda_p) + 1/\tau} - \frac{\sigma_a(\lambda_e)\left(I_p\sigma_e(\lambda_p)N + 1/\tau N\right)}{I_p\sigma_a(\lambda_p) + I_p\sigma_e(\lambda_p) + 1/\tau} \quad 1.\ 17,$$

from the eqs. 1.11 and 1.12 the saturation fluence I_{ls} where the gain g become half can be described as

$$I_{ls}(I_p) = \frac{I_p\left[\sigma_a(\lambda_p) + \sigma_e(\lambda_p)\right] + 1/\tau}{\sigma_a(\lambda_e) + \sigma_e(\lambda_p)} \qquad 1.\ 18,$$

$$= I_{ls}(I_0)[1 + \frac{I_p}{I_{ps}(0)}]$$

by assuming the $\sigma_a(\lambda_e) = 0$, the eq. 1.17 become well known equation

$$I_s(\lambda_e) = \frac{1}{\sigma_e(\lambda_e)\tau} \qquad 1.\ 19,$$

from eqs. 1.6 and 1.7 critical pump power I_{cr} (λ), which is required to achieve a gain coefficient of zero at the gain medium can be defined below

$$I_{cr} = \frac{1}{\tau}\frac{1}{\sigma_a(\lambda_p)\left(\sigma_e(\lambda_e)/\sigma_a(\lambda_e)\right) - \sigma_a(\lambda_p)} \qquad 1.\ 20,$$

1.3 Multi-mode laser operation

Inside a laser cavity, there are many longitudinal modes depending on an optical length l of the cavity ($v = m \times c/2l$, Fig.1.2). Each longitudinal mode has possibility of lasing and they strongly compete each other. In the case of homogeneous broadened gain material pumped by continuous wave pump source, ideally, the laser operation occur with one longitudinal mode where threshold population inversion N_u^{th} has the lowest value (see section 1.2). However, in general cases, lasing occurs with multi-longitudinal modes with random phase relationship that is caused by spatial-hole burning effect [6]. The spatial-hole burning effect is simply expressed by Fig. 1.3 (a). Except for a ring cavity, counter-propagating waves inside the cavity make a standing wave interference pattern, which makes spatially depending saturated gain profile inside the gain material. The gain saturation becomes weak at node points and strong at antinode points of interference pattern. Such spatially distributed saturated gain profile allows other longitudinal mode, which has different spatial frequency (period of standing wave) to lase. In addition, the spatially distributed saturated gain profile appears not only along z-axis but also across z-axis (Fig1.3 (b)). Distributed saturated gain profile across z-axis lead to multi-transverse mode operation. The available transverse mode depends on a mode matching between a distributed intensity profile of lasing and pumping

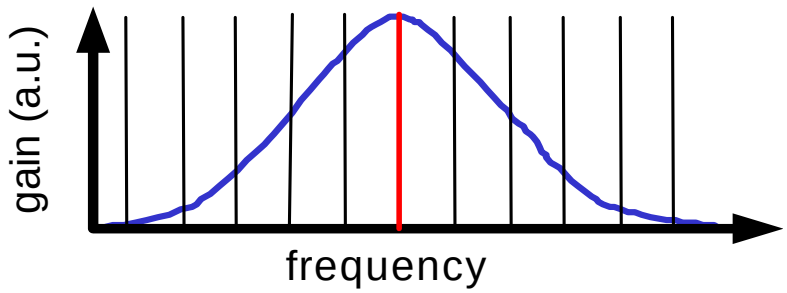

Fig. 1. 2. Transverse modes of the cavity and gaussian gain profile is shown. Each transverse mode has finite bandwidth. Ideally the laser operation occurs at one transverse mode having a lowest thresh hold (highest gain, red line).

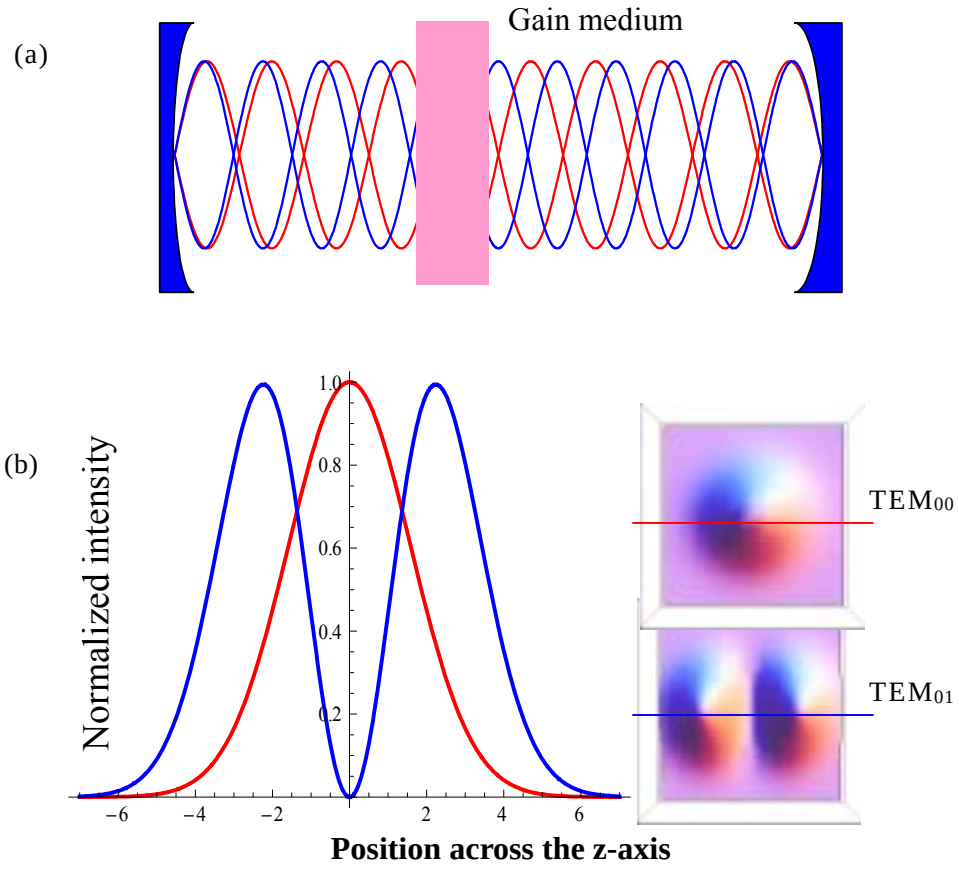

Fig. 1. 3. Spatial-hole-burning. (a) Standing waves inside the cavity along the z-axis are shown. Red curve and blue curve have 10 % different frequencies. (b) Intensity distribution across the z-axis. Red curve shows TEM_{00} and blue curve shows TEM_{01} mode.

transverse modes. To take account for them, the point rate eqs 1.6 and 1.7 are modified to 2-dimentional rate eqs. below

$$\frac{I_{total}}{dt} = \int [cS_l(x,y,z)\sigma_e(\lambda_e)N_u(x,y,z) - cS_l(x,y,z)\sigma_a(\lambda_e)N_l(x,y,z)]dV - \frac{cLI_{total}}{2l_{cavity}} \quad 1.21,$$

$$\frac{dN_u(x,y,z)}{dt} = cS_p(x,y,z)(\sigma_a(\lambda_p)N_u - \sigma_e(\lambda_p)N_l) - \frac{N_u(x,y,z)}{\tau} - S_l(x,y,z)c\times\int [N_u(x,y,z)\sigma_e(\lambda_e) - N_1(x,y,z)\sigma_a(\lambda_e)]dV \quad 1.22,$$

where I_{total} is total laser photon number inside the cavity, c is velocity of light, $S_l(x,y,z)$ and $S_p(x,y,z)$ are distribution functions of the lasing and

pumping photon densities inside the cavity, $N_l(x,y,z)$ and $N_u(x,y,z)$ are distribution function of the lower and upper state Yb^{3+} ion density, l_{cavity} is cavity length, L is round-trip cavity loss coefficient and $R_p(x,y,z)$ is pumping rate distribution function.

1.4 Mode-locked pulses

Ultrashort pulses consist of phase-locked multi-longitudinal modes laser beam (Fig.1.4). By an interference effect, they construct ultrashort pulse in the time domain. In the time domain, their electric field can be written below

$$E(t) = \varepsilon(t)\exp[i\phi(t) - i\omega_0 t] + c.c. \qquad 1.\ 23,$$

where $\varepsilon(t)$ is envelop function (Fig.1.5), $\Phi(t)$ is time depending phase shift

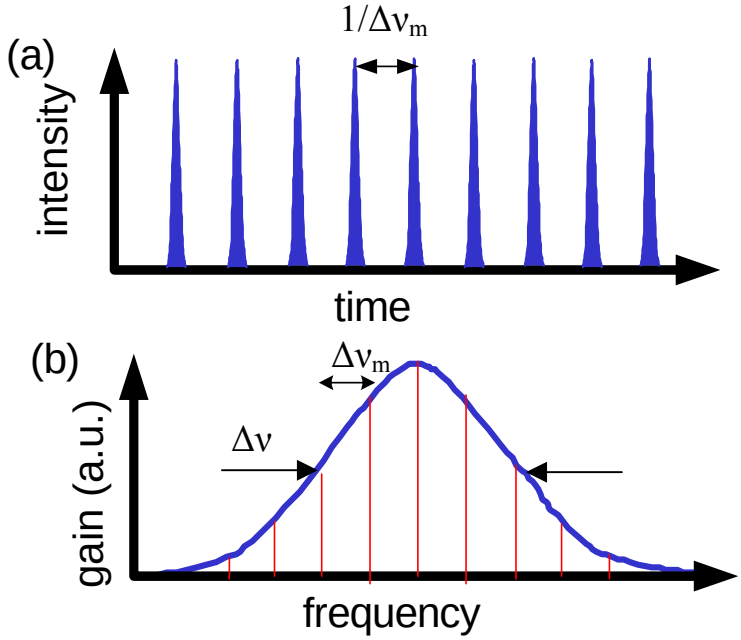

Fig. 1. 4. Ultrashort pulses in time domain (a) and frequency domain (b) are shown. In case of the 100 fs pulses with a one-meter length cavity, there are above 100,00 transverse modes in the spectrum.

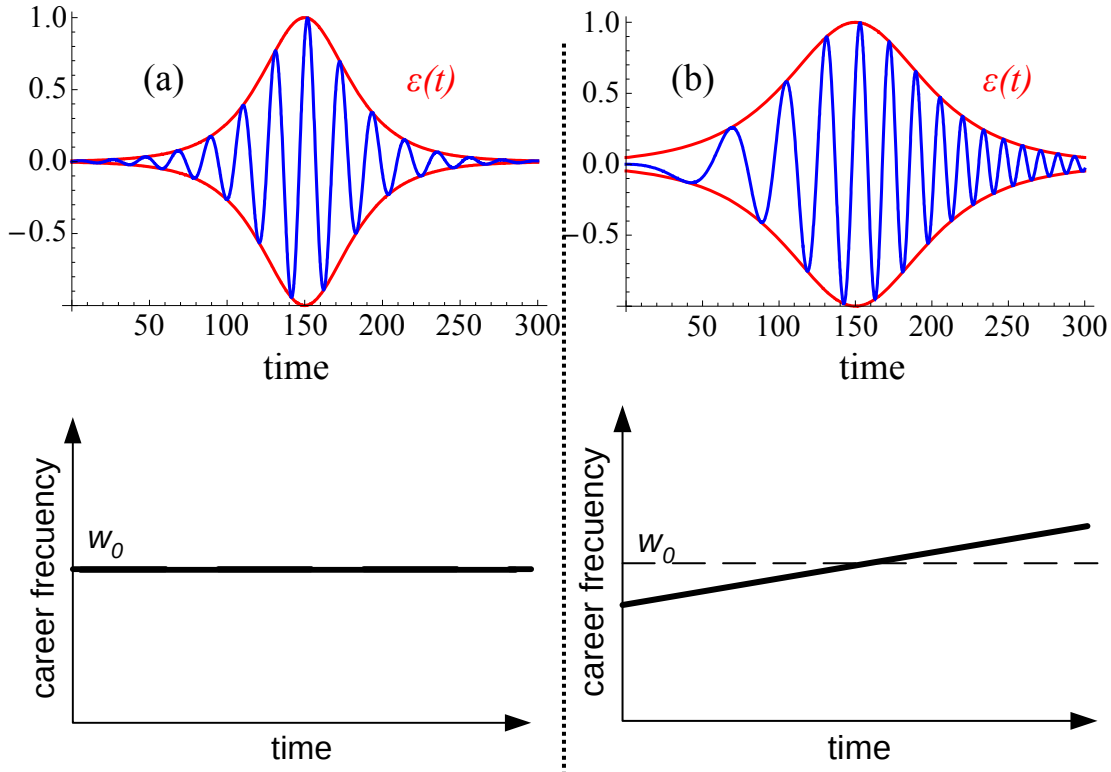

Fig. 1. 5. (a) Transform-limited pulse. (b) Up chirped pulse.

that express chirping of the pulses. When the $\Phi(t)$ becomes 0, the pulse is called transform-limited pulse and has shortest pulse duration. When $\Phi(t)$ increases (decreases) with time, the pulse is called up (down) chirped pulse and its pulse duration becomes longer than that of transform-limited pulse. ω_0 is career frequency and *c.c.* is complex conjugate. The energy of each pulse is proportional to the number of longitudinal modes. In a frequency domain their electric field can be written as

$$E(t) = \frac{1}{\sqrt{2\pi}} \int_0^\infty \varepsilon(\omega) \exp[i\phi(\omega) - i\omega t] d\omega + c.c. \qquad 1.\ 24,$$

In case of the transform-limited pulses ($\Phi(t)$=0), $\Phi(w)$ become 0 (or having linear relationship) in each longitudinal mode. In case of up (down) chirped pulse, $\Phi(w)$ increase (decrease) with w. Such chirping is mainly caused by material dispersion (dependence of refractive index on frequency, $n(v)$) and SPM effect (via the dependence of refractive index on a pulse temporal

intensity profile, $dI/dt \times n_2$). The repetition rate of the pulse train v_m in the time domain corresponds to the period of transverse modes in the frequency domain. The available pulse duration Δt and its frequency bandwidth Δv have the relationship written below

$$\Delta t \times \Delta \nu \geq K \qquad 1.25,$$

the K is pulse shape constant [7] (table. 1.1). The relationship of the frequency bandwidth and pulse duration can be considered similar to a relationship of far field beam pattern (wave vector profile) and near field beam pattern size of the laser light. It can also be considered as a relationship of Uncertainty principle.

Table 1. 1. Relation ships between pulse shape and K constant. [7]

Field envelope	Intensity profile	Auto correlation (FWHM)	Power spectrum	Constant K
Gauss	$\mathrm{Exp}[-2(t/\tau_g)^2]$	$1.18\tau_g$	$\mathrm{Exp}[-(\omega\tau_g)^2/2]$	0.441
Sech	$\mathrm{Sech}^2(t/\tau_s)$	$1.76\tau_s$	$\mathrm{Sech}^2(\pi\omega\tau_s/2)$	0.315
Lorentz	$[1+(t/\tau_l)^2]^{-2}$	$1.29\tau_l$	$\mathrm{Exp}[-2\lvert\omega\rvert\tau_l]$	0.142

1.5 Dispersion compensation

To obtain transform-limited pulses (short pulse duration) dispersion compensation becomes very important. The frequency depending phase shift can be expressed in a Taylor express

$$\phi(w) = \phi(w_0) + \frac{\partial \phi}{\partial w}(w - w_0) + \frac{1}{2}\frac{\partial^2 \phi}{\partial w^2}(w - w_0)^{2+} + \frac{1}{6}\frac{\partial^3 \phi}{\partial w^3}(w - w_0)^3 + \cdots \qquad 1.26$$

the third term of right side of the eq. 1.26 is caused by group velocity dispersion and the forth term is caused by third order dispersion. Such

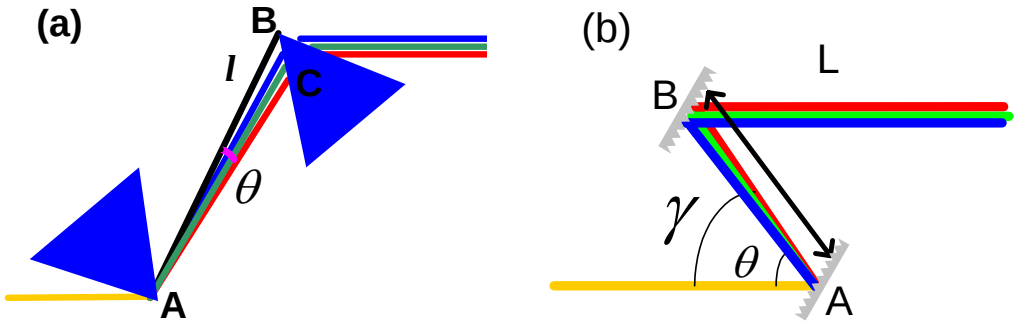

Fig. 1.6. Frequency depending optical pass (spatially dispersion) of prism pair (a) and grating pair (b) are shown.

dispersion can be compensated for by a prism pair, grating pair and/or chirped mirror (GTI mirror) [8,9,10]. In case of the prism pair or grating pair, the optical pass has spatially dispersion (frequency depending optical pass length), which can make dispersion compensation (Fig. 1.6). In case of the chirped mirror, it has chirped coating structure where longer wavelength light is reflected its top (bottom) surface and shorter wavelength light is reflected bottom (top) surface. In case of the GTI mirror, it has frequency depending complex reflectance, where the imaginary part can make dispersion compensation. In this thesis, we considered second order dispersion and ignored much higher order dispersion, which generally should be considered in case of sub-40 fs pulse generation. In the experiments of this thesis, we used SF 10 prism pair as a dispersion compensation element. The second order dispersion of the prism pair can be written below

$$\frac{d^2\phi}{dw^2} = \frac{\lambda^3}{2\pi^2 c^2}\frac{d^2P}{d\lambda^2} \qquad 1.27$$

$$\frac{d^2P}{d\lambda^2} = 4\left[\frac{d^2n}{d\lambda^2} + (2n - n^{-3})\left(\frac{dn}{d\lambda}\right)^2\right] l\sin\theta - 8\left(\frac{dn}{d\lambda}\right)^2 l\cos\theta \qquad 1.28$$

The GVD of SF 10 prism pair used in this thesis is estimated to

$$-33.5\times l\cos\theta(\text{cm}) + 140\times l\sin\theta\ (\text{mm}) \quad [\text{fs}^2] \qquad 1.29$$

where l is distance between prisms.

1.6 High power laser operation

In this section, we briefly consider limitation factors of high power operation in three operation types: CW oscillator, pulsed oscillator, and pulse amplifier. There are several limitation factors for each operation mode (see table 1.2). Among them, the heat loads are common problem in all operation modes. During the laser operation, nonradiative decay process of pumped active ions generates heat load inside the gain material, which makes temperature distribution. Due to the thermo-optical effect, such temperature distribution makes a thermal lens inside the gain material and changes cavity state. Furthermore it also makes uncompensatable wave front distortion, which strongly degraded the laser beam quality. The thermal distribution also makes internal stress inside the gain medium via thermal expansion effect. When the internal stress become larger than the stress fracture toughness of the gain medium, the gain medium will be broken. Thermal fracture toughness of materials can be evaluated by thermal shock parameter R_t written below [11]

$$R_t = \frac{\kappa(1-\nu)}{\alpha E}\sigma_{stress(MAX)} \qquad 1.30,$$

where k is thermal conductivity, ν is Poisson's ration, α is thermal

Table 1. 2. Limitation factors for high power laser operation

CW oscillator	Pulse Oscillator	Pulse amplifier
Available pump power	Available pump power	Available pump power
Thermal fracture limit	Thermal fracture limit	Thermal fracture limit
Thermal lens	Thermal lens	Thermal lens
Damage at the coating	Damage at the coating	Damage at the coating
	Nonlinear phase shift	Nonlinear phase shift
		Damage at material surface
		Parasitic oscillation & ASE
		Available storage energy

expansion coefficient, E is Young module and σ_{stress} is stress fracture limit. R_t indicates the limitation of Heat generation per material length. The available laser power P_{ex} can be written below [12]

$$P_{ex} \le \frac{12R_t}{\chi}\left(\frac{A}{t}\right) \qquad 1.31,$$

where χ is the heating parameter defined as heat deposited per unit stored energy. A and t are surface area and material thickness. In this thesis we used the gain material having high thermal conductivity and high thermal shock parameter for further power scalability. The coating damage at the material surface also becomes problem (especially in case of the pulse oscillator and amplifier). The damage threshold of the coating strongly depends on a wavelength, coating material, coating type, surface roughness, temperature and pulse duration. The shorter wavelength and the shorter pulse duration tend to cause lower damage threshold. Generally the coating damage is more critical than the damage at the bulk material surface [13]. The damage threshold at 1 μm wavelength and ~300 fs pulse duration is roughly about 1 J/cm^2 (HfO_2/SiO_2 multi-layer). In case of the thin-disk laser, coating damage at material top surface becomes problem. It is probably caused by its high temperature at top surface, which is caused by its buck surface cooling constructor. The bonding of nondoped material its top surface might be useful to decrease temperature at top surface. In case of the pulsed laser operation, the total amount of nonlinear phase shift becomes important. It is evaluated by B-integral parameter written below

$$B = \frac{2\pi}{\lambda}\int n_2(z) I_l(z) dz \qquad 1.32$$

where $n_2(z)$ is nonlinear refractive index. The critical value of B integral depends on cavity configuration, in a roughly evaluation B integral values should be smaller than 2π. Using a material with a low nonlinear refractive index and/or thin material can reduce the B integral value.
For relax above limitations, the thin-disk laser concept is desirable [14].

Ideally thin-disk has one-dimensional heat flow at the same direction of the laser beam axis and suffers less heat loads. It also has power scalability based on its scalable laser mode size. The Parasitic oscillation and amplified spontaneous emission (ASE) also become problem in high power amplifier system at low repetition rate and high power laser system based on large aperture size or long gain medium such as thin-disk, slab, and fiber. To suppress them, undesirable parasitic cavity should be eliminated and maximum temporal gain at interval of the pulses also should be limited. The ASE may make a limitation in the power scalability of thin-disk laser based on its scalable laser mode size.

The available storage energy is inversely proportional to the upper state lifetime. The Yb^{3+} ion have about 2~3 order longer lifetime than that of Ti^{3+}:Al_2O_3 and therefore it is also very suitable for high energy amplifier system.

References

[1] T. Y. Fan "Heat generation in Nd:YAG and Yb:YAG," IEEE J. of Quantum Electronics **29**, 1457-1459 (1993).
[2] V.A. French, R.R. Petrin, R.C. Powell, and M. Kokta, "Energy-transfer processes in $Y_3Al_5O_{12}$:Tm, Ho," Phys. Rev. B **46**, 8018-8026 (1992).
[3] H. M. Pask, R. J. Carman, D. C. Hanna, A. C. Tropper, C. J. Mackechnie, P. R. Barber, and J. M. Dawes, "Ytterbium-Doped Silica Fiber Lasers: VersatileSources for the 1-.2 pm Region" IEEE J. Sel. Topics Quantum Electron. **1,** 2 (1995).
[4] Jörg Neuhaus, "Passively mode-locked Yb:YAG thin-disk laser with active multipass geometry," Ph.D thesis, University of Konstanz, Germany, (2009).
[5] P. KLOPP. "New Yb^{3+} doped laser materials and their application in continuous wave and mode-locked lasers," Dissertation, Humboldt Universit¨at zu Berlin, 2006.
[6] C. L. Tang, H. Statz, and G. deMars, "Spectral output and spiking behavior of solid-state lasers," J. Appl. Phys. **34**, 2289 (1963).
[7] Jean Claude Diels and Wolfgang Rudolph, "Ultrashort Laser Pulse Phenomena, Fundamentals, Techniques and Applications on a Femtosecond Time scale," published from Academic Press Inc. (1995).
[8] R. L. Fork, C. H. Brito Cruz, P. C. Becker, and C. V. Shank, "Compression of optical pulses to six femtoseconds by using cubic phase compensation," Opt. Lett. **12**, 483-485 (1987).
[9] R. L. Fork, O. E. Martinez, and J. P. Gordon, "Negative dispersion using pairs of prisms," Opt. Lett. **9**, 150-152 (1984).
[10] J. Kuhl and J. Heppner, "Compression of femtosecond optical pulses with dielectric multilayer interferometers," IEEE J. Quantum Electron. **22**, 182-185, (1986).
[11] W. F. Krupke, M. D. Shinn, J. E. Marion, J. A. Caird, and S. E. Stokowski, "Spectroscopic, optical, and thermomechanical properties of neodymium- and chromium-doped gadolinium scandium gallium garnet," J. Opt. Soc. Am. B **3**, 102 (1986).
[12] T. Taira, "RE^{3+}-Ion-Doped YAG Ceramic Lasers," IEEE JSTQE. **13**, 798-809 (2007).
[13] W. Koechner, "Solid-State Laser Engineering 6^{th} version," Springer (2006).
[14] A. Giesen and J. Speiser "Fifteen Years of Work on Thin-Disk Lasers: Results and Scaling Laws," IEEE JSTQE **13**, 598-609 (2007).

Chapter 2. Ultrashort pulse laser operation

Short pulse duration with the order of sub-nanosecond can be obtained by a *Q*-switch laser, active or passive mode locked lasers. Particularly sub-ps pulse duration can be obtained by mode locking. Due to a broad spectral bandwidth (non-monochromatic spectrum) of mode-locked pulses, a mode-locked operation normally has higher threshold than a CW operation so that an additional loss/gain or phase modulation is required to achieve stable mode-locked laser operation.

2.1 Active mode locking

In case of the active mode locking, time depending gain/loss or phase modulation is applied to the cavity by an Electro-Optical Modulator (EOM) or Acoustic-Optical Modulator (AOM) with a period corresponding to the cavity round trip time of $c/2L$ (Fig.2.1). The modulation generates $\nu_0 \pm c/2L$ sideband in the frequency domain and they lock each other. In case of the AOM or EOM mode locking, the available pulse duration depends on the response time and timing jitter of the electrical components.

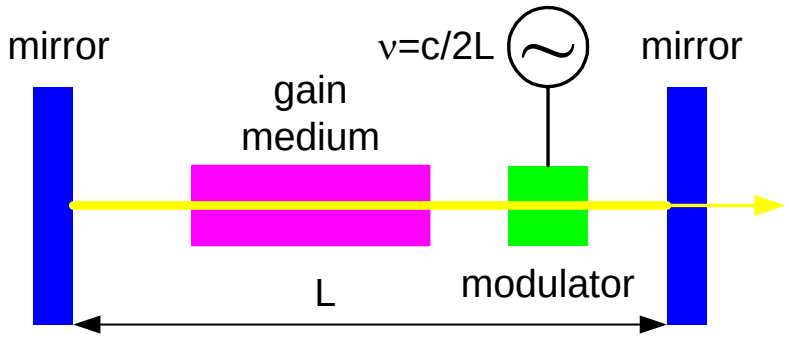

Fig. 2. 1. Schematic picture of active pulsed mode-locked laser cavity.

2.2 Passive mode locking

In the passive mode locking, an intensity depending loss and/or gain modulation element is inserted in the cavity. Saturable absorbers are the most popular elements to achieve a passive mode locking. They can be classified to “slow saturable absorber” and “first saturable absorber” by their response times and target pulse duration. The former has slower response (recovery) time of saturable absorption effect than the pulse duration and the latter has comparable response time to the pulse duration [1,2,3]. Ultrashort pulse laser operation based on a combination of slow saturable absorber and dye gain solution was intensively investigated in 1970s. The dye gain media have very broad gain bandwidths and large stimulated emission cross sections, which lead to a dynamic gain saturation. In 1972, sup-ps pulse duration was obtained from a mode-locked CW dye laser [4]. In 1981, sub-100 fs pulse duration was obtained from a colliding pulse mode locked dye laser [5]. These results were sustained by a very short time positive total gain window that was caused by a combination of slow saturable absorber and dynamic gain saturation effect in one pulse (fig.2.3 (a)). They had opened new door of sub 100 fs ultrafast sciences. The dye gain media, however, have several difficulties for handling. They generally have toxicity and easy to decay so that they have to be renewed in a short time period. Additionally the critical alignment also changes with the decay. Therefore, easy handling ultrashort pulse lasers based on chemically inert solid-state materials were desired. The combination of

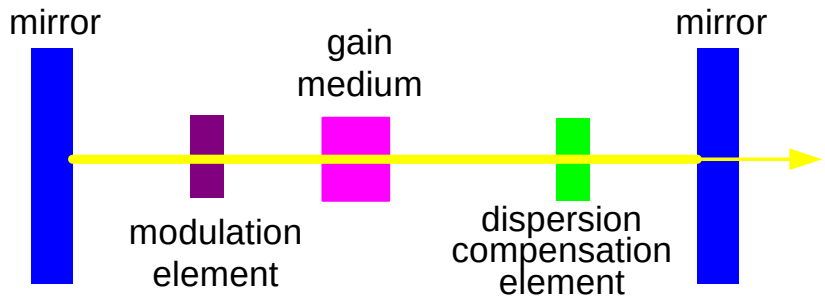

Fig. 2. 2. Schematic picture of solitonlike mode-locked laser cavity.

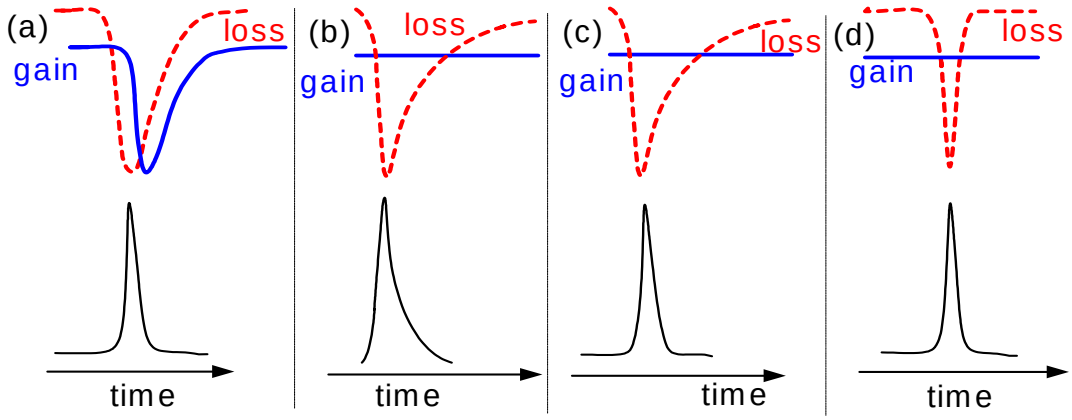

Fig. 2. 3. Temporal dependence of gain, loss and pulse shape in short pule operation are shown. (a) Slow saturable absorber with dynamic gain saturation, which can be seen in dye lasers. (b) Slow saturable absorber without dynamic gain saturation (c) soliton mode locking with slow saturable absorber and time independent gain (d) first saturable absorber with time independent gain. Referred from [1] and the author added one picture.

dynamic gain saturation and saturable absorption effect, however, is difficult to be used with solid-state gain materials. Because, generally solid-state gain media have 100~1000 times smaller stimulated emission cross sections than those of dye gain media so that the dynamic gain saturation effect in one pulse is very small and therefore short time positive total gain window can not be made in them (fig.2.3 (b)). In case of the solid-state lasers, sub-ps pulses can be obtained by a Soliton (sometimes solitonlike) mode locking [6]. In the soliton mode locking, the cavity includes dispersion compensation elements such as prism pair, grating pair and/or chirped mirror (GTI mirror) [7,8,9]. These elements compensate and balance with dispersion caused by material dispersion and SPM effect inside the cavity. The pulse duration can be estimated (defined) by the solution of nonlinear Schrödinger equation (Master equation introduced by Haus. Equation 2.1 [10,11]) and can be much shorter than response (relaxation) time of saturable absorber [12]. The solitonlike mode locking became very popular for solid-sate mode-locked lasers and all of experiments done in this thesis are based on solitonlike mode locking. The pulse duration can be expressed by the equations below [13]

$$\left[-j\psi -(L+j\chi)+g\left(1+\frac{1}{\Omega_g^2}\frac{d^2}{dt^2}\right)+jD\frac{d^2}{dt^2}+(\gamma-j\delta)|a|^2 \right]a=0 \quad 2.\ 1$$

$$\tau_{\text{soliton}}=\frac{1.76\lambda A_{eff}}{\pi n_2}\frac{|\beta_2|}{E_p} \quad \text{:soliton solution in the fiber lasers.} \quad 2.\ 2,$$

$$\tau_{\text{soliton}}=\frac{1.76\lambda A_{eff}}{\pi n_2 l}\frac{|D_2|}{E_p} \quad \text{:solitonlike solution in solid-state lasers.} \quad 2.\ 3,$$

where $j\psi$ is phase shift per pass, jx is linear reactive contribution of the media, g is gain, Ω_g is gain bandwidth, γ shows saturable absorption effect, δ is phase shift caused by SPM, λ is center wavelength, A_{eff} is effective laser mode-field area in side the nonlinear medium, β_2 is group velocity dispersion (GVD) parameter, D_2 is total GVD of the cavity, l is length of nonlinear medium and E_p is pulse energy. In roughly speaking, in the soliton (solitonlike) mode locking, parasitic components not satisfying the soliton solution suffer non-zero dispersion and diverge over time domain (diverge to outside the positive gain time window). Therefore they suffer negative total loss. In the soliton mode locking, the pulse (spectral) shape obeys the equation and become sech^2 shape by nonlinear shaping effect even though the shape of temporal gain window is not sech^2. Completely flat gain spectral is not always needed. In the experiments of this thesis, very large gain modulations were induced by Kerr-lens effect. Combination with such nonlinear shaping effect, it enabled generation of ultrashort pulses having broader spectral bandwidth than its material gain bandwidth limitation as in the case of previous Kerr-lens mode locked Ti^{3+}:Al_2O_3 laser [14] .

2.3 SESAM mode locking

In case of the solid-state mode-locked lasers, a solid-state saturable absorber also replaced a dye solution saturable absorber. Today the most popular solid-state saturable absorber is semiconductor saturable absorber mirror (SESAM). They have Anti resonant Fabry-Perot (AFP) structure consisting of semiconductor saturable absorber sandwiched by top and bottom Bragg reflectors (Fig.2.4) [15]. Comparison with balk semiconductor saturable absorber, the AFP structure enables artificial control of saturation fluence and modulation depth with lower insertion loss. The semiconductor saturable absorber used in SESAM itself is growth in low temperature to achieve short recovery time of saturable absorption effect. SESAM has been strongly developed in the past decade and accelerated the development of femtosecond solids-state lasers very well. The saturable absorption effect depends on only its pulse energy and does not depend on its pulse duration unless the pulse duration becomes longer than SESAM's recovery time (Fig.2.5). Today the wavelength range from 740 nm to 2000 nm, saturable absorption depth (ΔR) of 0.3 - 50 %, recovery time of 10 ps - 500 fs and saturation fluence ($F_{sat,a}$) of 10-120 μJ/cm^2 are commercially available (BATOP GmbH). One of the problems of the SESAM mode locking is tendency of transition to a multi-pulsed laser operation [16]. Because, SESAM's saturation effect depends only on

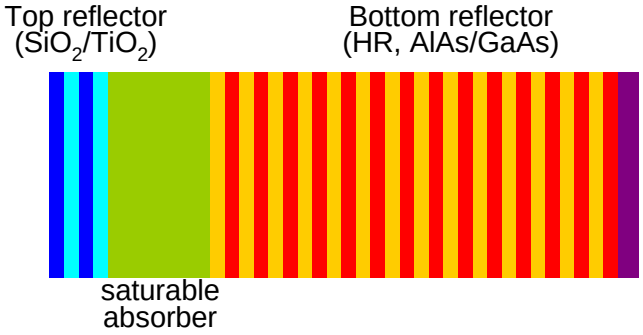

Fig. 2. 4. Schematic picture of Anti resonant Semiconductor saturable absorber mirror is shown. The material composition is change for target specifications.

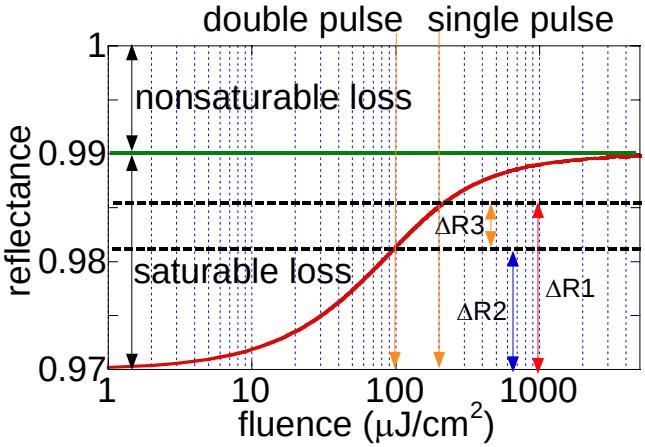

Fig. 2. 5. Fluence depending reflectance of SESAM. Red curve shows reflectance of SESAM. ΔR1 shows modulation depth between single pulse and cw operations. ΔR2 shows modulation depth between double pulse and cw operations. ΔR3 shows modulation depth between single and double pulse operations. Laser fluence of 200 μJ/cm^2 for single pulse and 100 μJ/cm^2 for double pulse operations were assumed.

a laser fluence and at the fully saturation pulse energy level, a double pulsed operation mode (half laser fluence) can strongly saturate the SESAM and becomes stable. To suppress such multi-pulsed laser operation, the laser fluence onto the SESAM is limited to be below its saturation fluence. A large saturable absorption depth ΔR is also can suppress such multi-pulsed operation. The available saturable absorption depth ΔR of the SESAM, however, is also limited to suppress Q-switch instability (Fig.2.6) [17]. The critical pulse energy E_p to suppress the Q-switch mode locking is written as

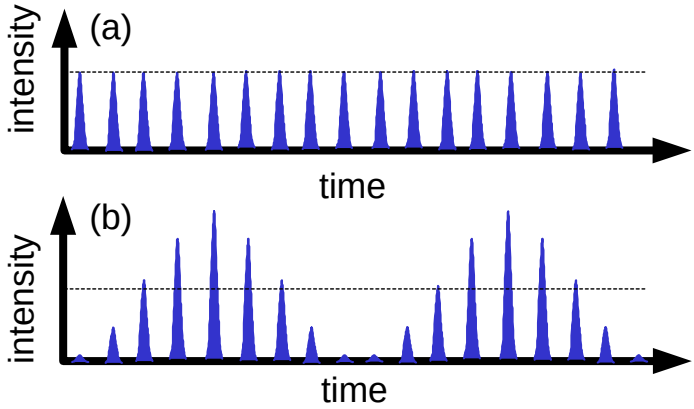

Fig. 2. 6. Schematic pictures of CW mode locked pulse train (a) and Q switch mode locked pulse train (b) are shown.

$$E_p = \sqrt{F_{sat,l} \cdot A_{eff,g} \cdot F_{sat,a} \cdot A_{eff,A} \cdot \Delta R} \qquad 2.4,$$

where $F_{sat,l}$ is saturation fluence of gain medium. $A_{eff,g}$ and $A_{eff,A}$ are effective laser mode area inside the gain medium and effective laser mode area onto the SESAM, respectively. In the case of *Q*-switch mode locking, the pulse energy is not constant and therefore stable soliton mode locking is difficult. On the other hand, their maximum pulse energy become very large, which tends to make a significant damage on the SESAM. The available saturable absorption depth ΔR of the SESAM is also limited by increasing nonsaturable loss. From above points, the available modulation depth of SESAM is limited so far. For further large modulation depth (further short pulse operation) Kerr-lens mode locking becomes powerful tool.

2.4 Kerr-lens mode locking

In case of the fast saturable absorber mode locking, Kerr-lens mode locking (KLM) became the most popular method. In 1991, Spence reported the first KLM [18,19]. At first, the mechanism of KLM was not clear and was called “magic mode locking”. The mechanism was understood that it is caused by self-focusing effect via Kerr nonlinearlity (Kerr-lens) [12]. The KLM is classified to fast saturable absorber, but there is no real saturable absorber. It is sustained by an intensity depending self-focusing effect caused by Kerr nonlinearity with a femtosecond scale response time. Due to the effect, the KLM laser cavity shows intensity dependent gain or loss modulation effect as in a saturable absorber mode locking and therefore it called fast saturable absorber. There is two type KLM: one is called “Hard aperture KLM” and another is called “soft aperture KLM” (Fig.2.7). In case of the hard aperture KLM (Fig.2.7 (a)), an aperture element such as pinhole or slit is inserted in the cavity. We consider here in case of the pinhole. When a pinhole is inserted in the cavity, its transmittance can be written as

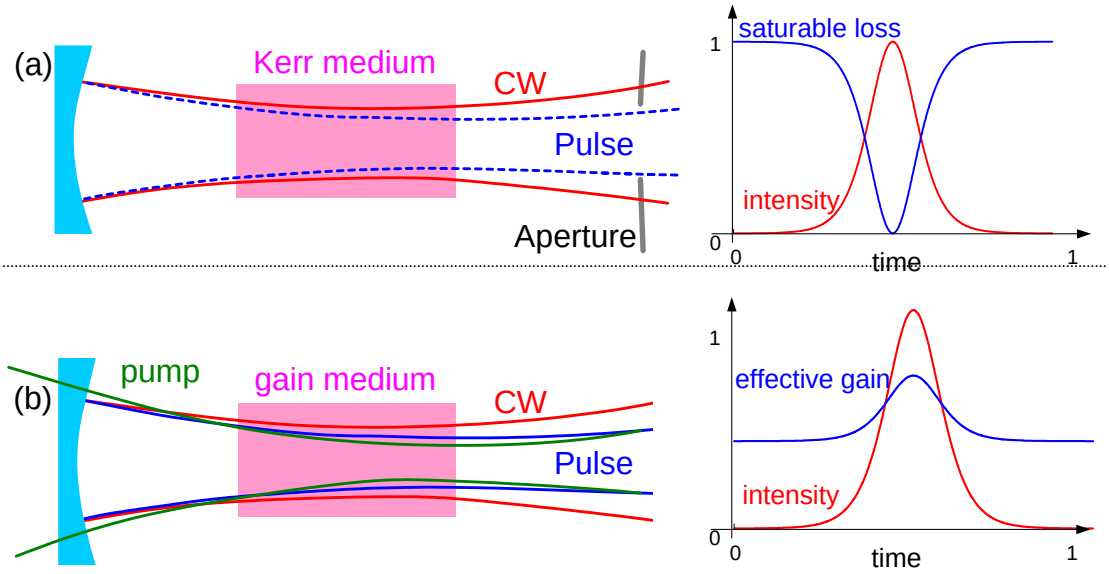

Fig. 2. 7. Schematic pictures of KLM are shown. (a) Hard aperture KLM and (b) soft aperture KLM.

$$T_{pinhole} = \frac{\int_0^{2\pi}\int_0^{a_p} S_l(r,\theta,z_0)drd\theta}{\int_0^{2\pi}\int_0^{\infty} S_l(r,\theta,z_0)drd\theta} \qquad 2.5,$$

where z_0 is the position where the pinhole is inserted in, a_p is a hole radius of the pinhole, $S_l(r;\theta,z_0)$ is distribution function of the lasing photon density (see chapter 1), which depends on the laser peak intensity via self-focusing effect. Therefore the transmittance also depends on the laser peak intensity via self-focusing effect. In addition the pinhole also change beam divergence and it make additional diffraction loss. In case if the below equation is satisfied, positive loss modulation effect can be obtained.

$$\frac{dT_{pinhole}}{dI_l} > 0 \qquad 2.6,$$

where I_l is laser peak intensity. Without the proper cavity configuration the modulation become negative and KLM operation never obtained. The magnitude of the hard aperture Kerr-lens effect strongly depends on the cavity configuration and it also need severe alignment. The hard aperture KLM is sustained by a nonlinear intensity depending internal loss modulation.

In case of the soft aperture KLM (Fig.2.7 (b)), although there is no additional aperture inside the cavity, the pumping light mode profile make virtual aperture (soft aperture) inside the gain medium. Let us consider two-dimensional model (r and θ perpendicular to the optical axis z) here for a simplification. We also assume a singe transverse mode operation (in case of the mode-locked operation, the laser generally becomes single transverse mode. A multi-transverse mode leads to slightly different longitudinal mode period in each mode, which obstructs mode-locked operation). The total magnitude of the stimulated emission inside the gain medium η_{ts} can be written below

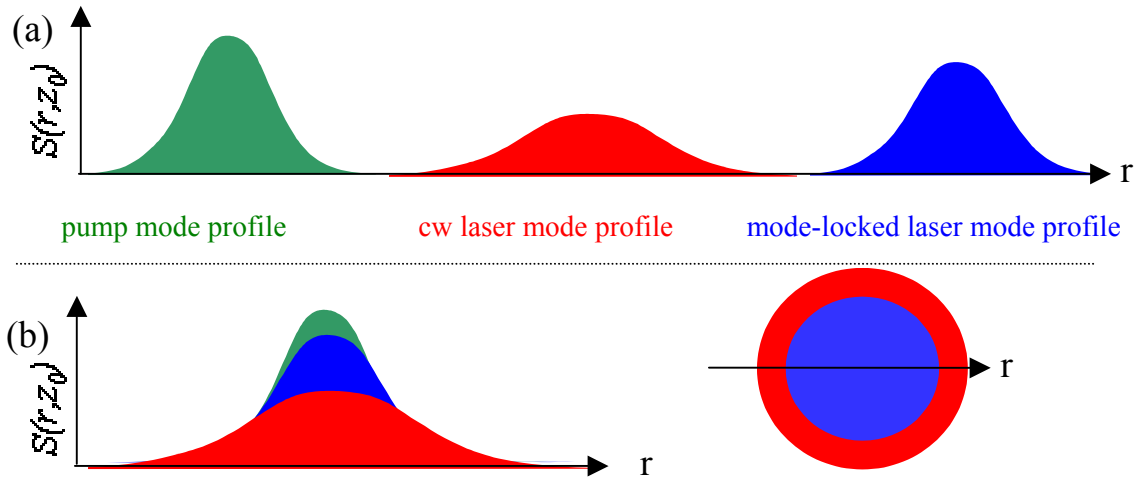

Fig.2.8 Scamatic picture of laser mode profiles in soft aperture KLM. (a) Side views of laser mode profiles in each mode are shown. (b) Side view (left side) and top view (right side) of overlapped laser modes profiles are shown.

$$\eta_{ts} = \int_0^{2\pi} \int_0^{\infty} cS(r, z_0) N_u(r, z_0) \sigma_e(\lambda_e) dr d\theta \qquad 2.\ 7.$$

The laser-mode cross sections at the gain medium in soft aperture KLM are shown in Fig. 2.8. In the case of soft aperture KLM, mode matching between the pump mode and mode-locked laser mode become better than that of cw laser mode, which effectively increases gain. The better mode matching also decreases diffraction loss. The pump mode having narrower spatial profile than its cavity mode can be considered as the gain medium having narrower gain bandwidth than amplified pulse's spectral bandwidth. For further simplification, we assume top-hut laser and pump mode profiles. We also use intra cavity pump power P_p and laser power $P_l(w_l, w_p)$ where w_l and w_p is laser mode radius and pumping mode radius, respectively. In case of the soft aperture KLM, the w_l is setted to be larger than the w_p. For roughly estimation $S(r, z_0)$ can be written as

$$S(r, z_0) = \frac{P_l(w_l, w_p)}{c\pi w_l^2} = \frac{\eta_e P_p}{c\pi w_l^2} \qquad w_l \geq w_p \qquad 2.\ 8,$$

where η_e is local point extraction efficiency. Then the total photon number

contributing to the stimulated emission inside the gain medium N_{ts} can be written as

$$N_{ts} = \int_0^{2\pi}\int_0^{w_p} S(r,\theta,z_0)drd\theta$$
$$= \eta_e P_p \left(\frac{w_p}{w_l}\right)^2 \qquad w_l \geq w_p \qquad 2.\ 9,$$

the equation 2.9 shows that the larger laser mode radius w_l leads to the smaller N_{ts}. With the combination of temporal intensity depending laser mode profile (radius) inside the gain material, the soft aperture makes intensity dependent effective gain modulation effect. In case if below equation is satisfied, positive modulation effect can be obtained.

$$\frac{dw_l}{dI_l} < 0 \quad (w_l > w_p) \qquad 2.\ 10,$$

In case if $w_l < w_p$ it decrease laser efficiency and multi-mode operation (multi transverse mode, multi-single-transverse-mode consisting of single transverse cw and mode-locked operation) tends to occur. The key to obtain soft aperture KLM is achieving a laser mode radius larger than the pump laser mode radius in cw operation and equivalent laser mode radius to the pump laser mode radius in mode-locked operation. The pumping laser beam quality is strongly important for soft aperture mode locking. Without the proper cavity configuration the Soft aperture Kerr-lens modulation effect can become negative and it restrict mode locked operation. The soft aperture Kerr-lens effect also appears in case of the hard aperture KLM and has a large influence on the mode-locked operation. One of the big difference between SESAM mode-locking and KLM is that the saturable absorption effect of SESAM depends on pulse energy, but both of hard and soft aperture KLM depends on laser intensity, which depends on not only pulse energy but also pulse duration. We suppose the differences are important to suppress multi-pulsed operation and Q-switch mode-locked instability. Additionally hard and soft aperture mode locking has difference.

The former is based on induced loss modulation and therefore front and tail of the pulses where intensity is low suffers hard aperture loss (of course it shorten the pulse.). On the other hand, the latter is based on effective gain modulation where center of the pulses feel higher gain and pulses do not suffer additional loss.
In the experiments of this thesis a SESAM was used as a mode-lock starter and soft aperture KLM effect was used for achieving large modulation depth.

As a first saturable absorber mode-locking, synchronous pumping was also reported. The gain modulation is applied by mode-locked pump source with a period corresponding to round trip time of pumped cavity. By this method sub-ps pulse duration have been obtained from dye laser [20,21]. The method, however, is needs severe alignment and mode-locked pump source so that the system is complicated and the available output power is also limited. We did not use synchronous pumping in this thesis.

References

[1] Haus, H, **"**Theory of mode locking with a slow saturable absorber,**"** IEEE J. of Quantum Electronics **11**, 736 -746 (1975).
[2] H. A. Haus, "Theory of mode locking with a fast saturable absorber," J. Appl. Phys. **46**, 3049 (1975).
[3] R. Paschotta, U. Keller, "Passive mode locking with slow saturable absorbers" Appl. Phys. B **73**, 653 (2001).
[4] E. P. Ippen, C.V. Shank, and A. Dienes, "Passive mode locking of the cw dye laser," Appl. Phys. Lett. **21**, 348 (1972).
[5] R. L. Fork, B. I. Greene, and C. V. Shank," Generation of optical pulses shorter than 0.1 psec by colliding pulse mode locking," Appl. Phys. Lett. **38**, 671 (1981).
[6] F. X. Kärtner and U. Keller, "Stabilization of solitonlike pulses with a slow saturable absorber," Opt. Lett. **20**, 16 (1995).
[7] R. L. Fork, C. H. Brito Cruz, P. C. Becker, and C. V. Shank, "Compression of optical pulses to six femtoseconds by using cubic phase compensation," Opt. Lett. **12**, 483-485 (1987).
[8] R. L. Fork, O. E. Martinez, and J. P. Gordon, "Negative dispersion using pairs of prisms," Opt. Lett. **9**, 150-152 (1984).
[9] J. Kuhl and J. Heppner, "Compression of femtosecond optical pulses with dielectric multilayer interferometers," IEEE J. Quantum Electron. **22**, 182-185, (1986).
[10] H. A. Haus, J. G. Fujimoto, and E. P. Ippen, "Structures for additive pulse mode locking," J. Opt. Soc. Am. B **8**, 2068-2076 (1991).
[11] H. A. Haus, J. G. Fujimoto, "Analytic Theory of Additive Pulse and Kerr Lens Mode Locking," IEEE J. Quantum Electron. **28**. 2086-2096 (1992).
[12] F. X. Kärtner, I. D. Jung, and U. Keller, "Soliton Mode-Locking with Saturable Absorbers," IEEE J. Sel. Top. Quantum Electron. **2**, 540 (1996).
[13] H. A. Haus, "Mode-Locking of Lasers," IEEE J. Sel. Top. Quantum Electron. **6**, 1173 (2000).
[14] R. Ell, U. Morgner, F. X. KÃÂrtner, J. G. Fujimoto, E. P. Ippen, V. Scheuer, G. Angelow, T. Tschudi, M. J. Lederer, A. Boiko, and B. Luther-Davies, "Generation of 5-fs pulses and octave-spanning spectra directly from a Ti:sapphire laser," Opt. Lett. **26**, 373-375 (2001).
[15] L. R. Brovelli, U. Keller, and T. H. Chiu, "Design and operation of antiresonant Fabry–Perot saturable semiconductor absorbers for mode-locked solid-state lasers," J. Opt. Soc. Am. B **12**, 311-322 (1995).
[16] M. J. Lederer, B. Luther-Davies, H. H. Tan, C. Jagadish, N. N. Akhmediev, and J. M. Soto-Crespo, "Multipulse operation of a Ti:sapphire laser mode locked by an ion-implanted semiconductor saturable-absorber mirror," J. Opt. Soc. Am. B **16**, 895-904 (1999).
[17] C. Hönninger, R. Paschotta, F. Morier-Genoud, M. Moser, and U. Keller, "*Q*-switching stability limits of continuous-wave passive mode locking," J. Opt. Soc. Am. B **16**, 46-56 (1999).
[18] D. E. Spence, P. N. Kean, and W Sibbett, "Sub-100 fs pulse generation from a self-modelocked titanium-sapphire laser," in *Digest of Conference on Lasers and*

Electro-Optics (Optical Society of America, Washington, D.C., 1990), paper CPDP10-1, p. 619.
[19] D. E. SPENCE, P. N. KEAN, W. SIBBETT. "60 fs pulse generation from a selfmode-locked Ti:sapphire laser," Opt. Lett. **16,** 42 (1991).
[20] J. P. Heritage and R. K. Jain, "Subpicosecond pulses from a tunable cw mode-locked dye laser," Appl. Phys. Lett. **32**, 101 (1978).
[21] N. Frigo, C. Hemenway, and H. Mahr, "Cavity-length stabilization technique for synchronously pumped mode-locked lasers," Appl. Phys. Lett. **37**, 981 (1980).

Chapter 3. Properties of Yb^{3+}-doped gain materials

Yb^{3+}-doped materials have interesting properties, which has some advantage over Nd^{3+}-ion doped materials for high power laser operations. The properties of Yb^{3+}-doped materials strongly depend on their host materials. In this chapter, first we introduce general properties of Yb^{3+}-doped material by comparing with Nd^{3+}-ion doped material. Second, comparisons of the properties with different host materials are shown. Third the measured spectroscopic properties of Yb^{3+}-doped materials used in this thesis are shown. Fourth we show the problem of Yb^{3+}-doped femtosecond laser with our previous works. Fifth we introduce a multi-gain media oscillator.

3.1 Properties of Yb^{3+} ions

Laser operations based on Yb^{3+}:CaF_2 and Yb^{3+}:$Y_3Al_5O_{12}$ (Yb:YAG) have been reported in 1967 [1] and 1974 [2], respectively. Yb^{3+}-ion doped materials have quasi-three (sometimes it called quasi-four) level laser scheme consisting of ${}^2F_{5/2} \leftrightarrow {}^2F_{7/2}$ inter manifold transition (Fig. 3.1.). Today Yb^{3+}-doped materials are recognized as gain media for highly efficient high power laser system due to their small quantum defect and high quantum efficiency [3]. They, however, had not been considered as great candidates for highly efficient high power laser operation till 1990s. Furthermore Yb^{3+}-ion doped materials were considered quite inefficient gain media by several reasons. Comparison with Nd^{3+} ions, Yb^{3+} ion has only a single

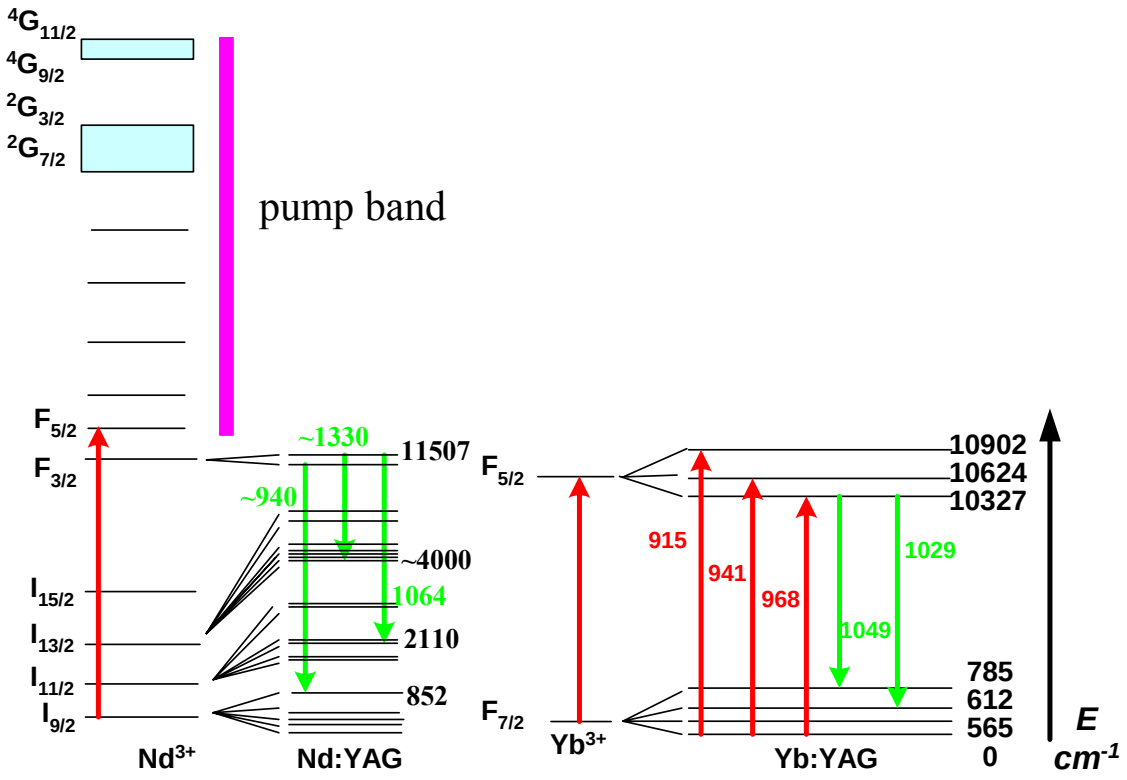

Fig. 3. 1. Energy levels of Nd:YAG and Yb:YAG.

absorption band around 940 nm and does not have any absorption band at visible range. Therefore, the available absorption efficiency with a conventional lamp pumping was strongly limited so that Nd^{3+} ion was used as sensitizing ions for Yb^{3+}-doped laser [1,2]. Yb^{3+} ion also has broader fluorescence spectrum than that of Nd^{3+} ion that leads to smaller stimulated emission cross section and increases a threshold pump power. Additionally Yb^{3+} ion has the quasi-three-level laser scheme so that its terminal level near the ground state level has thermally induced population, which leads to reabsorption loss. Especially incase of the lamp pumping, its large heat loads increase such reabsorption loss.

The situation has been strongly changed by an emergence of a high intense high power InGaAs LD emitting at a wavelength around 940 nm. Yb^{3+} ion's single absorption band around 940 nm is suitable for InGaAs LD pumping and the absence of other absorption band leads to an absence of undesirable processes such as excited state absorption and cross relaxation so that very high absorption efficiency and quantum efficiency are available by LD pumping. Furthermore when pumped by 940 nm LD, their quantum defects is less than 10 % so that highly efficient laser operation

Table 3. 1. Comparison of Nd:YAG and Yb:YAG.

Material	Nd:YAG	Yb:YAG
Lifetime τ	230 μs	950 μs
Emission cross section σ_e	2.8×10^{-19} cm^2 @ 1064 nm	2.1×10^{-20} cm^2 @ 1030 nm
Absorption cross section σ_a	≈0 @ 1064 nm	$0.1\times 10^{-20} cm^2$ @ 1030 nm
Emission bandwidth	0.6 nm	6.3~8.5 nm
$\sigma_e \times \tau$	6.44×10^{-23} s ·cm^2	1.99×10^{-23} s ·cm^2
Quantum Defect	24 % 808 nm→1064 nm	9 % 940 nm→1030 nm
Quantum effecieny	~0.6	~1
Opt-to-opt efficiency	~45%	~90%
Transparency intensity I_t	0	1.4 kW cm^{-2}

with low thermal loads is possible [4] (table 3.1, see section 1.1) and therefore they becomes quite suitable for high average power laser operation. Moreover their broad emission bands around the wavelength of 1 μm enable tunable laser operation and femtosecond laser operation. Their spectroscopic properties are strongly depends on the crystal field of the host materials. For a femtosecond laser oscillator, broad emission bandwidth, large emission cross section and less reabsorption loss are generally desirable. For a highly efficient high average power laser operation, host material's properties itself such as thermal conductivity, thermal expansion, isotropic structure and stress fracture toughens are very important. For a high average power femtosecond laser operation, gain medium satisfying both properties are desirable. To find a new material satisfying above properties, several kinds of Yb^{3+}-doped materials have been composed and their spectroscopic properties and laser operation have been investigated in the past decade [5—17] (table 3.2). They, however, generally have trade off relation ship. For instance, the glass materials have inhomogeneous broadening fluorescence spectra, but their thermal conductivities are roughly about one order lower than those of crystalline materials. The disordered materials also have broad fluorescence spectra, but the disordered structures also tend to degrade thermal and mechanical properties. In case of the Yb^{3+}-doped materials, the broad emission

Table 3. 2. Properties of remarkable materials are shown.

Host material	Thermal conductivity (W/mK)	FWHM of gain bandwidth (nm)	Emission cross section (10^{-20} cm^2)	Lifetime (μs)
YAG	10.1	8.5*	1.9	1020
KGW	3.3	25*		600
KYW	3.8	24*	3.0	600
YVO_4	12.1//c 8.9⊥c	~30	~1	250
GdCOB	2.1	44	0.35	2600
$CaGdAlO_4$	6.3//c 6.9⊥c	~70	0.75	420
BOYS	1.8	60*	0.2	1100
SYS	2.85//c 1.5⊥c	~40	0.5	1100
Phosphate Glass	0.8	35	0.05	1300

* With an assumption of β=0.5.

spectrum also has broad absorption spectrum. It read reabsorption losses and decreases the effective gain bandwidth of the gain material. The effective gain bandwidth depends on population inversion ratio β.

$$\beta = N_u / (N_u + N_l) \qquad 3.1$$

where N_u and N_l are upper and lower states Yb^{3+} ion density. The Yb^{3+}-doped gain medium having very broad gain bandwidth with great thermal and mechanical properties are sill not founded yet.

3.2 Ceramic materials

Recently the ceramic materials are well considered as gain media for high power laser systems, because they have several advantages over other solid-state laser materials. Single crystal materials have favorable thermal properties and can be used for high average power operation. However, the available crystal size is generally limited to several cm and generally could not be used for ultrahigh average power and ultrahigh peak power laser system based on large beam aperture size >10 × 10 cm^2. Glass materials have size scalability so that meter size glass material can be available. They, however, show about one-order smaller thermal conductivities than those of crystalline materials and therefore suffer large heat problem such as thermal fracture, thermal lens and so on. Consequently, due to the their size scalability, they can used for ultrahigh peak power laser system based on large beam aperture size, but the available average power (repetition rate) is strongly limited by large heat loads. Our polycrystalline ceramic materials are fabricated based on vacuum sintering and nanotechnology (VSN) method [18,19]. They are composed of innumerable grains only with few ppm-order defects. Each grain size is less than 10-μm. The grain boundaries have a thickness of less than 1 nm, which is further small than visible laser wavelength and therefore they have grate transparency [20]. The chemical compositions of ceramics are almost the same as those of single crystals, except for little SiO_2 as a sintering stimulator. The crystal fields of the grains composing ceramic materials are the same as single crystals. Consequently they show almost the same spectroscopic properties and comparable thermal conductivities as those of single crystals. In addition, the VSN gives ceramic glass-like size scalability. In case of the YAG ceramic, as large as 1 m × 1 m × a few cm material size can be available. The ceramic materials have crystalline thermal properties with glass-like size scalability. Further more they have superior uniformity and mechanical properties. In case of the YAG, Y_2O_3 and CaF_2 ceramics, they showed 3~5 times higher stress fracture toughness than those of single

Table 3. 3. Comparison of fracture toughness

	Ceramic					Single crystal		
Material	YAG	Nd^{3+}: YAG	Y_2O_3	Lu_2O_3	CaF_2	YAG	Y_2O_3	CaF_2
Knoop hardness (Gpa)	16.0	15.0	10	12.5	260 (micro hardness)	14.5	7.6	200 (micro hardness)
Fracture toughness (Mpa)	8.7	5.2	2.5	4.1	4.7	1.8	1	1.5

crystals (table 3.3) [21,22,23]. The fracture toughness, however, depend on ceramic quality so that poor quality ceramics (large impurity and defect, surface polish, average grain size and its size homogeneity) may show lower fracture toughness. The scattering coefficients of YAG ceramics were also measured and were smaller than that of single crystal [24]. One of the reasons of lower scattering loss of ceramic is that in case of the single crystal, some defect and/or internal stress tends to be made during a growing process (increasing its size), but innumerable grains of ceramic are very small and could be considered as an aggregate of perfect small single crystals. In addition, their defects and impurities at grain boundaries were smaller than visible laser wavelength.

Additionally, fabrication process based on sintering enables to make some unique materials such as sesquioxide materials and disordered material that have some difficulty to be fabricated in single crystal. The sintering process also gives another advantage that the composite ceramic material can be available. Their bonding is easier than the optical contact and important for many applications [25]. One of the disadvantages of ceramic materials is solarization problem, which is induced by irradiation of ultraviolet light and probably caused by little SiO_2 stimulator. The solarization becomes problem when a flash lamp is used as a pump source and a generally UV cut filter is used to avoid it [26]. In the case of LD pumping the solarization does not make problem.

The ceramic materials enable ultrahigh peak, ultrahigh average power laser systems due to its size scalability, superior fracture toughness and favorable thermal properties.

3.3 Sesquioxide materials

Yb^{3+}-ion doped rare earth sesquioxide materials (Yb^{3+}:Re_2O_3, Re = rare earth ion: Y,Lu,Sc) are recognized as promising candidates for high power femtosecond laser since they have high thermal conductivities, good mechanical toughness and relative broad fluorescence spectra with small reabsorption loss. Additionally they have isotropic structure and therefore do not suffer anisotropy problems. Fabrication of laser grade sesquioxide material by conventional Czochralski method, however, is difficult due to their high melting points of above 2400 C^o. In the last decade, a heat exchanger method using a high-purity rhenium crucible and VSN method enable fabrication of laser grade sesquioxide single crystals [27,28] and ceramics [29,30], respectively. In this thesis, three kinds of Yb^{3+}-ion doped sesquioxide ceramics: Y_2O_3, Lu_2O_3 and Sc_2O_3 and two kinds of Yb^{3+}-ion doped sesquioxide single crystals: Lu_2O_3 and Sc_2O_3 were used. Their absorption cross sections and stimulated emission cross sections are shown below. Absorption cross sections were calculated by divining a measured absorption coefficient α (λ) by a doping Yb^{3+} ion density N.

$$\sigma_a(\lambda) = \frac{\alpha(\lambda)}{N} \qquad 3.2,$$

Yb^{3+} ion has only one transition route ($F_{5/2} \leftrightarrow F_{7/2}$) so that the emission cross section can be calculated with a measured upper state lifetime and emission spectrum as follows [31].

$$\sigma(\nu) = \frac{\lambda^2}{8\pi c n^2 \tau} \frac{I(\nu)}{\int I(\nu) d\nu} = \frac{\lambda^4}{8\pi c n^2 \tau} \frac{I(\lambda)}{\int I(\lambda) d\lambda} \qquad 3.3,$$

where $I(\nu)$ and $I(\lambda)$ are measured emission spectra shapes and n is

refractive index. We used low Yb^{3+} concentration materials in spectroscopic measurements to avoid influence of reabsorption and assume that the measured lifetimes were not strongly affected by nonradiative transition process and radiation trapping effect [32].

$$\frac{1}{\tau} = \frac{1}{\tau_{radiative}} + \frac{1}{\tau_{nonradiative}} \approx \frac{1}{\tau_{radiative}} \qquad 3.4,$$

The measured spectra, however, still include some reabsorption effect. Especially, emission cross sections near the absorption peak have some uncertainty. We have measured the spectra both of ceramic and single crystal materials and not much difference was observed. Experimental uncertainty caused by such reabsorption effect is larger than the intrinsic difference (Fig.3.2) and therefore we do not mention the difference between cross sections of ceramics and those of single crystals in this thesis.

In case of the Yb^{3+} ions, emission and absorption cross sections were effectively expressed with taking account for a thermally distributed population in the inter manifolds. The absorption and emission cross sections have a temperature depending relationship [33]

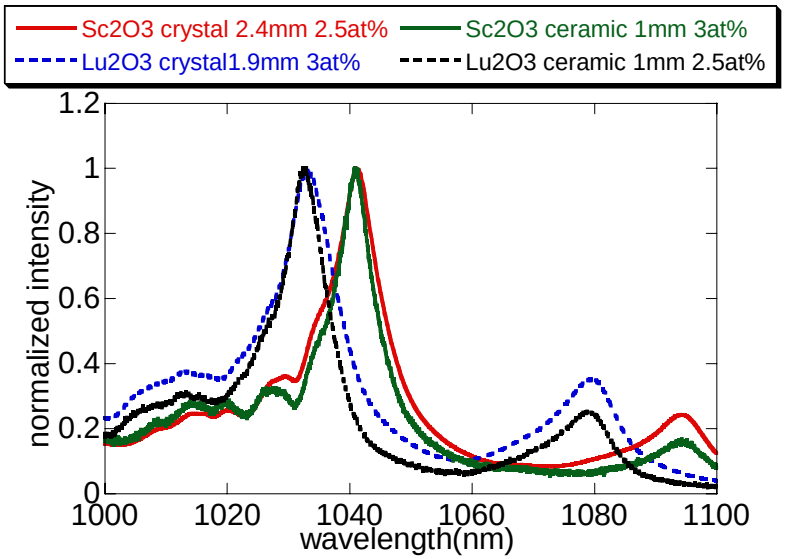

Fig. 3. 2. Fluorescence spectra of Yb:sesquioxides ceramics and single crystals.

$$\sigma_e(\nu)Z_u = \sigma_a(\nu)Z_l \exp\left(\frac{E_u - E_l - h\nu}{kT(x,y,z)}\right) \qquad 3.\ 5,$$

where Z_u and Z_l are total population in an upper level $F_{5/2}$ and lower level $F_{7/2}$, E_u and E_l are energies of inter manifolds state in upper and lower level. This relation ship can be used to estimate temperature dependence of absorption cross section.

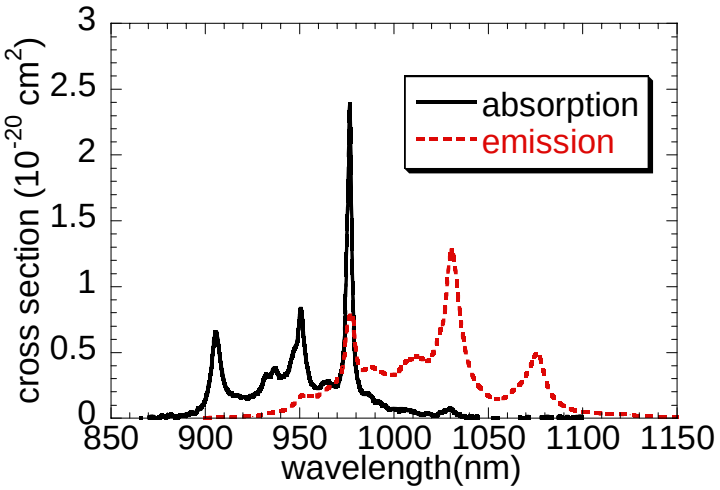

Fig. 3. 3. Emission and absorption cross section of Yb:Y_2O_3 ceramic (1.8 at.%, 1.5 mm plate) are shown. The solid black curve and dashed red curve shows emission cross-section and absorption cross section, respectively.

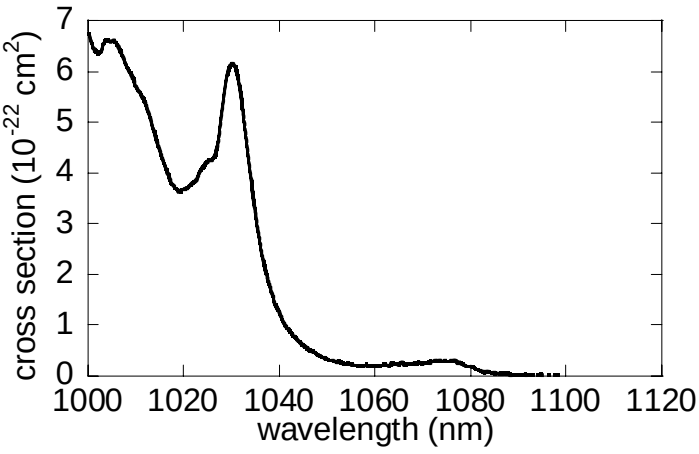

Fig. 3. 4. Absorption cross section of Yb:Y_2O_3 ceramic (10 at.% 2 mm plate) is shown.

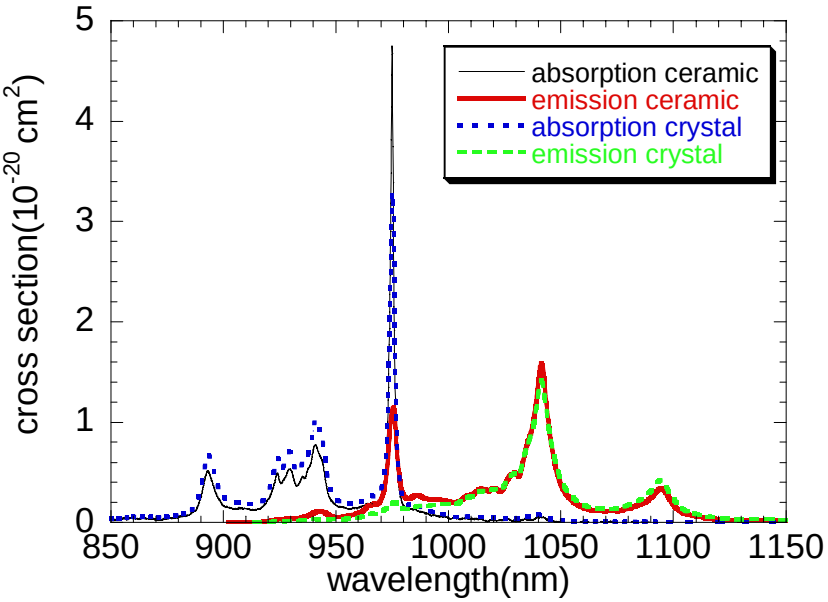

Fig. 3. 5. Emission and absorption cross sections of Yb:Sc_2O_3 are shown. Ceramic(2.5 at.% 1mm thick plate), Crystal (2.5 at.%, 2.4 mm thick plate).

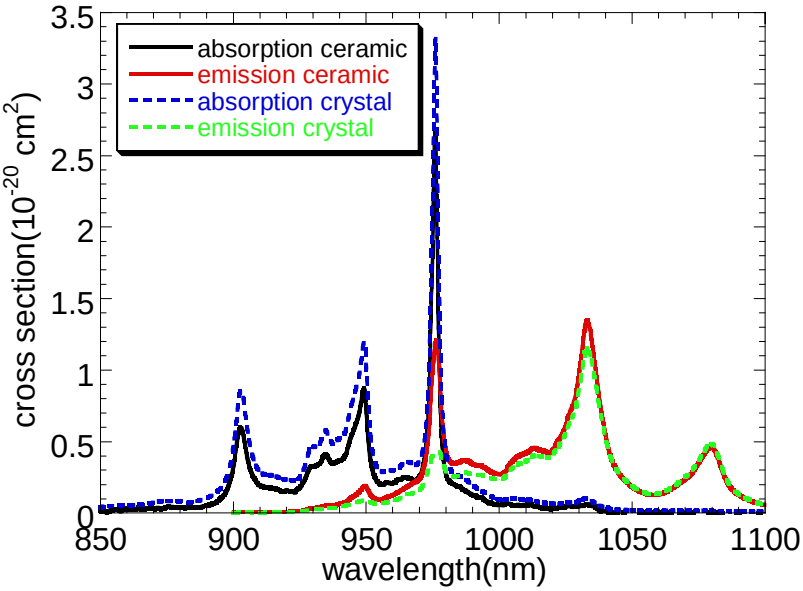

Fig. 3. 6. Emission and absorption cross sections of Yb:Lu_2O_3 are shown. . Ceramic (3 at.%, 1mm thick plate), Crystal (3 at.%, 1.9 mm thick plate).

In the table 3.4, the properties of sesquioxide materials are shown. Comparison with Yb:YAG, Yb^{3+}-doped sesquioxide materials have comparable thermal properties and 1.5~2 times broader fluorescence spectral bandwidths. They also have a high nonlinear refractive induces ($\gamma = 4.19 \times 10^{-3} \times n_2 / n_0$ [34]), which enable to induce large nonlinear effect such as Kerr-lens effect.

In the case of Yb^{3+}-doped materials, the thermally induced population at the terminal laser level makes the reabsorption, which increases the threshold of lasing at shorter wavelength peak. Consequently the lasing wavelength depends on cavity's Q parameter. In case of the Yb^{3+}-doped sesquioxide materials, they also tend to lase at longer wavelength side with high Q cavity.

Table 3. 4. Properties of Yb-doped sesquioxide materials

Host material	Y_2O_3	Lu_2O_3	Sc_2O_3
Melting points (C^o)	2430	2450	2430
**Thermal conductivity k non dope (W/mK)	13.6	*12.5 10.9 ± 0.6	*16.5 12.5 ± 0.6
**Thermal conductivity, [Yb ion density (10^{-20} cm^{-3})]	*7.7 [7.22]	*11.0 [7.69]	*6.6 [9.45]
FWHM of fluorescence spectrum(nm) [λ_{center} (nm)]	15 [1031] 16 [1076]	13 [1032] 15 [1080]	11[1041] 17 [1094]
Transform limited pulse duration (fs)	74 [1031] 76 [1076]	86 [1032] 82 [1080]	99 [1041] 74 [1094]
Emission cross section (10^{-20} cm^2) [λ_{center} (nm)]	1.28 [1031] 0.49 [1076]	1.35 [1032] 0.46 [1080]	1.59 [1041] 0.34 [1094]
Absorption cross section (10^{-20} cm^2) [λ_{center} (nm)]	3.5 [976] 0.061[1031]	3.3 [976] 0.066 [1032]	3.3 [975] 0.068 [1041]
FWHM of absorption spectrum (nm) [λ_{center} (nm)]	2 [976]	2 [976]	1.8[975]
Refractive index [λ (nm)]	1.893 [1031]	1.91 [1032]	1.96 [1041]
Nonlinear refractive index γ(10^{-13}esu)	5.79±1.45	3.96±1.77	5.32±1.33
Lifetime (μs)	~820	~820	~800

*crystals's values.

**Thermal conductivities of YAG are 10.1 at nondoping and 6.8 at almost the same Yb doping label.

3.4 Yb^{3+}:$\{YGd_2\}[Sc_2](Al_2Ga)O_{12}$ ceramic material

Disordered materials are also very interesting for ultrashort pulse laser operation due to their broad fluorescence spectral bandwidth. $\{YGd_2\}[Sc_2](Al_2Ga)O_{12}$ ceramic material is an interesting candidate for ultrashort pulse laser operation. It is a solid solution of $(Y_3Sc_2Al_3O_{12})_{0.33}$ and $(Gd_3Sc_2Al_3O_{12})_{0.66}$ that has partially disordered isotropic garnet structure (Fig. 3.7) [35]. Sc^{3+} ions occupy octahedral *a* positions. Al^{3+} and Ga^{3+} ions occupy the tetrahedral *d*-sites in the ratio of 2:1. Y^{3+} and Gd^{3+} ions occupy the dodecahedral *c*-sites (distorted cubes) in the ration of 1:2 and they are substituted by Yb^{3+} ions. In case of the single crystal it has reported in 1993 with Nd^{3+}-ion doping and succeeded in generating as short as 260 fs pulses by additive-pulse mode locking [36]. Solid solution, however, has some difficulty to be fabricated in single crystal and Yb^{3+}:$\{YGd_2\}[Sc_2](Al_2Ga)O_{12}$ single crystal has not been fabricated. Today VSN method enables to make it in ceramic with laser grade quality.

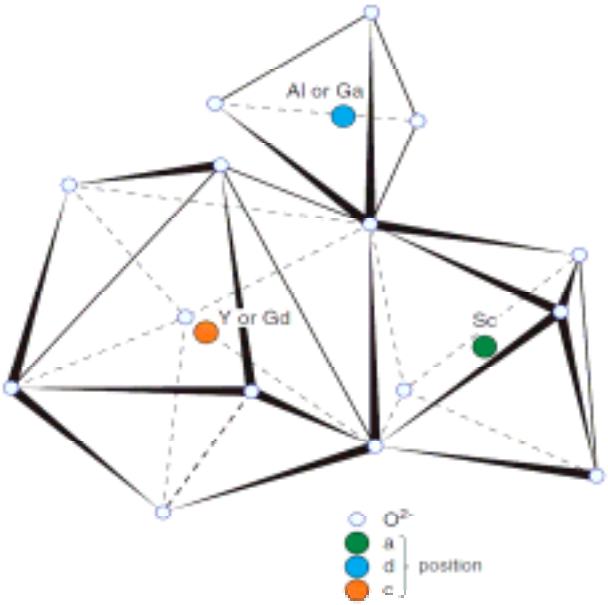

Fig. 3. 7. Motif of garnet crystal structure as applied to the $\{YGd_2\}[Sc_2](Al_2Ga)O_{12}$ ceramics with the explanation of host-cation occupations.

Comparison with Yb:YAG, it has about twice times broader florescence spectral bandwidth. The emission and absorption spectra of Yb:YAG and Yb^{3+}:{YGd_2}[Sc_2](Al_2Ga)O_{12} are shown in Fig. 3.8 and Fig. 3.9, respectively. Additionally it might have good thermo-mechanical properties due to its garnet structure similar to YAG ceramic.

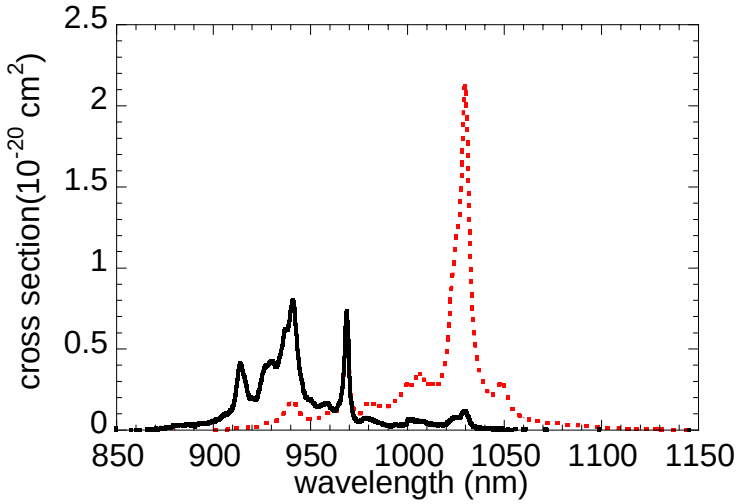

Fig. 3. 9. Emission and absorption cross section of Yb:YAG are shown. The black solid curve and red doted curves show absorption cross-section and stimulated emission cross-section.

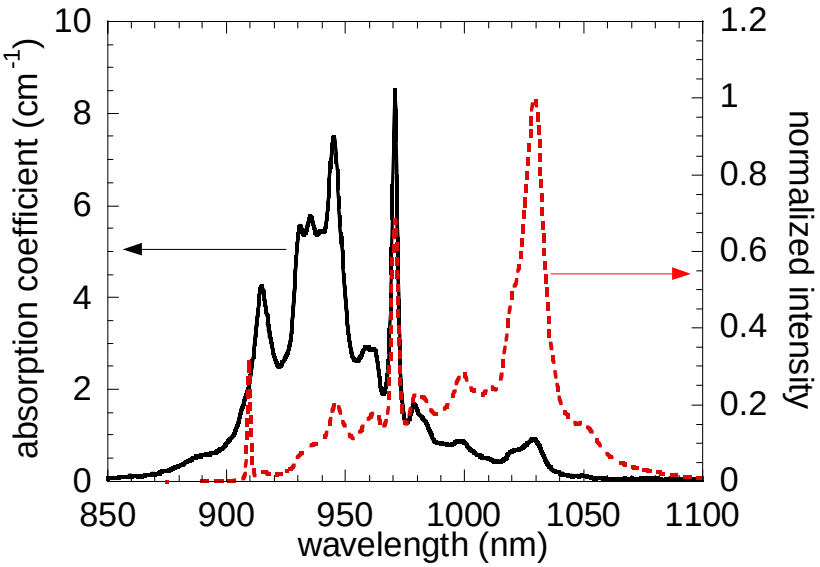

Fig. 3. 8. Absorption coefficient (10 at.% Yb^{3+}-ion doped) and emission cross section (1.9 at.% Yb^{3+}-ion doped Yb^{3+}:{YGd_2}[Sc_2](Al_2Ga)O_{12} ceramic are shown. The black solid curve is absorption and red doted curve is emission.

3.5 Previous results of SESAM mode-locked Yb^{3+}-doped sesquioxide lasers

The sesquioxide materials have superior thermal and mechanical properties and relative broad fluorescence spectra. However, the available gain bandwidths with them are narrower than those of other gain media used for ultrashort pulse (<100 fs) laser operation (e.g. glass materials, disordered materials.). Yb-doped sesquioxide mode-locked lasers based on SESAM have been already reported. In case of the single crystals, pulses as short as 220 fs and 230 fs were obtained from Yb^{3+}:Lu_2O_3 and Yb^{3+}:Sc_2O_3 single crystals, respectively [37,38]. In case of the ceramics, we have obtained pulses as short as 188 fs, 352 fs and 1 ps from Yb^{3+}:Y_2O_3, Yb^{3+}:Lu_2O_3 and Yb^{3+}:Sc_2O_3 ceramics, respectively (Fig. 3.10) [39,40]. In above SESAM mode locking, the shortest pulse duration was limited by an appearance of cw component and/or transition to the multi-pulsed operation (Fig. 3.11). In the solitary mode locking, the pulse duration obeys the solution of nonlinear Schrödinger equation (Chapter 2.2)

$$\tau_{\text{soliton}} = \frac{1.76\lambda A_{eff}}{\pi n_2 l}\frac{|D_2|}{E_p} \quad \text{: solitonlike solution in solid-state lasers.} \quad 3.\ 6,$$

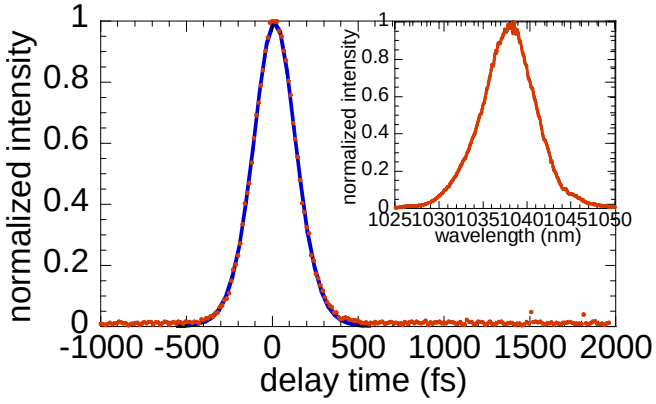

Fig. 3. 10. Autocorrelation trace and spectrum (inset) of the 188 fs mode-locked pulses. The experimental data (points) and a $sech^2$-fitting curve (solid curve) are shown.

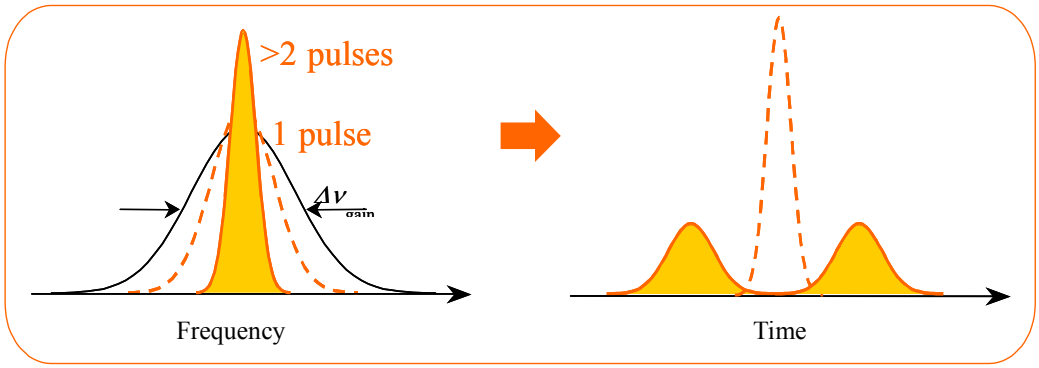

Fig. 3. 11. Schematic picture of multi-pulsing in frequency domain and time domain.

the equation 3.6 obviously shows that the larger pulse energy lead to the shorter pulse duration. The shorter pulse duration, however, needs the broader spectral bandwidth that tends to decrease the total gain (the detail discussion is shown in chapter 6). The amount of such gain decreasing strongly depends on the bandwidth of gain medium. Unless the total amount of the gain decreasing effect becomes larger than the modulation depth of SESAM (*ΔR1* of Fig. 2.3 in section 2.3), the short pulse operation without cw component can be obtained (Fig. 3.12 (a)). If the total amount of the gain decreasing become equal to the modulation depth of the SESAM, the narrow cw component appear in the spectrum (Fig. 3.12 (b)). In case of the multi-pulse operation, the pulse energy is divided each pulse and therefore the pulse duration become longer and spectral bandwidth become narrower than those in single pulse operation. Their narrower spectral bandwidth has larger gain than that of single short pulse operation. When the divided pulse energy becomes large enough for saturating most saturable loss of the SESAM, the difference of saturated loss of SESAM between single pulse and double pulsed operation become very small (*ΔR3* of Fig. 2.3 in section 2.3). If the total gain of the multi-pulse operation (narrower spectral and lower loss saturation) becomes larger than that of single pulsed operation, the double pulse (multi-pulse) operation become more suitable for the cavity.

The very interesting question is that how we can suppress such multi-pulsed operation and appearance of the cw component. By increasing the laser mode area on the SESAM, we can suppress excess saturation of the SESAM and the multi-pulse operation can be suppressed, but the

appearance of cw component can not be suppressed and it make the limitation of the shortest pulse duration. To suppress such cw component and obtain short pulse duration, a large modulation depth of SESAM is required, but such large modulation depth leads to *Q*-switching mode-locked instability and unsaturable loss (see chapter 2.3) [41]. By using high *Q* cavity (based on low loss optical component and low output coupling efficiency), short pulse also can be obtained. On the other hand, mode-locked lasers tend to have slightly large cavity losses (caused by dispersion compensation elements and saturable absorber), which make requirement of slightly large output coupling efficiency for achieving highly efficient laser operation and therefore such high *Q* cavity is suitable for neither highly efficient laser operation nor high power laser operation. Most of the previous results reporting on the sub-100 fs ultrashort pulse generation were based on a high *Q* cavity and therefore their efficiency and average power were also strongly limited. We have to overcome above problems to obtain highly efficient high power ultrashort pulse laser operation.

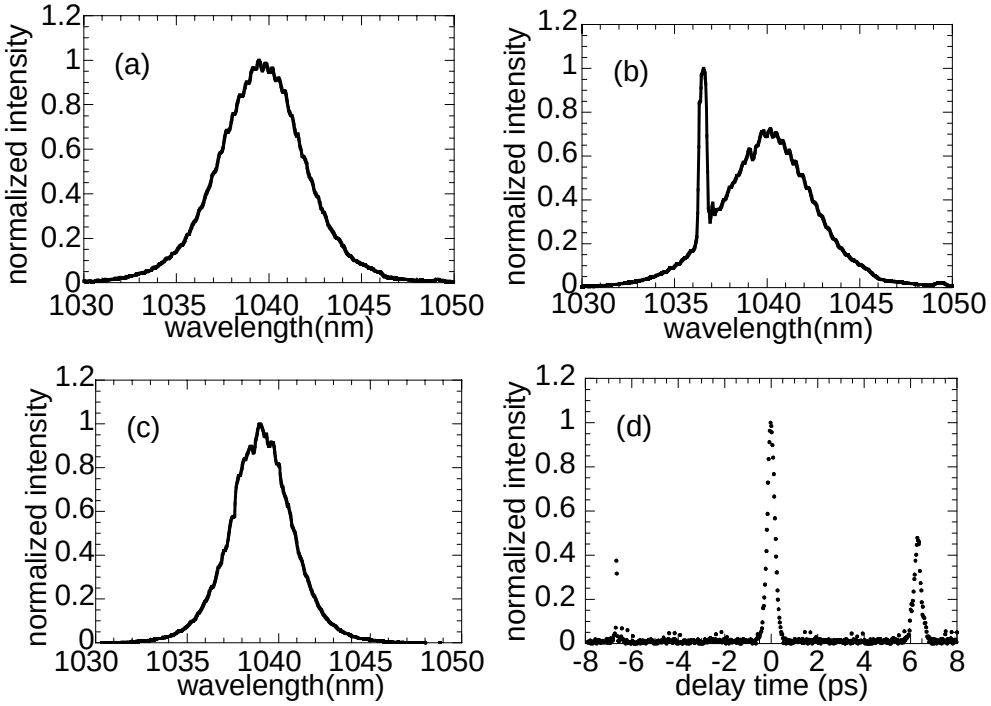

Fig. 3. 12. Spectra and autocorrelation trace of the mode-locked Yb^{3+}:Y_2O_3 ceramic laser are shown. (a) Spectrum of single pulse operation. (b) Spectrum of single pulse with narrow cw component. (c) Spectrum of multi-pulsed operation. (d) Autocorrelation trace in the multi-pulse operation.

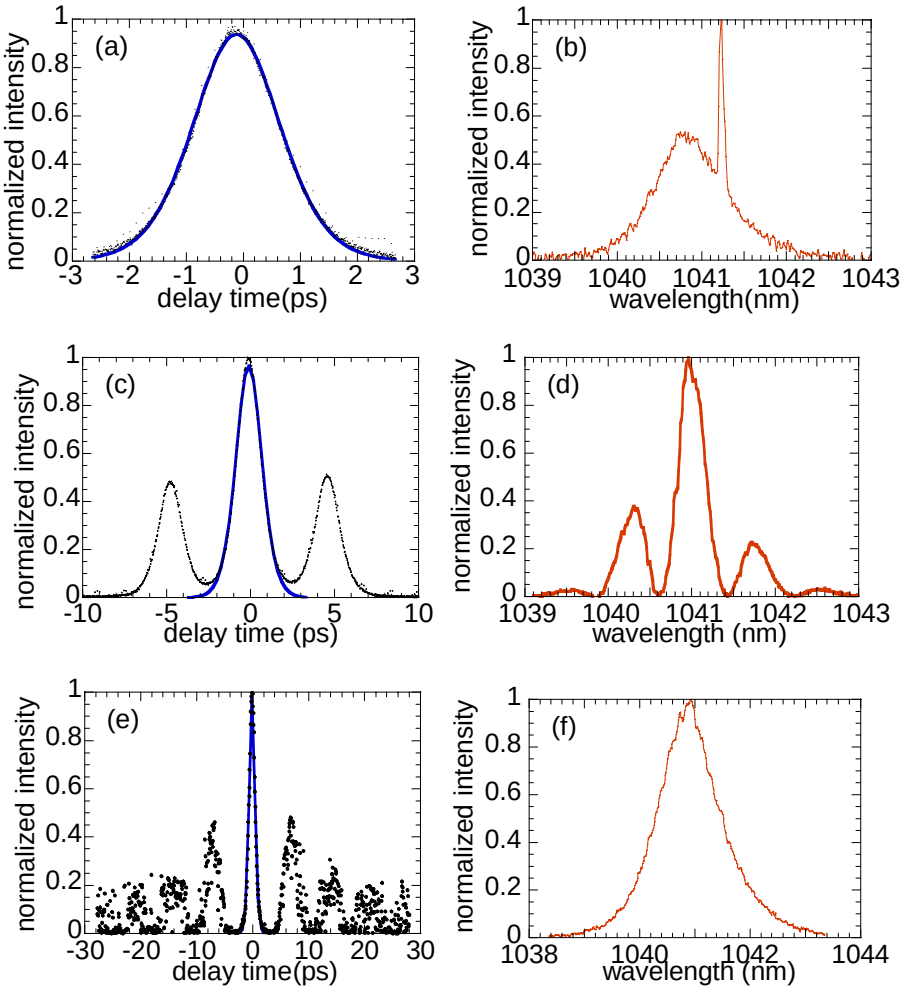

Fig. 3. 13. Spectra and autocorrelation traces of the mode-locked Yb^{3+}:Sc_2O_3 ceramic laser are shown. (a)(b) Autocorrelation trace and spectrum of single pulse operation. (c)(d) Autocorrelation trace and spectrum with narrow cw component. (e)(f) Autocorrelation trace and spectrum in multi pulsed operation (measured with slightly different experimental setup from (a)-(d)).

3.6 Multi-gain media oscillator

The simplest way to obtain much short pulse duration is to use a gain medium having broad gain bandwidth such as glass material and disordered material. Their thermal and mechanical properties, however, were generally poor and suffer large heat loads and therefore they could not be used in a high power laser operation. Seeking for a new desirable gain material having broad gain bandwidth with good thermal and mechanical properties has been important subject to achieve highly efficient high power ultrashort pulse laser operation. Beside the seeking new gain material, a multi-gain media oscillator is interesting for above purpose. The multi-gain media ultrashort pulse oscillator was demonstrated with Nd^{3+}-doped glass materials [42]. In case of the multi-gain media oscillator, different kinds of gain media having different gain spectra are used in the same cavity simultaneously. As a result of them, the total gain bandwidth become broader than each gain medium (Fig.3. 14). Furthermore it can keep the thermal and mechanical properties of each gain medium. By using it with crystalline gain materials, they show artificial glasslike inhomogeneous

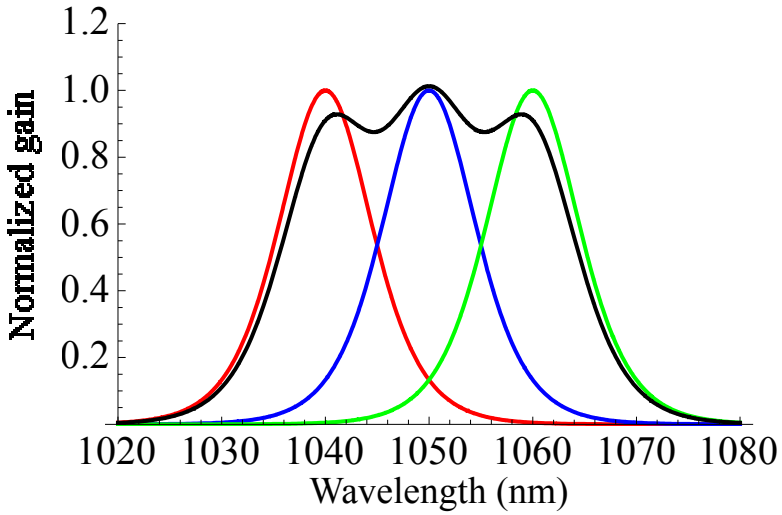

Fig. 3. 14. Schematic picture of multi-gain media is shown. Red curve, blue curve and Green curve show gain spectrum of each gain medium. Black curve shows total gain of multi-gain media

broadened gain bandwidth with crystalline thermal and mechanical properties. For instance we show here multi-gain media based on Yb^{3+}:Sc_2O_3 and Yb^{3+}:Y_2O_3, which was used in the experiment of this thesis. The effective total gain cross-section σ_g can be written below

$$\sigma_{\text{gain}} = \beta_1(1-\alpha)\sigma_{\text{e1}} - (1-\beta_1)(1-\alpha)\sigma_{\text{a1}} + \beta_2\alpha\sigma_{\text{e2}} - (1-\beta_2)\alpha\sigma_{\text{a2}} \qquad 3.7,$$

where σ_{e1}, σ_{a1}, σ_{e2} and σ_{a2} are emission and absorption cross sections of Yb^{3+}:Sc_2O_3 and Yb^{3+}:Y_2O_3, respectively. β_1 and β_2 indicate population inversion ratios of Yb^{3+}:Sc_2O_3 and Yb^{3+}:Y_2O_3, respectively. α indicates ratio of the Yb^{3+}-ion number in the Yb^{3+}:Y_2O_3 gain part against the total Yb^{3+}-ion number interacting with the laser mode. The effective total gain cross sections for different ratios α and β are shown in Fig. 3.15. Its FWHM strongly depends on the ratios α and β. With proper α and β, the FWHM around 1035 nm becomes broader than 25 nm, more than 1.5 times broader than that of Yb^{3+}:Sc_2O_3 (11.6 nm) or Yb^{3+}:Y_2O_3 (15 nm). The comparison of the multi-gain media and disorder materials is shown in table 3.5 [43,44]. The multi-gain media shows broad gain bandwidth with very high thermal conductivity, which is suitable for high average power ultrashort pulse laser operation.

Table 3.5. Comparison of multi-gain medium and disorder material

Host material	HWHM of gain bandwidth [nm]	Thermal conductivity [W/mK] (Yb doping density [10^{-20} cm^{-3}])
Y_2O_3+Sc_2O_3 multi-gain media	>20	7.7 (7.2) 6.6 (9.4)
$ScLuO_3$ disordered crystal	>20	~3.5
$(YGd_2)Sc_2(Al_2Ga)O_{12}$ partially disordered ceramic	~16	~5 [nondoped]
YAG crystal	~8.5	6.8 (5 at.%)

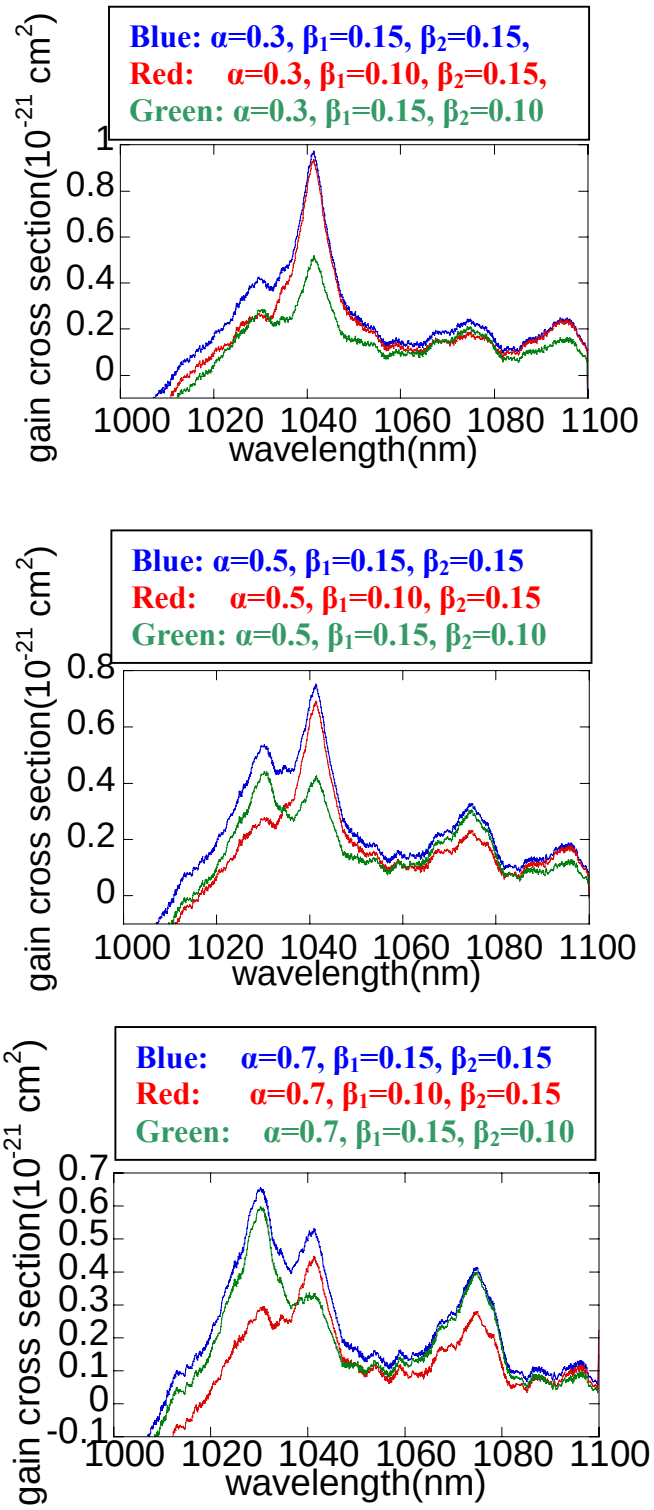

Fig. 3. 15. (a)-(c) Estimated effective total gain cross sections of the multi-gain media based on Yb^{3+}:Sc_2O_3 and Yb^{3+}:Y_2O_3. (a) for α = 0.3, (b) for α = 0.5 and (c) for α = 0.7 with different β's are shown.

References

[1] M. Robinson and C. K. Asawa, "Stimulated Emission from Nd^{3+} and Yb^{3+} in Noncubic Sites of Neodymium- and Ytterbium-Doped CaF_2," J. Appl. Phys. **38**, 4495 (1967).
[2] K h. S. Bagdasarov, G. A. Bogomolova, D. N. Vylegzhanin, A. A. Kaminskii, A. M. Kevorkov, A. G. Petrosyan, "Luminescence and stimulated emission of Yb^{3+} ions in aluminum garnets," Sov. Phys.-Doki **19**, 358-359 (1974).
[3] W. F. Krupke, "Ytterbium solid-state lasers-the first decade," IEEE J. Sel. Top. Quantum Electron. **6**, 1287-1296 (2000).
[4] C. Hönninger, R. Paschotta, M. Graf, F. Morier-Genoud, G. Zhang, M. Moser, S. Biswal, J. Nees, A. Braun, G.A. Mourou, I. Johannsen, A. Giesen, W. Seeber, and U. Keller, "Ultrafast ytterbiumdoped bulk lasers and laser amplifiers," Appl. Phys. B, **69**, 3-17 (1999).
[5] J. Saikawa, Y. Sato, and T. Taira, "Passive mode locking of a mixed garnet $Yb:Y_3ScAl_4O_{12}$ ceramic laser," Appl. Phys. Lett. **85**, 5845 (2004).
[6] H. Liu, J. Nees, and G. Mourou, "Diode-pumped Kerr-lens mode-locked $Yb:KY(WO_4)_2$ laser," Opt. Lett. **26**, 1723-1725 (2001).
[7] F. Druon, D. N. Papadopoulos, J. Boudeile, M. Hanna, P. Georges, A. Benayad, P. Camy, J. L. Doualan, V Ménard, and R. Moncorgé, "Mode-locked operation of a diode-pumped femtosecond $Yb:SrF_2$ laser," Opt. Lett. **34**, 2354-2356 (2009).
[8] A. A. Lagatsky, V. E. Kiselb, F. Baina, C. T. A. Browna, N. V. Kuleshovb, and W. Sibbetta," Advances in femtosecond lasers having enhanced efficiencies," Proc. of SPIE **6731**, 673103, (2007).
[9] S. Rivier, A. Schmidt, C. Kränkel, R. Peters, K. Petermann, G. Huber, M. Zorn, M. Weyers, A. Klehr, G. Erbert, V. Petrov, and U. Griebner, "Ultrashort pulse $Yb:LaSc_3(BO_3)_4$ mode-locked oscillator," Opt. Express **15**, 15539-15544 (2007).
[10] F. Thibault, D. Pelenc, F. Druon, Y. Zaouter, M. Jacquemet, and P. Georges, "Efficient diode-pumped $Yb^{3+}:Y_2SiO_5$ and $Yb^{3+}:Lu_2SiO_5$ high-power femtosecond laser operation," Opt. Lett. **31**, 1555-1557, (2006).
[11] J. Boudeile, F. Druon, M. Hanna, P. Georges, Y. Zaouter, E. Cormier, J. Petit, P. Goldner, and B. Viana, "Continuous-wave and femtosecond laser operation of $Yb:CaGdAlO_4$ under high-power diode pumping," Opt. Lett. **32**, 1962-1964 (2007).
[12] U. Griebner, V. Petrov, K. Petermann, and V. Peters, "Passively mode-locked $Yb:Lu_2O_3$ laser," Opt. Express **12**, 3125-3130 (2004).
[13] V. Petrov, U. Griebner, D. Ehrt, and W. Seeber, "Femtosecond self mode locking of Yb:fluoride phosphate glass laser," Opt. Lett. **22**, 408-410 (1997).
[14] A. Chong, W. H. Renninger, and F. W. Wise, "All-normal-dispersion femtosecond fiber laser with pulse energy above 20nJ," Opt. Lett. **32**, 2408-2410 (2007).
[15] Xiangyu Zhou, Dai Yoshitomi, Yohei Kobayashi, and Kenji Torizuka, "Generation of 28-fs pulses from a mode-locked ytterbium fiber oscillator," Opt. Express **16**, 7055-7059 (2008).
[16] S. Chénais, F. Druon, F. Balembois, P. Georges, R. Gaumé, P. H. Haumesser, B. Viana, G. P. Aka, and D. Vivien, "Spectroscopy and efficient laser action from diode pumping of a new broadly tunable crystal: $Yb^{3+}:Sr_3\ Y(BO_3)_3$," J. Opt. Soc. Am. B **19**,

1083-1091 (2002).
[17] F. Druon, S. Chenais, P. Raybaut, F. Balembois, P. Georges, R. Gaume, G. Aka, B. Viana, D. Vivien, J.P. Chambaret, S. Mohr, D. Kopf, "Largely tunable diode-pumped sub-100-fs Yb:BOYS laser" Appl. Phys. B **74**, S201 (2002)
[18] T. Yanagitani, H. Yagi, and M. Ichikawa, Japanese Patent No.10-101333 (1998).
[19] T. Yanagitani, H. Yagi, and Y. Yamasaki, Japanese Patent No.10-101411 (1998).
[20] A. A. Kaminskii, S. N. Bagayev, K. Ueda, K. Takaichi, A. Shirakawa, S. N. Ivanov, E. N. Khazanov, A. V. Taranov, H. Yagi, and T. Yanagitani, "New results on characterization of highly transparent nanocrystalline C-modification Lu_2O_3 nanocrystalline ceramics: room-temperature tunable CW laser action of Yb^{3+} ions under LD-pumping and the propagation kinetics of non-equilibrium acoustic phonons," Laser Phys. Lett. **3**, 375 (2006).
[21] A. A. Kaminskii, M. Akchurin, R. Gainutdinov, K. Takaichi, A. Shirakawa, H. Yagi, T. Yanagitani, and K. Ueda, "Microharness and fracture toughness of Y_2O_3- and $Y_3Al_5O_{12}$-based nanocrystalline laser ceramics," Crystallography Report **50**, 869 (2005).
[22] O. K. Alimov, T. T. Basiev, M. E. Doroshenko, P. P. Fedorov, V. A. Konyushkin, S. V. Kouznetsov, A. N. Nakladov, V. V. Osiko, H. Jelinkova, and J. Šulc, "Spectroscopic and Oscillation Properties of Yb^{3+}Ions in BaF_2-SrF_2-CaF_2 Crystals and Ceramics," in *Advanced Solid-State Photonics*, OSA Technical Digest Series (CD) (Optical Society of America, 2009), paper **WB25**.
[23] A.A. Kaminskii, M.Sh. Akchurin, P. Becker, K. Ueda, L. Bohatý, A. Shirakawa, M. Takurakawa, K. Takaichi, H. Yagi, J. Dong, T. Yanagitani, "Mechanical and optical properties of Lu_2O_3 host-ceramics for Ln^{3+} lasants," Laser Physics Letters, **5**, 300 (2008).
[24] G. Quarles, Paper 5707-19-Photonics West 2005-January 25, (2005).
[25] H. Yagi, K. Takaichi, K. Ueda, Y. Yamasaki, T. Yanagitani and A. A. Kaminskii, "The Physical Properties of Composite YAG Ceramics," Laser Physics, **15**, 1338 (2005).
[26] H. Yagi, T. Yanagitani, K. Takaichi, K. Ueda and A. A. Kaminskii, "Characterizations and laser performances of highly transparent Nd^{3+}:$Y_3Al_5O_{12}$ laser ceramics," Opt. Materials, **29**, 1258-1262 (2007).
[27] K. Petermann, L. Fornasiero, E. Mix, V. Peters, "High melting sesquioxides: crystal growth, spectroscopy, and laser experiments," Optical Materials **19** 67-71 (2002).
[28] K. Petermann G. Huber, L. Fornasiero, S. Kuch, E. Mix, V. Peters and S.A. Basun," Rare-earth-doped sesquioxides" Jounal of Luminescence, **87-89**, 973-975, (2000).
[29] J. Lu, J. F. Bisson, K. Takaichi, T. Uematsu, A. Shirakawa, M. Musha, K. Ueda, H. Yagi, T. Yanagitani, and A. A. Kaminskii, "Yb^{3+}:Sc_2O_3 ceramic laser," Appl. Phys. Lett. **83**, 1101 (2003).
[30] K. Takaichi, H. Yagi, A. Shirakawa, K. Ueda, S. Hosokawa, T. Yanagitani and A. A. Kaminskii, "Lu_2O_3:Yb^{3+} ceramics - a novel gain material for high-power solid-state lasers," phys. stat. sol. (a) **202**, R1–R3 (2005).
[31] W. F. Krupke, M. D. Shinn, J. E. Marion, J. A. Caird, and S. E. Stokowski, "Spectroscopic, optical, and thermomechanical properties of neodymium- and

chromium-doped gadolinium scandium gallium garnet," J. Opt. Soc. Am. B **3**, 102-114 (1986).
[32] D. S. Sumida and T. Y. Fan, "Effect of radiation trapping on fluorescence lifetime and emission cross section measurements in solid-state laser media," Opt. Lett. **19**, 1343-1345 (1994).
[33] L. D. DeLoach, S. A. Payne, L. L. Chase, L. K. Smith, W. L. Kway, and W. F. Krupke, "Evaluation of absorption and emission properties of Yb^{3+}-doped crystals for laser applications," IEEE J. Quantum Electron. **29**, pp. 1179-1191, (1993).
[34] W. Koechner, "Solid-State Laser Engineering 6^{th} version," Springer (2006).
[35] A.A. Kaminskii, S.N. Bagaev, K. Ueda, H. Yagi, H.J. Eichler, A. Shirakawa, M. Tokurakawa, H. Rhee, K. Takaichi, T. Yanagitani, "Nonlinear-laser $\chi^{(3)}$-effects in novel garnet-type fine-grained ceramic-host $\{YGd_2\}[Sc_2](Al_2Ga)O_{12}$ for Ln^{3+} lasants" Laser Phys. Lett. **6**, 671 (2009).
[36] E. Sorokin, M. H. Ober, I. Sorokina, E. Wintner, A. J. Schmidt, A. I. Zagumennyi, G. B. Loutts, E. W. Zharikov, and I. A. Shcherbakov, "Femtosecond solid-state lasers using Nd^{3+}-doped mixed scandium garnets," J. Opt. Soc. Am. B **10**, 1436-1442 (1993).
[37] U. Griebner, V. Petrov, K. Petermann, and V. Peters, "Passively mode-locked $Yb:Lu_2O_3$ laser," Opt. Express **12**, 3125-3130 (2004).
[38] Peter Klopp, Valentin Petrov, Uwe Griebner, Klaus Petermann, Volker Peters, and Götz Erbert, "Highly efficient mode-locked $Yb:Sc_2O_3$ laser," Opt. Lett. **29**, 391-393 (2004).
[39] M. Tokurakawa, K. Takaichi, A. Shirakawa, K. Ueda, H. Yagi, T. Yanagitani and A. A. Kaminskii, "Diode-pumped 188-fs mode-locked $Yb^{3+}:Y_2O_3$ ceramic laser," Appl. Phys. Lett. Vol.**90**, 071101 (2007).
[40] M. Tokurakawa, K. Takaichi, A. Shirakawa, K. Ueda, H. Yagi, S. Hosokawa, T. Yanagitani and A. A. Kaminskii, "Diode-pumped mode-locked $Yb^{3+}:Lu_2O_3$ ceramic laser," Opt. Express, Vol.**14**, 12832-12838 (2006).
[41] C. Hönninger, R. Paschotta, F. Morier-Genoud, M. Moser, and U. Keller, "*Q*-switching stability limits of continuous-wave passive mode locking," J. Opt. Soc. Am. B **16**, 46-56 (1999).
[42] S. Han, W. Lu, B. Y. Sheh, L. Yan, M. Wraback, H. Shen, J. Pamulapati, and P. G. Newman, "Generation of sub-40 fs pulses from a mode-locked dual-gain-medis Nd:glass laser," Appl. Phys. B **74**, s177–s179 (2002).
[43] A. Schmidt, V. Petrov, U. Griebner, R. Peters, K. Petermann, G. Huber, C. Fiebig, K. Paschke, and G.Erbert, "Diode-pumped mode-locked $Yb:LuScO_3$ single crystal laser with 74 fs pulse duration," Opt. Lett. **35**, 511-513 (2010).
[44] H. Okada, H. Kiriyama, M. Tanaka, Y. Ochi, Y. Nakai,A. Sugiyama, H. Daido, T. Yanagitani, H. Yagi, "Development of broadband mixed Nd doped laser ceramics," in proceeding of Japan Society of Appl. Phys. 70th Autumn meeting **10p-V-2** (2009).

Chapter 4. Cavity design

All the experiments in this thesis were carried out with a Z-shaped astigmatically compensated (controlled) cavity as shown in Fig.4.1. To optimize the cavity for many purposes (*e.g.* to keep stable cavity condition, to achieve highly efficient laser operation, to suppress excess saturation of SESAM and to obtain large Kerr-lens effect.), we have to understand the laser mode radius inside the cavity. The pump laser mode profile at the focusing point was measured by image transfer system with a CCD camera. The divergence of pump laser beam can be measured and estimated with beam quality value M^2. To calculate the laser mode radius inside the cavity, we consider a model cavity as shown in Fig. 4.2. The cavity was divided to 100 μm segments along the optical axis (z axis). The laser mode radii at each position (segment) were calculated by ABCD matrix with taking account for Kerr-lens effect, astigmatisms of holding mirrors and gain material arranged at Brewster angle. We assumed that the laser beam has TEM_{00} mode profile inside the cavity and the assumption agrees with

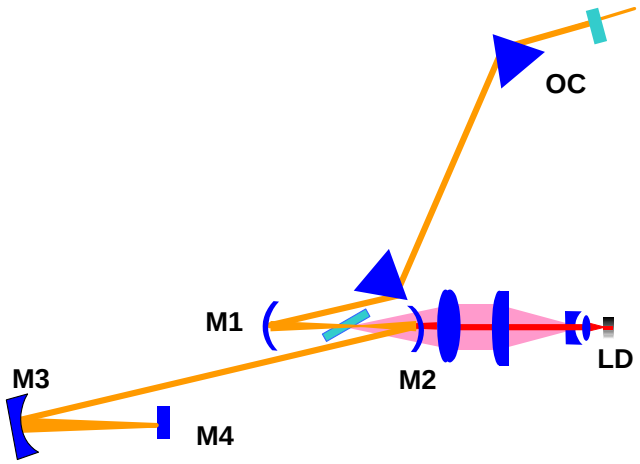

Fig. 4. 1. Schematic picture of Z-shaped astigmatically compensated cavity is shown.

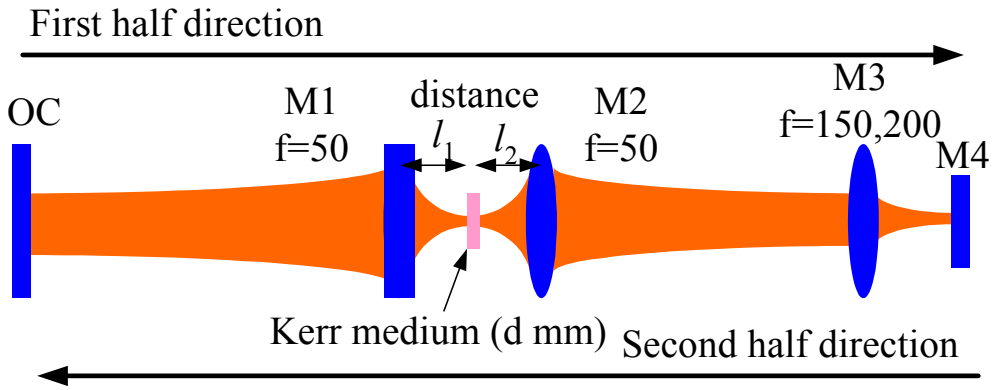

Fig. 4. 2. Model cavity used in the calculation is shown.

experimental observation. The thermal lens effect was ignored in the calculation that could make some mismatching between the calculated data and real experimental data. However, the most interesting point we would like to know from the calculation is that how large dynamic laser mode variation we can induce by Kerr-lens effect. Additionally the thermal lens effect can be considered smaller than the induced Kerr-lens effect [1] and therefore almost constant and small thermal lens effect was ignored.

4.1 Kerr-lens effect

Inside the nonlinear medium (Kerr medium), a distributed refractive index profile proportional to the incident laser mode profile is induced by Kerr nonlinearity. With spherical approximation, the profile can be expressed as [2,3]

$$n = \alpha - \frac{1}{2}\beta_{x(y)} r^2 \qquad 4.\ 1,$$

$$\alpha(z) = n_0 + n_2 I(z) \qquad 4.\ 2,$$

$$\beta_{x(y)}(z) = 2n_2 I(z) / w^2_{x(y)}(z) \qquad 4.\ 3,$$

where r is distance from optical axis z, n_0 is linear refractive index, n_2 is

nonlinear refractive index, *I(z)* is laser intensity and $w_{x(y)}(z)$ is beam radius. The ABCD matrix of Kerr medium *(Kl)* can be written as

$$Kl_{(x)y}(z) = \begin{bmatrix} \cos\sqrt{\frac{\beta_{(x)y}}{\alpha}} & \sqrt{\frac{\alpha}{\beta_{(x)y}}}\sin\sqrt{\frac{\beta_{(x)y}}{\alpha}} \\ -\sqrt{\frac{\beta_{(x)y}}{\alpha}}\sin\sqrt{\frac{\beta_{(x)y}}{\alpha}} & \cos\sqrt{\frac{\beta_{(x)y}}{\alpha}} \end{bmatrix} \qquad 4.4,$$

The Kerr-lens effect can make difference in light propagations between first half and second half directions of the cavity (see Fig. 4.2). We calculated them in both directions. At first we calculated the laser mode radii inside the cavity without Kerr-lens effect (Fig.4.3). Second we made ABCD matrix of the Kerr medium in each segment with the calculated beam radii and experimentally available data or expectable values (pulse energy and pulse duration). Third the laser mode radii inside the cavity were recalculated with Kerr-lens effect. The processes second and third were repeated with refreshed mode radii till the laser mode radii have converged.

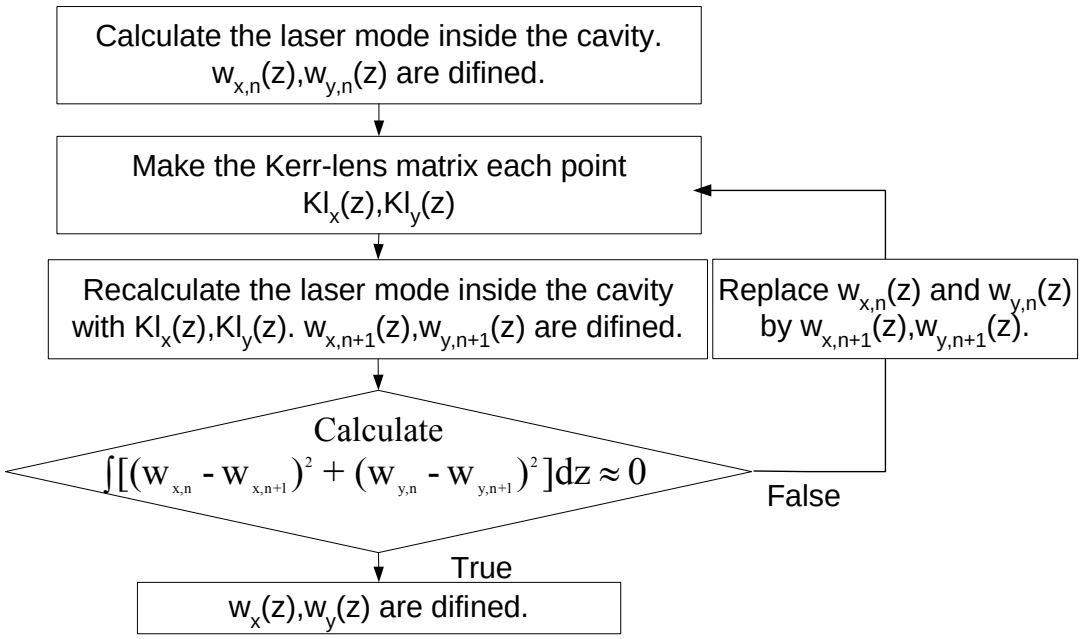

Fig. 4. 3. Flow chart of calculation of the cavity state with Kerr-lens effect.

4.2 Astigmatisms of gain medium and spherical mirror

It is well known that a gain medium (bulk material) shows astigmatism when a laser beam penetrates it with some incident angle. In the experiments of this thesis, gain media were arranged at the Brewster angles. If a gain medium has a thickness of d, its effective thickness in saggital plane and tangential plane are written below [4]

$$d_{\text{saggital}} = \frac{d\sqrt{n^2+1}}{n^2} \qquad 4.\ 5,$$

$$d_{\text{tangential}} = \frac{d\sqrt{n^2+1}}{n^4} \qquad 4.\ 6.$$

A spherical mirror also shows an astigmatism depending on an incident angle of a laser beam. If the original mirror has a focal length of f, it shows an effective focal length of $f_{\text{sagittal}} = f \times \cos\theta$ at sagittal plane and $f_{\text{tangential}} = f / \cos\theta$ at tangential plane with an incident angle of θ (Fig. 4.4). The astigmatisms of bulk medium and folding mirror can be compensated for by each other. The astigmatism compensation can be achieved when the following equation is satisfied.

$$d_{\text{sagittal}} - d_{\text{tangential}} \cong f_{\text{tangential}} - f_{\text{sagittal}} \qquad 4.\ 7,$$

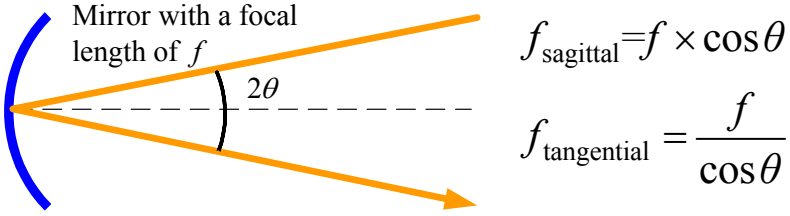

Fig. 4. 4. Astigmatism of spherical lens.

The astigmatism also appears in pump laser beam. We have to consider it when thick gain medium arranged at Brewster angle is used.

Eqs. 4.5,4.6 and 4.7 enable to calculate laser beam radii of cw laser operation based on astigmatically compensated cavity. In case of the mode-locked operation we have to consider a matrix of Kerr-lens effect (eq. 4.4). However, the Kerr-lens effect is also known to have astigmatism [5,6]. To calculate correct Kerr-lens effect of a gain material arranged at Brewster angle, we have to consider a correct laser mode profile inside the gain material in each segment so that the eqs. 4.5 and 4.6 (effective total length) cannot be applied. The eqs. 4.5 and 4.6 are caused by refractions at the material surfaces (Fig. 4.5). Due to the refraction, the physical length of the material become $d(n^2+1)^{1/2}/n$ (Fig. 4.5 (a) dotted red arrow). At the tangential plane, the laser mode radius is n times expanded at the material surface with the Brewster incident angle. By ray tracing, we also easily understand that the radius of curvatures become n times larger in saggital plane and n^3 times larger in tangential plane after the refraction (Fig. 4.5 (b), n times larger beam radius and n^2 times smaller $\Delta\theta$). The change of curvatures also can be understood from the expansion of beam radius, because the beam radius and numerical aperture angle have a relation ship of a Fourier transformation.

In the calculation, to take account for above points, we considered

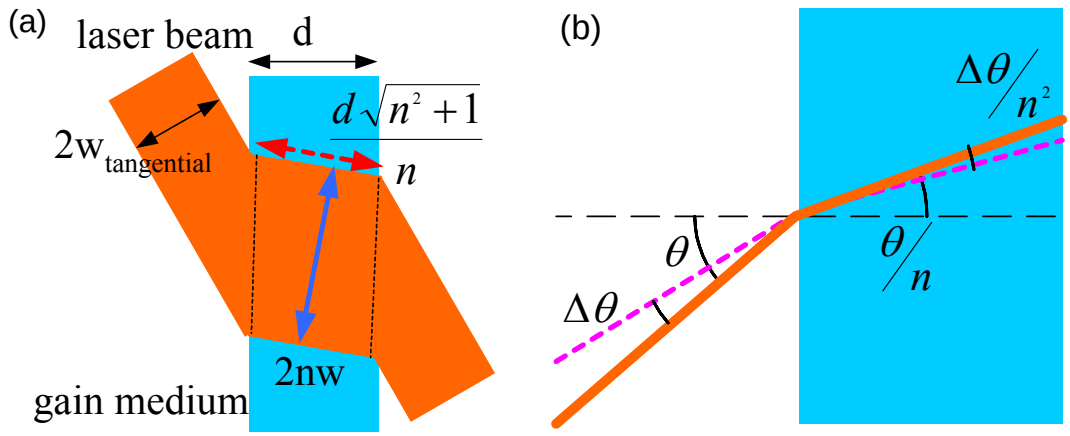

Fig. 4. 5. Astigmatisms of bulk material. (a) Refraction at Brewster angle. In tangential plane, the laser mode radius becomes n times larger after the refraction. (b) Radius of curvature becomes n tims larger in saggital plane and n^3 times larger in tangential plane after the refraction.

$(n^2+1)^{1/2}/n$ times longer material length and defined the refraction matrixes $R_{in,saggital}$, $R_{out.sagittal}$, $R_{in,tangential}$ and $R_{out,tangential}$ below

$$R_{in,saggital}=\begin{bmatrix}1 & 0\\ 0 & 1/n\end{bmatrix},\qquad R_{out.sagittal}=\begin{bmatrix}1 & 0\\ 0 & n\end{bmatrix}$$
$$R_{in,tangential}=\begin{bmatrix}n & 0\\ 0 & 1/n^2\end{bmatrix},\qquad R_{out,tangential}=\begin{bmatrix}1/n & 0\\ 0 & n^2\end{bmatrix} \qquad 4.8,$$

by the refraction effect, Kerr-lens effect inside the material become about n^2 times weaker in tangential plane due to the n times large beam radius in the tangential plane (see equation 4.4). The change of curvature inside the material, however, is about n^2 times enhanced outside the material by the refraction at the exit surface of material and therefore the total astigmatism of the Kerr-lens effect strongly depends on a situation (material length, laser intensity, nonlinear refractive index, focusing beam radius and so on.). We calculated the beam radii inside the gain material with above ABCD matrix.

4.3 Kerr-lens mode-locking with a broad-stripe LD pumping

Almost all experiments in this theses were done with a high power cheap broad-stripe laser diode pimping, which has an emitter size of about 1 × 100 μm (sagittal × tangential). Its beam quality values (M^2) are roughly about 1 at sagittal plane and 25 at tangential plane. In the experiment, the pump laser beam was focused by four beam shaping lenses and become ~25×110 μm rectangular-like beam profile (Fig.4.6). At the tangential plane, the focusing diameter is restricted due to a geometrical problem and requirement of a comparable confocal length to a crystal length (generally ~2 mm). In our experimental set up the cavity's laser mode diameter near the focusing point are about 50×50 μm (without Kerr-lens effect). The

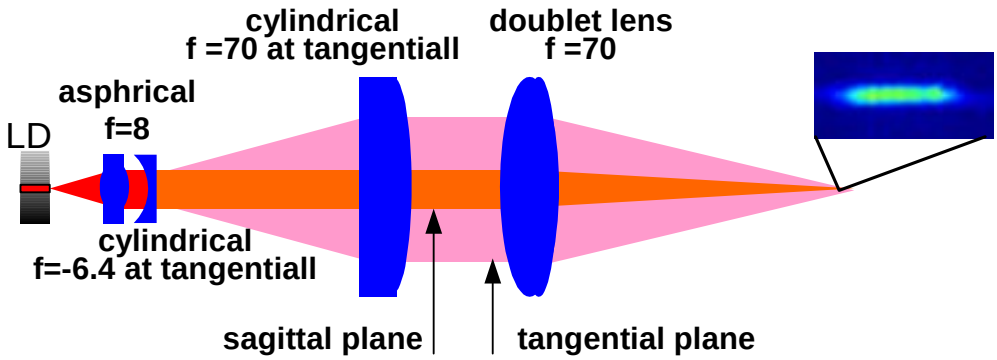

Fig. 4. 6. Schematic picture of pump beam shaping elements.

pump mode diameters are larger than the laser mode diameter at tangential plane and smaller than the laser mode diameter at sagittal plane. Therefore, the soft aperture Kerr-lens effect is not available at tangential plane. Furthermore, Kerr-lens effect (decreasing of laser mode diameter inside the gain material) at tangential plane could degrade a mode-matching factor between a laser mode and a pump mode. To obtain soft aperture Kerr-lens mode locking (KLM) with a broad-strip LD, we have to induce large soft aperture Kerr-lens effect only in saggital plane. In addition, the soft aperture Kerr-lens effect also appears in a hard aperture KLM and therefore we should suppress soft aperture Kerr-lens effect at tangential plan even if we use a hard aperture. It is well known that the Kerr-lens effect (change of laser mode diameter) can be strongly obtained in case if the cavity is aligned nearly unstable state [7,8,9]. By adjusting the astigmatisms of the cavity, we can make cavity nearly unstable at saggital plane and stable at tangential plane [10]. As a result, we can induce large soft aperture Kerr-lens effect only in saggital plane.

We show the result of calculations below. In the calculation, we assumed 2.5 mm material thickness, ~200-nJ pulse energy with ~80 fs pulse duration inside the cavity, which have been obtained in the experiment.

4.4 Calculation of laser mode radius inside the cavity

At first we show the calculated stability of the cavity. The model cavity is shown in Fig. 4.2. The cavity becomes stable when the following eq. is satisfied.

$$\left|\frac{D+A}{2}\right| \le 1 \qquad 4.9,$$

where the A and D are the elements of ABCD matrix of the cavity for one round trip. The calculated stability curves are shown in Fig.4.7. In the calculation we did not take account gain guiding effects, which may expand stable states. As can be seen in Fig. 4.7, the cavity remains a small astigmatism and stable region are slightly different in tangential and saggital planes. For the KLM operation, we would like to know how large change of the laser mode radii could be obtained by Kerr-lens effect. We have calculated them with several cavity states. To evaluate soft aperture Kerr-lens effect, we defined mode matching factor ($MMF_{x(y)}$) between pump laser modes and cavity lasing modes below.

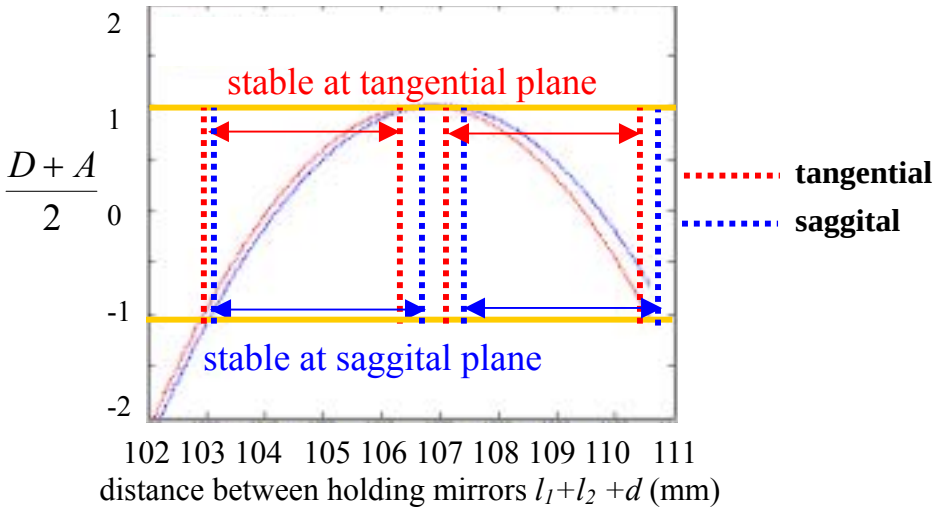

Fig. 4. 7. Calculated stability curves of a z shaped cavity.

$$MMF_{x(y)} = \frac{\int \left(w_l(z) \Big/ w_p(z) \right) dz}{d} \qquad 4.10,$$

where d is length of gain material. $w_l(z)$ and $w_p(z)$ are laser mode radius and pump mode radius. The integration is taken along the gain material.
We can optimize the cavity for MMF_x or MMF_y by slightly shifting the z-position of gain medium. We show here two calculated results, which were optimized for *MMFy* (Fig.4.8) and for *MMFx* (Fig. 4.9).
The calculated *MMFs* are also shown in Table 4.1. The subscript "cw" and "Kerr lens" indicate their operation mode. In Fig.4.8, Fig.4.9 and table 4.1, we can see large soft aperture Kerr-lens effects only at the saggital plane. The ratio of $MMF_{y\ cw}$ and $MMF_{y\ Kerr\text{-}lens}$ indicates the magnitude of the soft

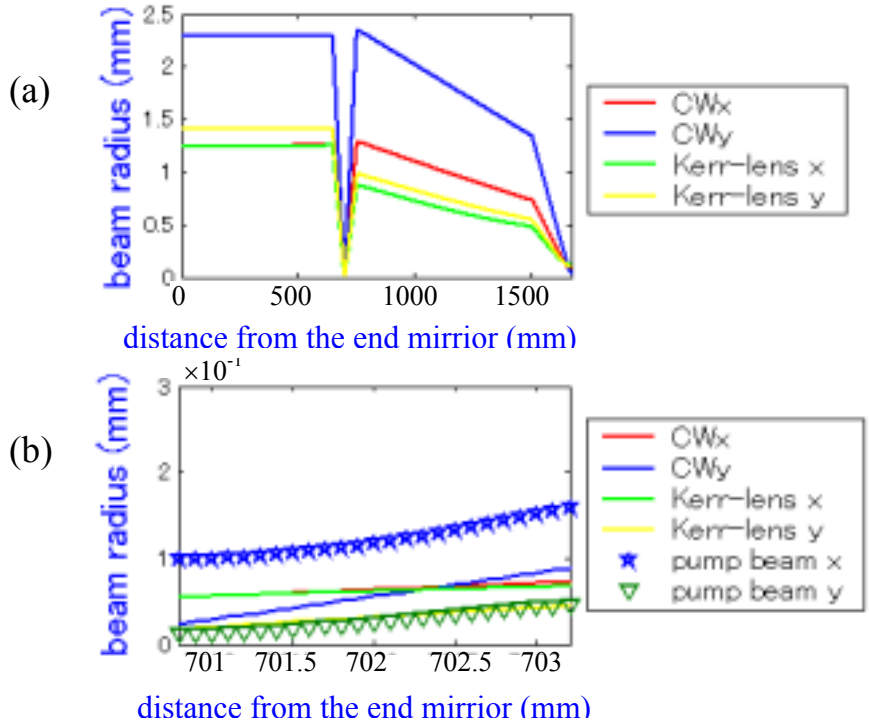

Fig. 4. 8. Calculated laser beam radii with and without the Kerr-lens effect. The characters x and y indicate tangential and saggital planes, respectively.(a) laser beam radii inside the cavity and (b) laser beam radii inside the gain material are shown. The cavity is aligned nearly unstable state (i) in Fig.4.10.

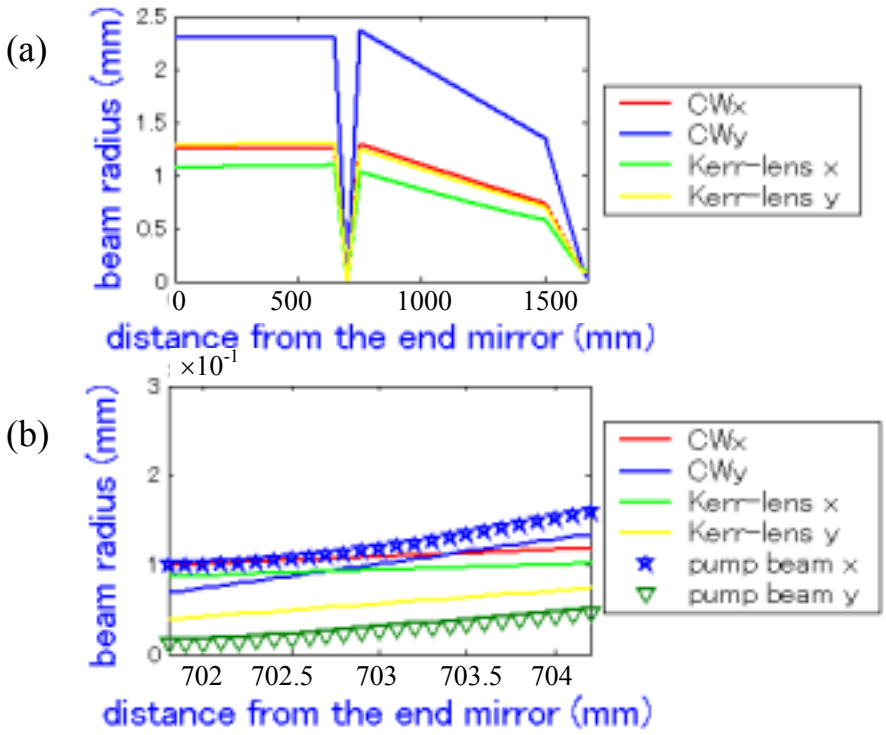

Fig. 4. 9. Calculated laser beam radii with and without the Kerr-lens effect. (a) laser beam radii inside the cavity and (b) laser beam radii inside the gain material are shown. The cavity is aligned nearly unstable state (ii) in Fig.4.10.

aperture Kerr-lens effect. In case if the laser mode diameters are larger than pump mode diameter (saggital plane in our experimental setup), the larger $MMF_{y\ cw}$ / $MMF_{y\ Kerr\text{-}lens}$ value indicates the larger soft aperture Kerr-lens effect and $MMF_{y\ cw}$ / $MMF_{y\ Kerr\text{-}lens}$ < 1 means negative soft aperture Kerr-lens effect (obstruct the short pulse operation). In case if the laser mode diameters are smaller than pump mode diameter (tangential plane in

Table 4.1 Comparison of mode matching factors in different cavity states

Cavity state	Optimized for MMF_y	Optimized for MMF_x
$MMF_{x\ Kerr\text{-}lens}$	0.536	0.810
$MMF_{x\ cw}$	0.530	0.923
$MMF_{x\ cw}$/ $MMF_{x\ Kerr\text{-}lens}$	1.01	1.14
$MMF_{y\ Ker\text{-}lens}$	1.31	2.44
$MMF_{y\ cw}$	2.24	4.34
$MMF_{y\ cw}$/ $MMF_{y\ Kerr\text{-}lens}$	1.71	1.78

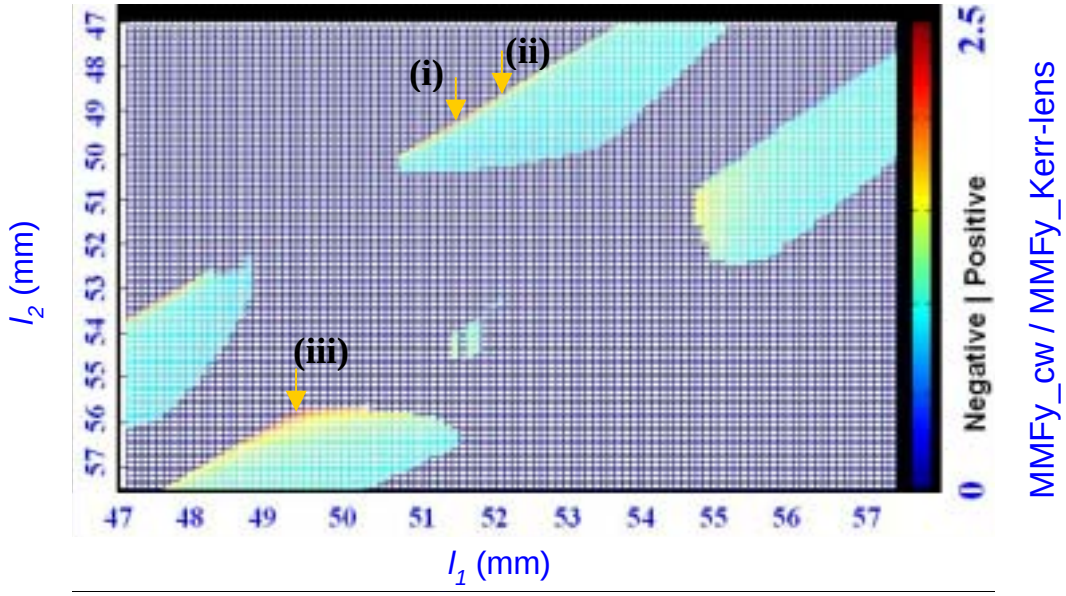

Fig. 4. 10. Two-dimensional map of soft aperture Kerr-lens effect. State (i) and (ii) indicate cavity state of Fig. 4.8 and Fig. 4.9, respectively.

our experimental setup), the smaller $MMF_{y\,cw} / MMF_{y\,Kerr\text{-}lens}$ value indicates the larger soft aperture Kerr lens effect and $MMF_{y\,cw} / MMF_{y\,Kerr\text{-}lens} > 1$ means negative soft aperture Kerr-lens effect. Fig. 4.8 and Fig.4.9 also show that due to the residual astigmatisms, the far fields laser mode profiles become elliptical only in cw operation modes.

We have also calculated the magnitude of soft aperture Kerr-lens effect at saggital plane with several l_1 and l_2 values. The two-dimensional map of soft aperture Kerr lens effect is shown in Fig. 4.10. The blank states in Fig 4.10 indicate the unstable state cavity. Fig. 4.10 obviously shows that the soft aperture Kerr-lens effect becomes large when the cavity is aligned nearly unstable state. Someone notice that near the state (iii) in Fig 4.10 is seem to have a large soft aperture Kerr-lens effect and higher stability than states (i)(ii). The calculated laser mode radii near the state (iii) are shown in Fig.4.11. The laser mode propagation profile (position on focusing points, diameter) are strongly different from states (i) and (ii). In addition the soft aperture Kerr-lens effect at tangential plane have large negative value and therefore we have done the experiment near the state (i) and (ii) in this thesis. The state (iii), however, is very interesting due to its stability. It might give us more stable cavity condition by further optimizations in future work (using hard aperture, removing M3 and SESAM and using

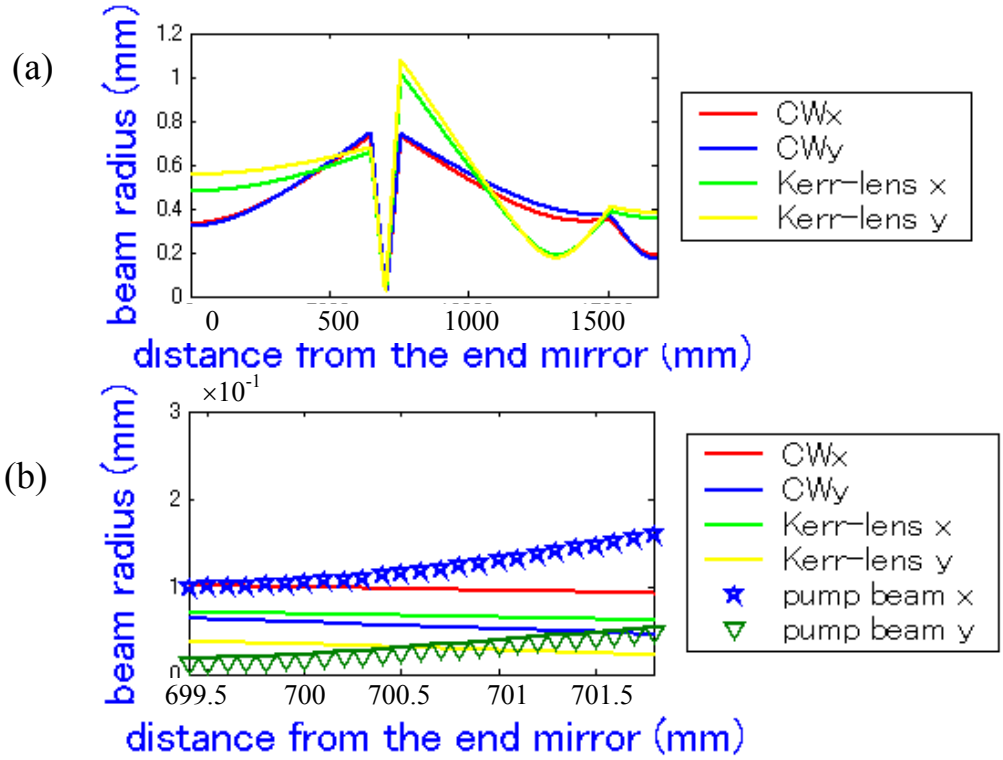

Fig. 4. 11. Calculated laser beam radii with and without the Kerr-lens effect. (a) laser beam radii inside the cavity and (b) laser beam radii inside the gain material are shown. The cavity is aligned nearly unstable state (iii) in Fig.4.10.

circular mode profile pump source, *etc.*). To obtain short pulse duration, the suppression of multi-pulsed operation is also very important (see chapter 2.3 and 3.5). We have calculated the magnitude of soft aperture Kerr-lens effect in case of the double-pulsed operation (Fig. 4.12. half pulse energy and twice pulse duration). Fig. 4.12 shows large soft aperture Kerr-lens effect even in case of the double-pulsed operation mode. The optimum points for large soft aperture Kerr-lens effect, however, are slightly different from those in single pulsed operation. To evaluate double pulse suppression effect, we have also calculated the ration of *MMFys* between single pulsed mode locked operation and double pulsed mode locked operation (Fig.4.13). Fig. 13. shows large suppression effect of double pulsed operation by soft aperture Kerr-lens effect. Probably it caused by a dependence of Kerr-lens effect not only on the pulse energy but also on the pulse duration.

From above points we have done the experiment with astigmatism controlled cavity near the unstable state to obtained large Kerr-lens effect.

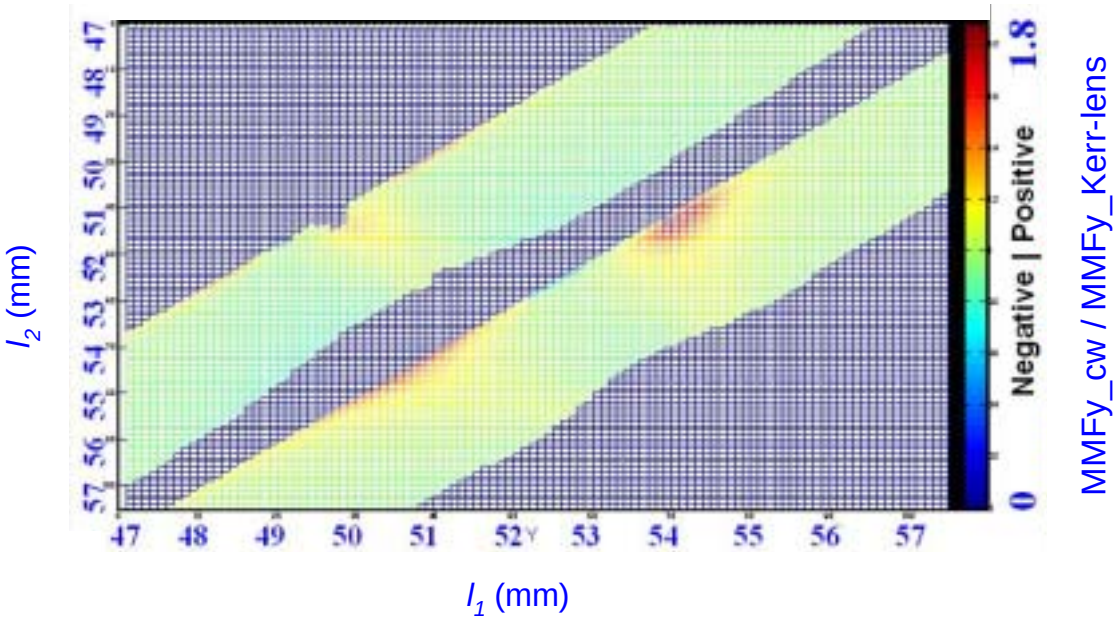

Fig. 4. 12. Two-dimensional map of soft aperture Kerr-lens effect in a double pulsed operation (assuming half pulse energy and twice pulse duration).

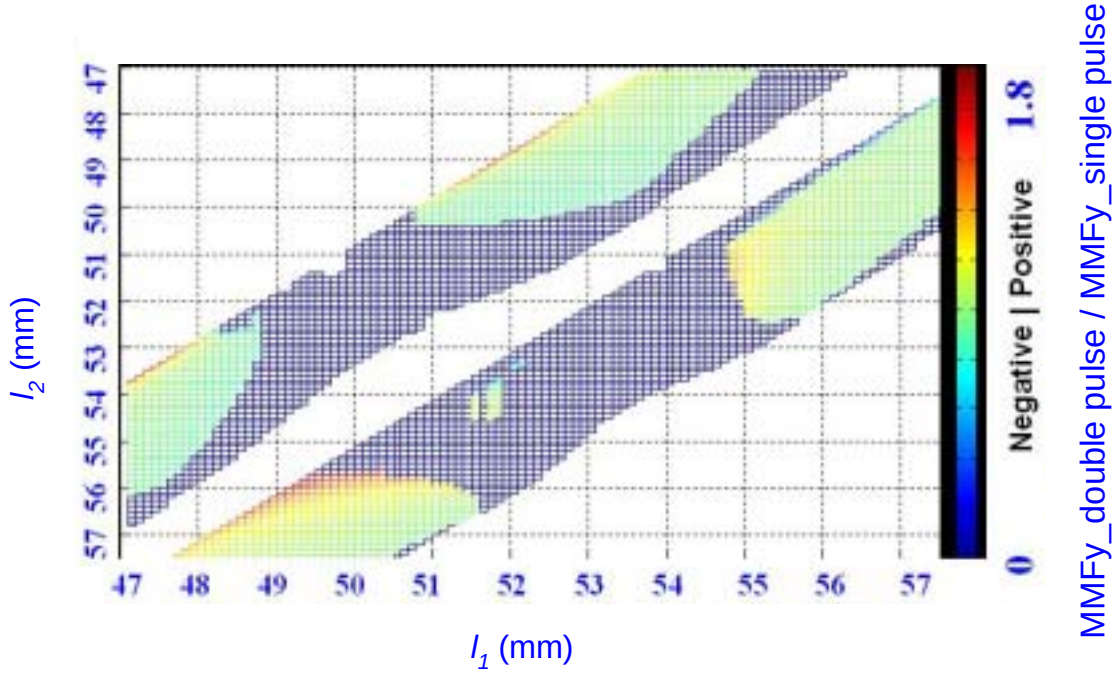

Fig. 4. 13. Two-dimensional map of soft aperture Kerr-lens effect between single pulsed mode locked operation and double pulsed mode locked operation.

References

[1] F. Friebel, F. Druon, J. Boudeile, D. N. Papadopoulos, M. Hanna, P. Georges, P. Camy, J. L. Doualan, A. Benayad, R. Moncorgé, C. Cassagne, and G. Boudebs, "Diode-pumped 99 fs Yb:CaF_2 oscillator," Opt. Lett. **34**, 1474-1476 (2009).
[2] A. Yariv, "Quantum Electronics, 3rd ed" John Wiley & Sons, Inc. (1989).
[3] H. Kogelnik, "On the Propagation of Gaussian Beams of Light Through Lenslike Media Including those with a Loss or Gain Variation," Applied Optics, **4**, 1562 (1965).
[4] H.W.Kogelnik, E.P.Ippen, A.Dienes, C.V.Shank "Astigmatically Compensated Cavities for CW Dye Lasers" IEEE J. Quant. Electr, QE-**8**, 373-379 (1972).
[5] Robert E. Bridges, Robert W. Boyd, and Govind P. Agrawal, "Effect of beam ellipticity on self-mode locking in lasers," Opt. Lett. **18**, 2026-2028 (1993).
[6] V. Magni, G. Cerullo, S. De Silvestri, and A. Monguzzi, "Astigmatism in Gaussian-beam self-focusing and in resonators for Kerr-lens mode locking," J. Opt. Soc. Am. B **12**, 476-485 (1995).
[7] T. Brabec, Ch. Spielmann, P. F. Curley, and F. Krausz, "Kerr lens mode locking," Opt. Lett. **17**, 1292-1294 (1992).
[8] M. Piché and F. Salin, "Self-mode locking of solid-state lasers without apertures," Opt. Lett. **18**, 1041-1043 (1993).
[9] Joachim Herrmann, "Theory of Kerr-lens mode locking: role of self-focusing and radially varying gain," J. Opt. Soc. Am. B **11**, 498-512 (1994).
[10] G. Cerullo, S. De Silvestri, V. Magni, and L. Pallaro, "Resonators for Kerr-lens mode-locked femtosecond Ti:sapphire lasers," Opt. Lett. **19**, 807-809 (1994).

Chapter 5. Experiments of mode-locked lasers

In this chapter we describe experimental detail of our mode-locked lasers. First we show SESAM mode-locked and KLM laser operations based on a broad-strip LD pumped Yb^{3+}:Sc_2O_3 ceramic. In case of the SESAM mode locked operation the shortest pulse duration was limited to be above 200 fs by transition to a multi-pulsed operation. In case of the KLM operation, sub-100 fs pulse duration was obtained. Second We show KLM laser operation based on fiber-coupled LD pumped Yb^{3+}:Lu_2O_3 ceramic with non-doped Y_2O_3 ceramic. The non-doped Y_2O_3 was used to enhance Kerr-nonlinearly. Third, we show KLM multi-gain media laser operation based on a broad-stripe LD pumped Yb^{3+}:Sc_2O_3 and Yb^{3+}:Y_2O_3 ceramics. Due to its broadened gain bandwidth and strong Kerr-lens effect, pulses as short as 53-fs with above 1-W average power were obtained. Fourth, we show KLM laser operation based on Yb^{3+}:Sc_2O_3 single crystal and Yb^{3+}:Lu_2O_3 single crystal, respectively. Almost the same short pulse generation as in the ceramic cases were obtained with single crystal materials. Fifth, we show cw and KLM laser operations based on Yb^{3+}:$\{YGd_2\}[Sc_2](Al_2Ga)O_{12}$ ceramic. $\{YGd_2\}[Sc_2](Al_2Ga)O_{12}$ is new ceramic material and very interesting for high power ultrashort pulse operation. Sixth we show KLM operation based on Yb:YAG ceramic. Pulses as short as 128-f with above 1-W average power were obtained from Yb:YAG.

5.1 Yb^{3+}:Sc_2O_3 ceramic SESAM mode-locked laser

The experimental setup is schematically described in Fig. 5.1. A z-shaped astigmatically compensated cavity was employed. As the gain material, a 3-mm thick Yb^{3+}:Sc_2O_3 (C_{Yb} ≈2.5 at.%) ceramic was used. The material was arranged at the Brewster angle and mounted in a copper holder without water cooling. The holder was mounted on 4-axis (x,y,z,θ) stage. As a pump source a broad-stripe LD (emission area of 1 × 100 μm, (sagittal × tangential), beam-quality values $M_y^2 \approx 1$, $M_x^2 > 20$, λ_{center} ~976 nm, $\Delta\lambda$ ~4 nm) with a maximum output power of 4.5 W was used. The pump beam was focused into the ceramic to $1/e^2$ diameters of 20 × 190 μm inside the gain medium by four beam-shaping lenses. Its Rayleigh lengths are ~2.3 mm in sagittal plane and ~1.7 mm in tangential plane. The maximum

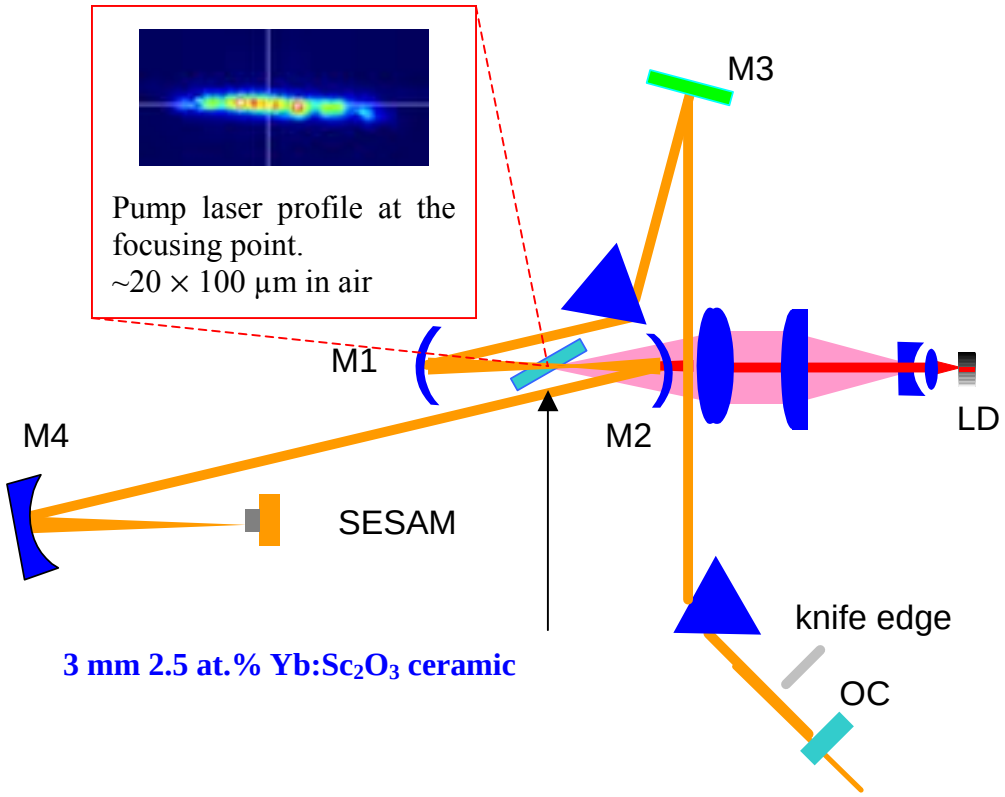

Fig. 5.1. Experimental setup of SESAM mode-locked Yb^{3+}:Sc_2O_3 ceramic laser.

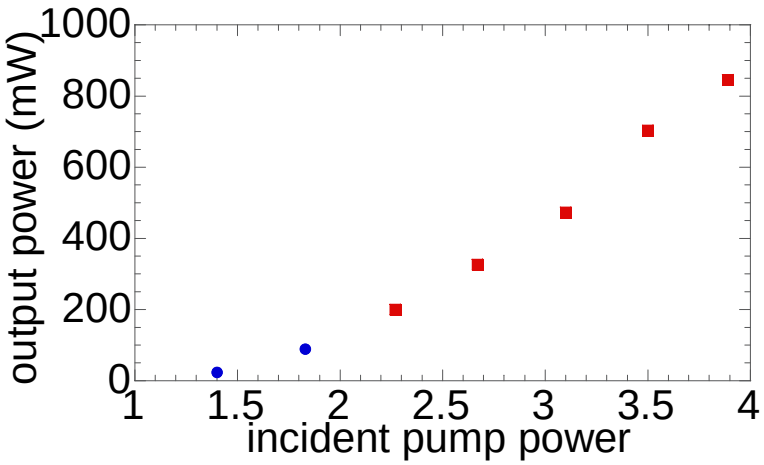

Fig. 5.2. Output power versus incident pump power. Circle points show output power in cw and single pulsed operation. Square points show output power in the muti-pulsed operation.

incident pump power was about 3.89 W. The pump beam passed through the folding mirror M2. The folding mirrors (M1, M2) have 100 mm radii of curvature (ROC) on both surfaces to eliminate a concave lens effect (for pump laser mode) and are antireflection coated for wavelength below 980 nm and high-reflection (HR) coated above 1020 nm. To achieve solitonlike mode locking, the Chirped mirror (M3, GDD~-900 fs^2) and SF10 Brewster prism pair (P) with the tip-to-tip separation of 70 cm were used. Neglecting the Kerr-lens effect the laser mode diameters inside the gain material were calculated to be about ~40 × 70 μm. The laser beam was focused onto SESAM (BATOP GmbH, 0.7 % saturable loss with 0.3 % linear loss (from data sheet), 30-μJ/cm^2 saturation fluence, 1-mJ/cm^2 damage threshold, 10

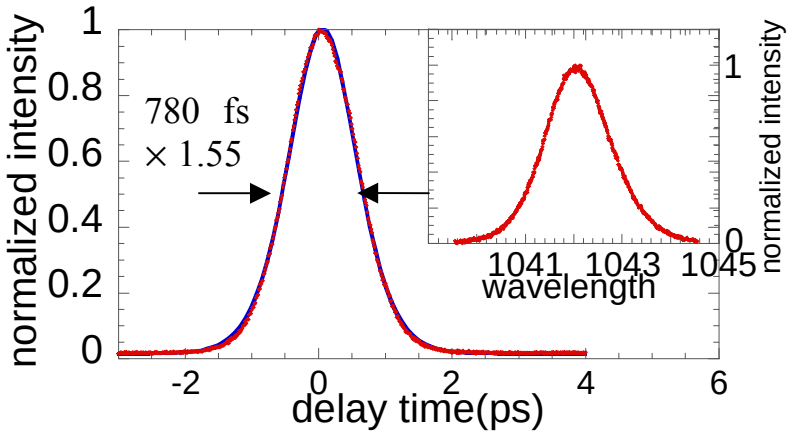

Fig. 5.3. Autocorrelation trace and spectrum (inset) are shown. Single pulse operation with the optimization of output power.

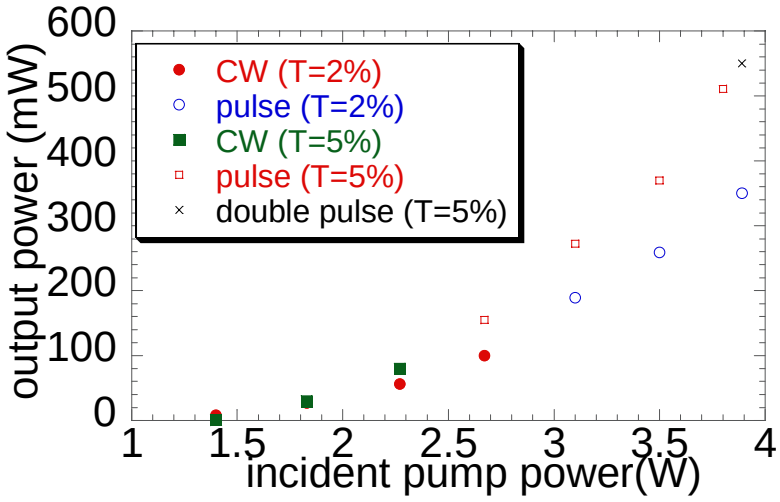

Fig. 5.4. Output power versus incident pump power.

ps recovery time) by a concave mirror (M4, ROC = 300 mm). The estimated laser mode diameters focused onto the SESAM4 were ~110 × 120 μm. A 5% transmittance output coupler (OC) was used. The all of OCs

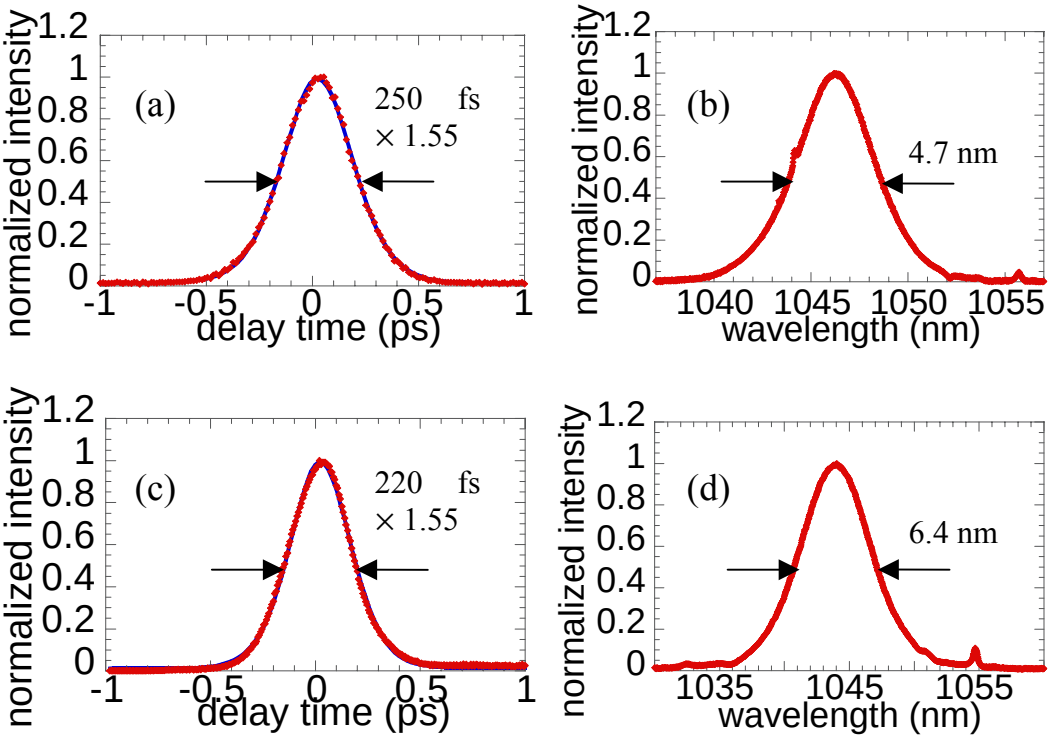

Fig. 5.5. Autocorrelation traces and spectra are shown. (a)(b) Autocorrelation trace and spectrum of 250 fs pulses. (c)(d) Autocorrelation trace and spectrum of 220 fs pulses.

used in this thesis were wedged for about 30 min. to avoid reflection at its back surface. If we use a parallel output coupler, it easily generates sub pulses separated by the time interval corresponding to the output coupler thickness, even though there is an antireflection coating on its back surface. At first we optimized the cavity for output power (Fig.5.2.). Under the optimization, we suffer a transition to a multi-pulsed operation and pulse duration was limited to be about 800 fs (Fig.5.3.). To suppress the multi-pulsed operation, The SESAM was replaced to a new SESAM having 1.2 % saturable absorption depth with 0.8 % linear loss. The concave mirror (M4) was also changed to new one having ROC of 400 mm to expand the focusing laser mode diameters on the SESAM. The estimated laser mode diameters focused onto the SESAM were changed to ~180 × 230 μm, which avoids excess saturation of the SESAM. With these changes, pulses as short as 220 fs and 250 fs were obtained with 2% OC and 5% OC, respectively (Fig.5.4, Fig. 5.5). The maximum average powers were 350 mW with 2% OC and 515mW with 5% OC. Comparison with the 5% OC, the 2% OC enables shorter pulse generation with a penalty of lower average power. By inserting the knife-edge as a spectral selective element behind the prism pair, tunable femtosecond laser operation was also obtained (Fig. 5.6). The shortest pulse duration, however, was still limited by a transition to the multi-pulsed operation and appearance of cw component.

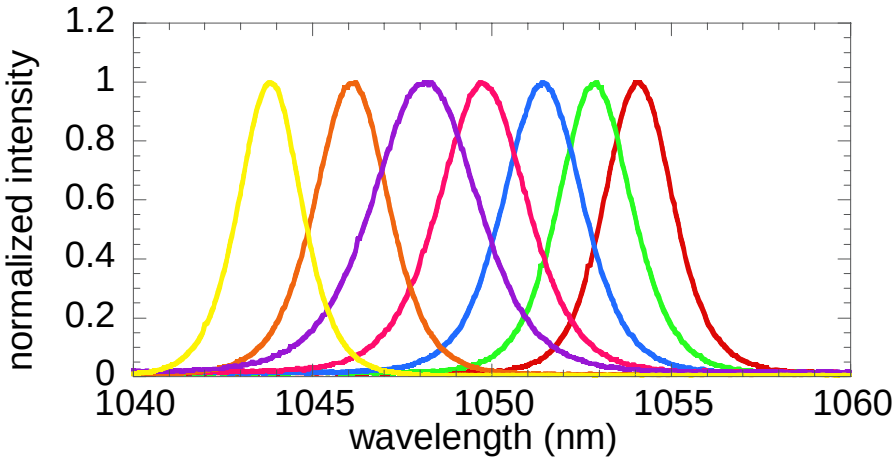

Fig.5.6. Spectra of pulses with different center wavelength are shown. The center wavelengths were tuned by the knife-edge.

5.2 Yb^{3+}:Sc_2O_3 ceramic Kerr-lens mode-locked laser

For further short pulse generation, we optimized the cavity for KLM. The chirped mirror M3 was removed (Fig. 5.7) to decrease total negative dispersion and the positions of concave mirrors (M1, M2) and gain medium were carefully adjusted to obtain large soft aperture Kerr-lens effect (see chapter 4). By the adjustment the resonator was in an almost unstable state in cw operation where the cavity became very sensitive to the Kerr-lens effect. A maximum average power of 650 mW with pulse duration of 92 fs (Fig.5.8) at the repetition rate of 83 MHz (Fig. 5.9) was obtained. The mode locking showed self-starting by increasing the pump power. The center wavelength was 1042 nm and the spectral bandwidth was 13.7 nm, which is about 1.2 times broader than the fluorescence spectral bandwidth of the Yb^{3+}:Sc_2O_3. The spectral shape and bandwidth obey solition equation and probably was supported by the nonlinear spectral shaping effect (e.g. SPM effect and Kerr shutter in the material). The time-bandwidth product was 0.340 that indicates almost the transform limited pulses were directly

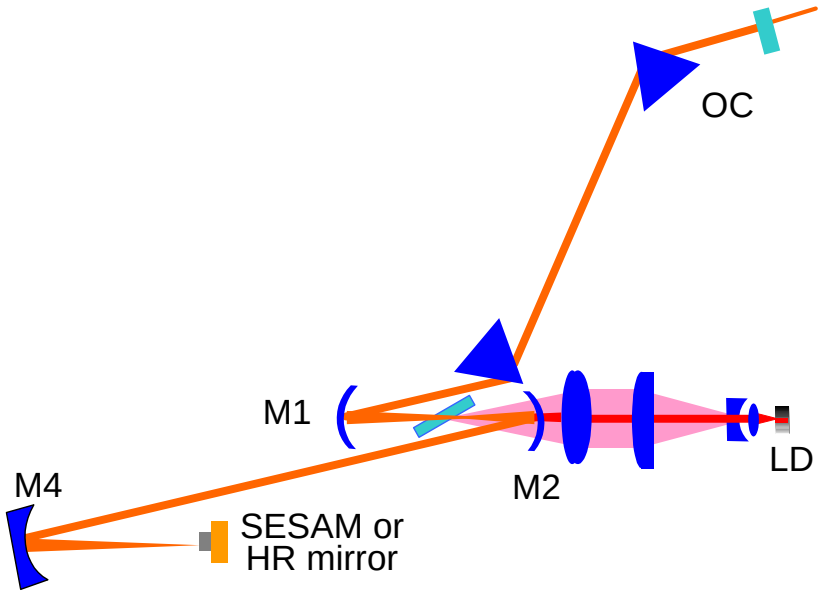

Fig. 5.7. Experimental setup of Yb^{3+}:Sc_2O_3 Kerr-lens mode locking.

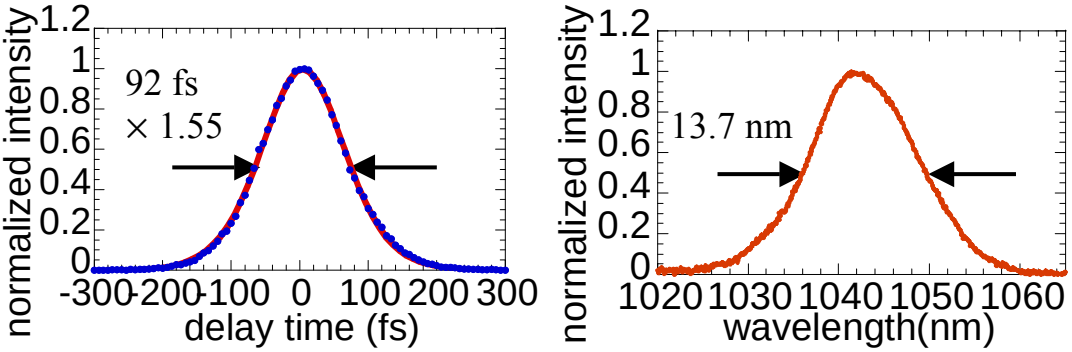

Fig. 5.8. Autocorrelation trace (a) and spectrum (b) of 92 fs pulses are shown. (a) The experimental data (dots) and $sech^2$-fitting curves (solid curve) are shown.

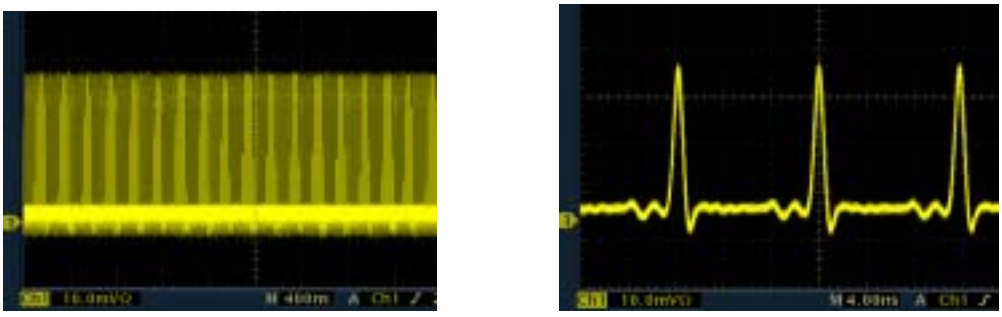

Fig. 5.9. Pulse trains of 92 fs pulses are shown.

obtained from the cavity. The mode-locked operation was stable for more than 3 hours. At the onset of mode locking the significant change of the laser mode profile was observed (Fig. 5.10), which indicates existence of large Kerr-lens effect and the change of the condition of the resonator to a stable state from an almost unstable state. However, the observed laser mode profiles are slightly different from the calculation (chapter 4, elliptical in cw and circular in mode-lockied). The difference was probably

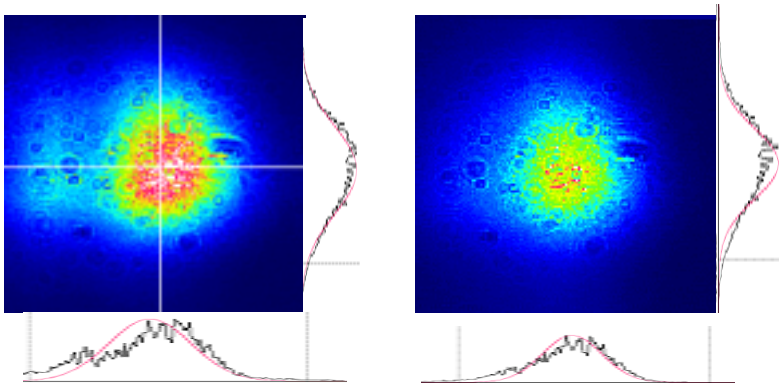

Fig. 5.10. Measured laser mode profiles (a) in cw (2350 × 2400 μm) and (b) in mode locked operations (1850 × 1970 μm) are shown.

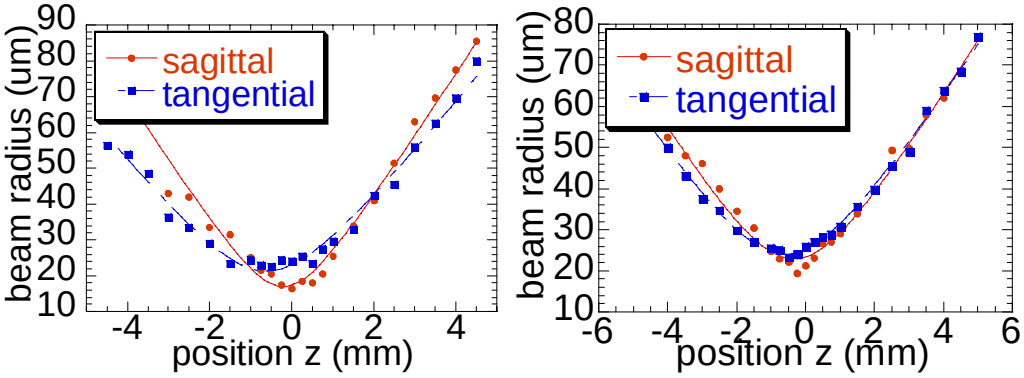

Fig. 5.11. Measured beam radiuses near the focusing point were shown. (a) In the cw operation. (b) In the mode-locked operation.

caused by imperfect control of astigmatism in this first KLM laser experiment. The laser beam quality values M_x^2 and M_y^2 were roughly measured and were smaller than 1.2 both in the cw and mode-locked operations (Fig. 5.11.). We supposed the pulse shortening was mainly sustained by the Kerr-lens effect. To verify it, the SESAM was replaced by an HR mirror. At the incident pump power of 3.1 W Kerr-lens mode locking was initiated by knocking the optical bench. At the onset of mode locking the average power jumped to ~580 mW from ~430 mW (Fig. 5.12). This large jump in average power also indicates large loss and/or gain modulation by Kerr lens effect. Due to the absence of the unsaturable loss of the SESAM the maximum average power increased to 850 mW with the maximum incident pump power of 3.89 W. The 92 fs pulse duration was the same as that at aforementioned KLM operation with a SESAM and the spectrum was almost the same, but the tendency of cw spiking appeared at the maximum pump power. The peak power was about 111 kW and the optical-to-optical efficiency was 21.9%, which was probably degraded by

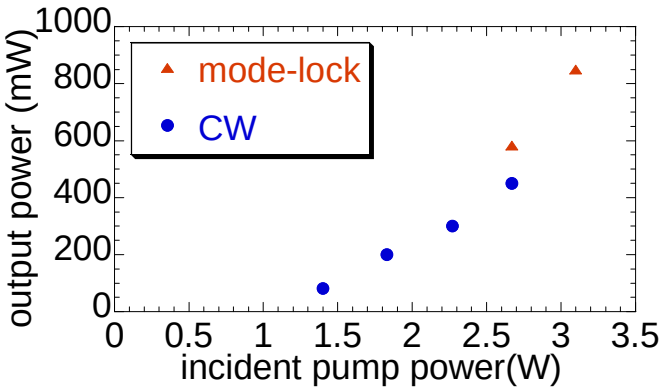

Fig. 5.12. Output power versus incident pump power.

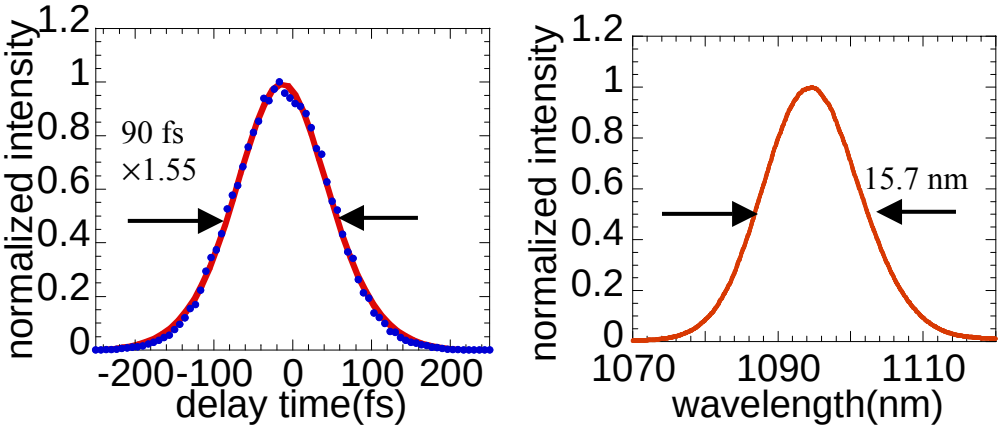

Fig. 5.13. Autocorrelation trace (a) and spectra (b) of 90 fs pulses are shown. (a) The experimental data (dots) and $sech^2$-fitting curves (solid curve) are shown.

the poor mode-matching factor between the lasing mode area and the pumping mode area. In this cavity setup, the mode-matching factor between pump mode and laser mode inside the cavity was less than 40%. Therefore, almost doubling the factor efficiency could be possible by improving the mode-matching factor.

By replacing the 5% OC to a 1% OC, the KLM laser operation at a center wavelength of 1092 nm was also achieved. The existence of the reabsorption loss around 1041 nm increases the threshold of lasing at 1041 nm. Consequently the lasing at 1092 nm selectively occurs with a high Q cavity. In this case the average power of 160 mW with the pulse duration of 90 fs was obtained at the same incident pump power (Fig. 5.13). The spectral bandwidth was 15.7 nm, and the time-bandwidth product was 0.354. Although the emission cross section of Yb^{3+}:Sc_2O_3 at 1094 nm is about 5 times smaller than at 1041 nm, the fluorescence spectrum bandwidth of 17 nm is about 1.5 times broader than at 1041 nm. Therefore the generation of much shorter pulses at 1094 nm is expected by further optimization. More efficient operation around 1094 nm also should be possible by using a higher transmission OC with some spectral selective element [1].

5.3 $Yb^{3+}:Lu_2O_3$ and Y_2O_3 ceramic Kerr-lens mode-locked laser

For the KLM laser operation with our experimental setup, the thickness of a gain medium (Kerr medium) is important factor. In this experiment, a 1 mm thick $Yb^{3+}:Lu_2O_3$ (C_{Yb} ≈3 at.%) ceramic and 2 mm thick non-doped Y_2O_3 ceramic were used simultaneously in the cavity. The 2 mm thick non-doped Y_2O_3 ceramic was used in order to increase the nonlinear effects. The reason why Y_2O_3 ceramic was used is that we did not have a Lu_2O_3 ceramic thicker than 1 mm and Y_2O_3 has almost the same values of the linear and nonlinear refractive induces as Lu_2O_3 [2]. This experiment also serves the test of multi-gain media oscillator (see next section). The experimental setup is shown in Fig. 5.14. The $Yb^{3+}:Lu_2O_3$ and non-doped Y_2O_3 ceramics were physically contacted to each other without any coating and arranged at the Brewster angle. The setup is almost the same as that in the $Yb^{3+}:Sc_2O_3$ experiment but the pump source was changed to a 5 W fiber-coupled LD (50-μm-core diameter with a numerical aperture of 0.15,

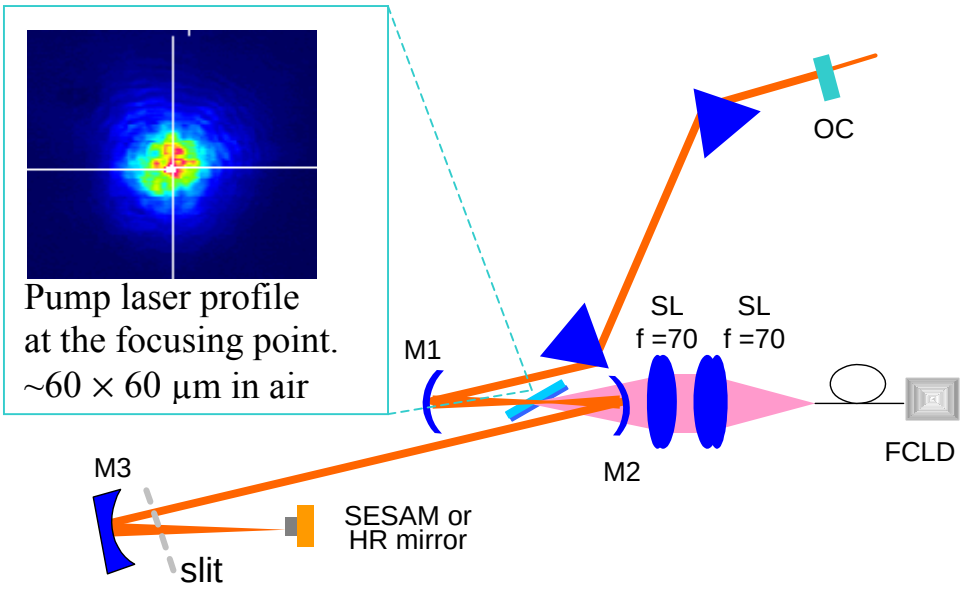

Fig. 5.14. Experimental setup of $Yb^{3+}:Lu_2O_3$ ceramic Kerr-lens mode-locked laser. SL is spherical lenses.

λ_{center} ~975 nm, $\Delta\lambda$ ~5 nm). Its output beam was focused into the ceramic to a $1/e^2$ diameter of ~60 × 110 μm through the folding mirror (M1) by two 70 mm focal length doublet lenses. As a starter and stabilizer of the mode locking, a SESAM (BATOP GmbH, 0.7 % saturable loss with 0.3 % linear loss, 30-μJ/cm^2 saturation fluence, 10 ps recovery time) was still used. To stabilize the Kerr-lens mode locking a slit (slit radius is about 3 mm) was also inserted near the M3 (The distance from M3 was about 5 cm) in the vertical direction. The KLM can be obtained without this slit, but the stability was improved by incorporation. Due to the poor pump laser mode qualities of fiber coupled LD, The soft aperture Kerr-lens effect is not strong and the slit make additional hard aperture Kerr-lens effect. The distance between the prisms was 45 cm and the OC has 5% transmittance.
By optimization of the cavity for a cw operation, an output power of about 500 mW was obtained. However, it suffered transition to a multi-pulsed operation. For the short pulse operation, the cavity was aligned at an almost unstable state in the vertical direction where the cavity became very sensitive to the Kerr-lens effect. On to the mode-locked operation the average power increased to 300 mW from ~200 mW and the significant change in the laser mode field diameters was also observed. The measured laser mode field diameters were about 1400 × 2200 μm in the cw operation and 1350 × 1600 μm in the mode-locked operation (Fig. 5.15). The disappearance of an interference pattern in Fig.5.15 (b) indicates decreasing of coherent length in ultrashort pulse operation. The significant change of the beam profile was apparent only in the vertical direction where the cavity was aligned almost unstable state. Similar behaviors have been

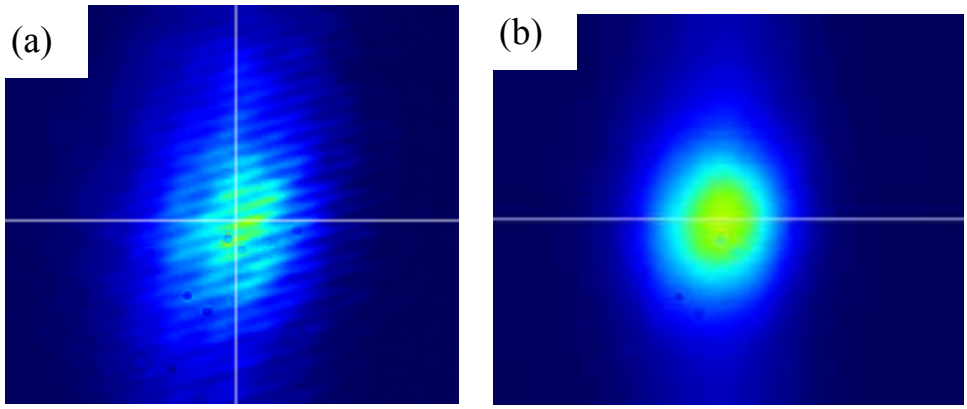

Fig. 5.15. Measured laser mode profile (a) in cw and (b) in mode locked operations was shown.

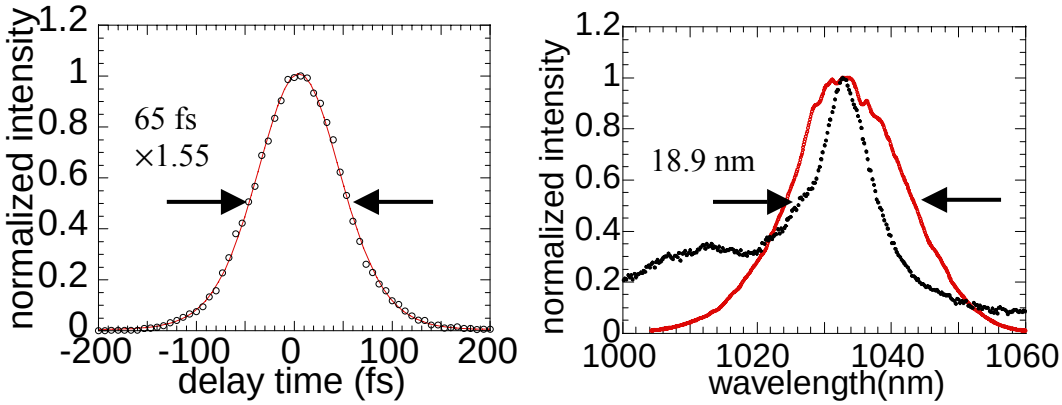

Fig. 5.16. (a) Measured autocorrelation data (dots) and sech^2-fitting curves (solid curve) are shown. (b) Fluorescence spectrum of Yb^{3+}:Lu_2O_3 (doted curve) and spectrum of 65 fs pulses are showen.

reported with KLM operation with a Brewster configuration [3,4]. The change also agrees with calculated result. The measured beam quality M^2 were almost the same value about 1.1 in the cw operation and mode-locked operation. The shortest pulse duration of 65 fs with a maximum average power of 320 mW at the repetition rate of 99 MHz was obtained (Fig. 5.16). The center wavelength was 1032 nm and the spectral bandwidth was 18.9 nm, which was about 1.4 times broader than the fluorescence spectral bandwidth of Yb^{3+}:Lu_2O_3. The time-bandwidth product was 0.345. The pulse duration was almost independent on the saturable absorption depth of the SESAM. The allowance of the distance between the folding mirrors was only several 100 μm to obtain an adequate Kerr-lens switching and varied with the pump power. The peak intensity was about 53 kW and the optical-to-optical efficiency was 6.4%, which was partly due to the poor mode-matching factor between the lasing mode area and the pumping mode area, and to the low absorption efficiency of the gain material (about 60 %). By changing the insertion depth of the prisms and the distance of the holding mirrors (M1, M2), the pulse duration changed (Fig. 5.17) due to the change of the total negative dispersion value and the laser mode field diameters inside the gain medium.

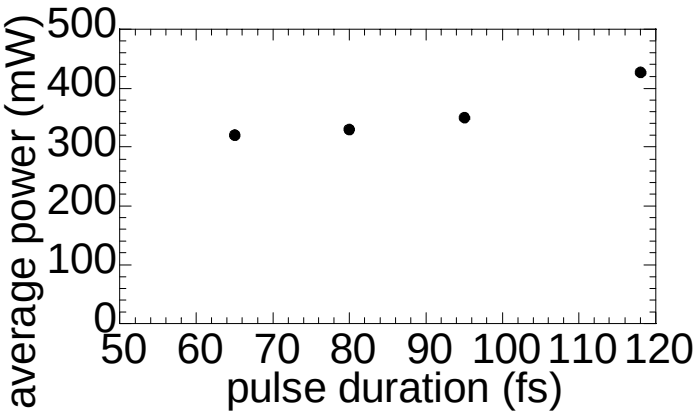

Fig. 5.17. Output power versus pulse duration.

We also demonstrated a mode-locked operation based on an Yb^{3+}:Y_2O_3 ceramic (3mm thick, C_{Yb} = 2 at.%) with the same cavity but with the 40 cm tip-to-tip prism separation distance. By the setup, the similar behaviors were observed and 68-fs pulses with an average power of 540 mW were obtained at the center wavelength of 1036 nm (Fig. 5.18). The spectral bandwidth was 20 nm and the repetition rate was about 99 MHz [5].

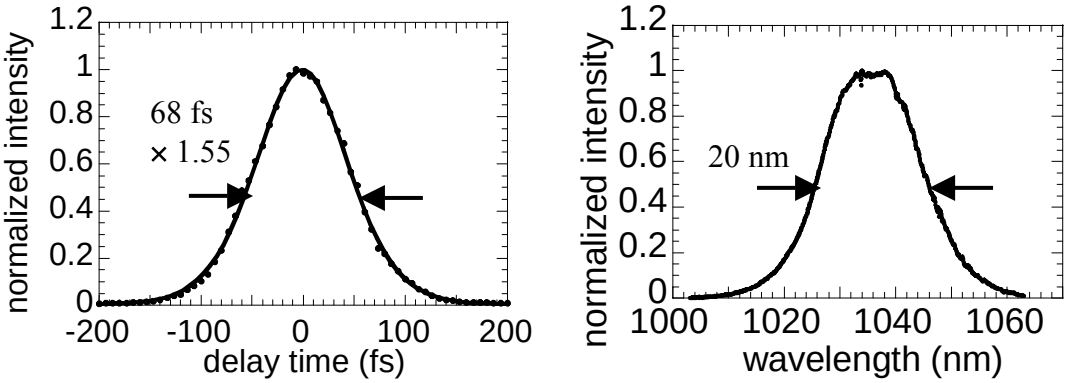

Fig. 5.18. Autocorrelation trace (a) and spectra (b) of 68 fs pulses are shown. (a) The experimental data (dots) and $sech^2$-fitting curves (solid curve) are shown.

5.4 $Yb^{3+}:Sc_2O_3$ and $Yb^{3+}:Y_2O_3$ ceramic multi-gain media Kerr-lens mode-locked laser

The experimental setup was schematically shown in Fig.5.19 and was almost the same as that in $Yb^{3+}:Sc_2O_3$ experiment. As the gain media, an $Yb^{3+}:Sc_2O_3$ (1 mm thick, C_{Yb}=2.5 at.%) and $Yb^{3+}:Y_2O_3$ (1.5 mm thick, C_{Yb}=1.8 at.%) ceramics were used simultaneously in the cavity. They correspond to α (ratio of the Yb^{3+}-ion number in the $Yb^{3+}:Y_2O_3$ gain part against the total Yb^{3+}-ion number interacting with the laser mode. See chapter 3.6.) of 0.46. They were physically contacted to each other without any coating and arranged at the Brewster angle. The $Yb^{3+}:Sc_2O_3$ ceramic was situated at the near side of the pump source and the $Yb^{3+}:Y_2O_3$ ceramic was situated at the opposite side. As the pump source an 8-W broad-stripe LD (Lumics GmbH, emission area of 1 × 95 μm, 976 nm, $\Delta\lambda$~5 nm) was used. The maximum incident pump power was 7.4 W. To achieve stable and self-starting mode-locked operation, the same SESAM as we used in

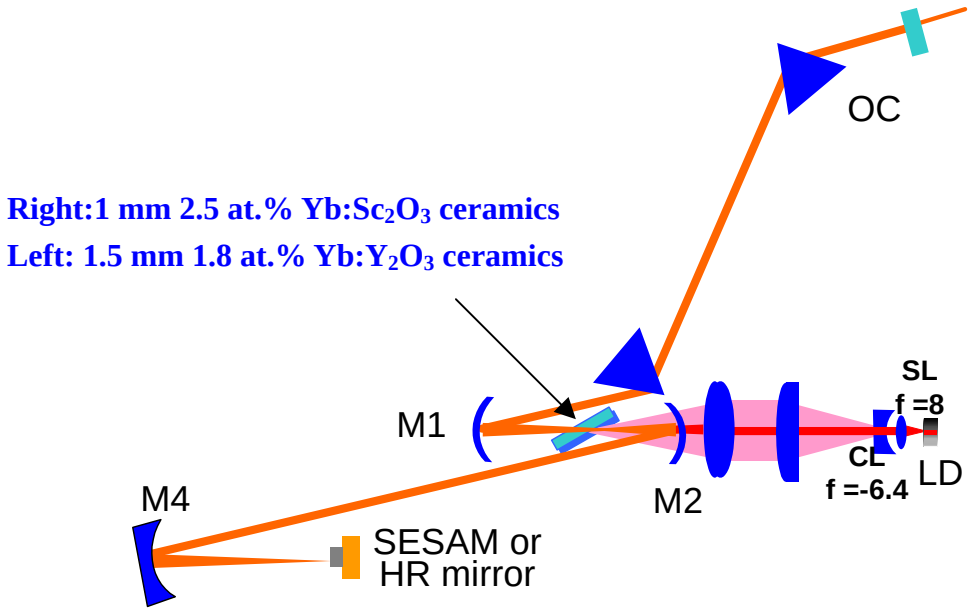

Fig. 5.19. Experimental setup of $Yb^{3+}:Sc_2O_3$ and $Yb^{3+}:Y_2O_3$ multi-gain media Kerr-lens mode-locked laser.

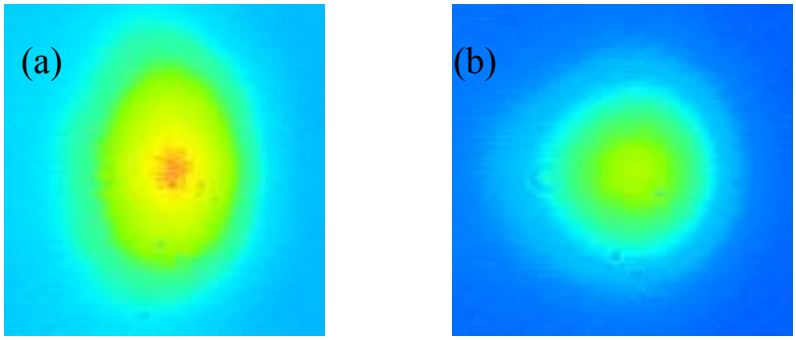

Fig. 5.20. Measured laser mode profiles of multi-gain media laser. (a) Before multi-pulse suppression: laser mode field diameters were 2900 × 1800 μm. (b) After multi-pulse suppression: laser mode field diameters were 2060 × 1800 μm.

Yb^{3+}:Lu_2O_3 Kerr-lens mode locked experiment was used. The distance between prism pair was 40 cm and OC has 10% transmittance.

In a cw operation (replacing the SESAM by a high-reflection mirror), an output power of about 1.9 W at the wavelength of 1041.5 nm was obtained. For the mode-locked operation, at first we optimized the cavity with respect to the average power. Under this optimization an average power of 1.7 W was obtained. The output pulses, however, suffered serious multi-pulsed operation and the pulse duration was limited to several hundred fs. Next, we optimized the cavity with respect to the pulse duration as same as aforementioned experiments. During the optimization the average power once decreased to about 1.3 W. At the same time of the multi-pulse suppression, the average power increased from 1.3 W to ~1.5 W and the spectral bandwidth broadened from several nm to ~20 nm. The large increase of the average power from 1.3 W to 1.5 W even with the low *Q* cavity (10% output coupling) indicates an existence of large gain and/or loss modulation. The significant change in the laser mode field diameter was also observed at the same time (Fig.5.20). The $sech^2$-fit pulse duration of 66 fs with the average power of 1.5 W at the repetition rate of 89 MHz was obtained (Fig. 5.21). The center wavelength was 1041 nm and the spectral bandwidth was 19.7 nm. The time bandwidth product was 0.36. The peak intensity was about 0.25 MW and the optical-to-optical efficiency was about 18.8% (against the LD power of 8 W). By changing the insertion depth of the prisms and the distance of the folding mirrors (M1, M2), the

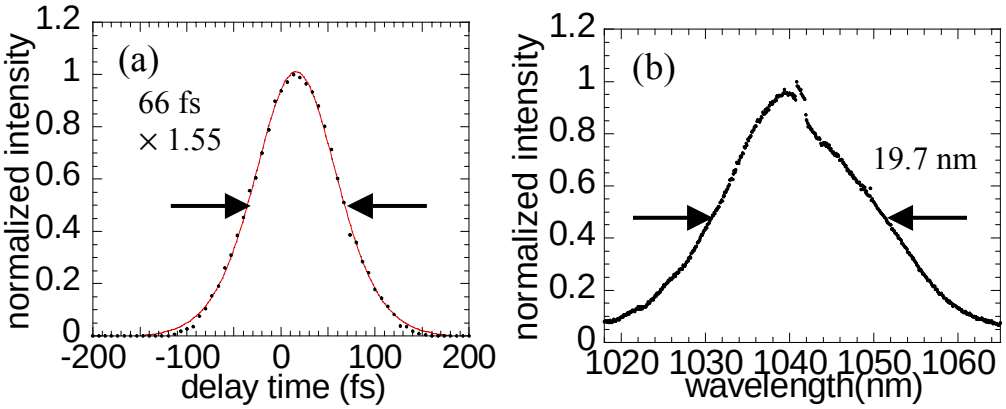

Fig. 5.21. Autocorrelation trace (a) and spectrum (b) of 66 fs pulses are shown. (a) The experimental data (dots) and sech^2-fitting curves (solid curve) are shown.

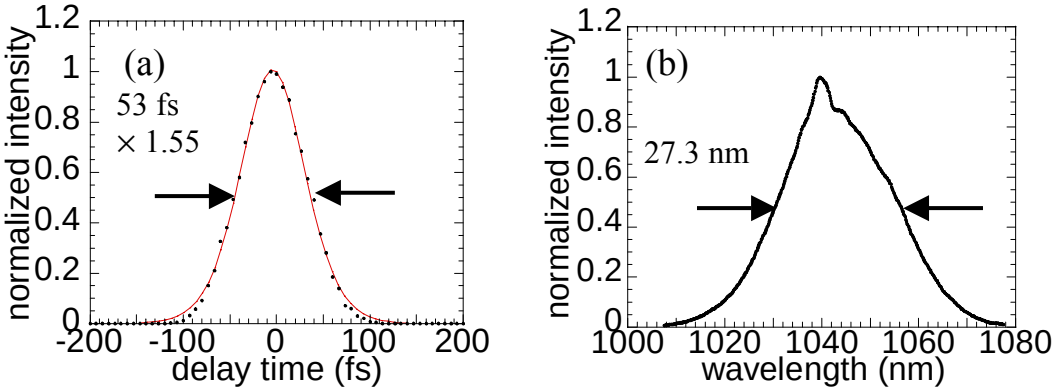

Fig. 5.22. Autocorrelation trace (a) and spectrum (b) of 53 fs pulses are shown. (a) The experimental data (dots) and sech^2-fitting curves (solid curve) are shown.

shortest pulse duration of 53 fs with a 1-W average power was also achieved (Fig. 5.22). The spectral bandwidth was 27.3 nm and the time bandwidth product was 0.40. The spectral includes little narrow cw component. About the stability, the short pulse operation kept for longer than 30 minutes. However, it showed an instant instability during the operation and the stable time decreased, as the pulse was shorter. The stable time is also very sensitive to the alignment. The mode-locked operation has also been investigated with a couple of SESAMs with different specifications (BATOP GmbH, saturable absorption depths of 0.5% and 1.3% with a recovery time of 500 fs). Pulses as short as sub 60 fs have been also obtained with both SESAMs. Therefore, the pulse durations are almost independent from the SESAMs.

.

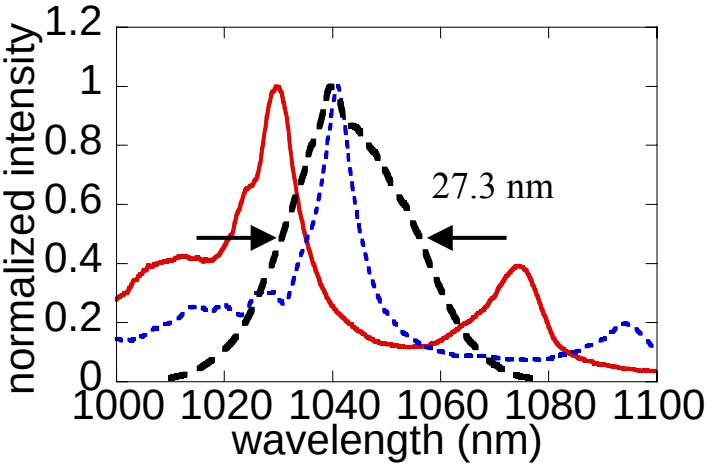

Fig. 5.23. Spectrum of the 53-fs pulses (broken curve) and normalized emission spectrum of the Yb^{3+}:Sc_2O_3 (dotted curve) and Yb^{3+}:Y_2O_3 (solid curve) are shown.

The spectrum of the 53-fs pulses was centered at 1042 nm and broadened to 1010 nm and 1075 nm (Fig. 5.23). At the shorter wavelength side, the folding mirrors (M1 and M2) do not keep the high reflectance (>99.9%) below 1020 nm and also have large high-order dispersion near 1010 nm, which limits the spectral range of the shorter wavelength side. At the longer wavelength side, the spectrum reached another gain peak of Yb^{3+}:Y_2O_3 at 1076 nm. This is greatly interesting, because it indicates that the presented operation made use of not only the different gain materials but also the separating different gain peaks simultaneously with the help of the large spectral broadening effect and the multi-gain media. Additionally, Yb^{3+}:Sc_2O_3 also has another gain peak at 1094 nm. Although the emission cross sections at the longer wavelength side are about 3~5 times smaller than those of the shorter wavelength side, the reabsorption at the shorter wavelength side can modify the effective gains to comparable values by optimizing the Yb^{3+}-ion concentration. Therefore, the effective gain bandwidth of Yb^{3+}:Sc_2O_3 and Yb^{3+}:Y_2O_3 multi-gain media can become much broader. It should be remarked that even though a Kerr-lens effect can broaden the spectrum with a large modulation depth, the broad gain bandwidth also plays an important role to sustain short pulse duration without multi-pulsing and/or cw component (see chapter 6). While Yb^{3+}:Sc_2O_3 and Yb^{3+}:Y_2O_3 were physically contacted in the present experiment, a composite ceramic technique will enable a monolithic

multi-gain media in the future. Additionally, the physical contact of the multi-gain media is dispensable, because their stimulated emissions are optically connected even if the gain media are spatially separated. We can select their configuration for different aims [6].

5.4 $Yb^{3+}:Sc_2O_3$ and $Yb^{3+}:Lu_2O_3$ single crystal Kerr-lens mode-locked lasers

In the above KLM Yb:sesquioxides ceramic laser experiments, we have succeeded in generating sub 100 fs ultrashort pulses, which is about 4 times shorter than the previously reported SESAM mode-locked lasers based on Yb:sesquioxides ceramics and single crystals. Our results also showed broader spectral bandwidth than the gain media. Then, one simple question arise: "whether similar short pulses can be obtained from single crystal or not?" Our answer was Yes and to verify it, we did almost the same experiments with $Yb^{3+}:Sc_2O_3$ or $Yb^{3+}:Lu_2O_3$ single crystals.

The experimental setup is shown in Fig. 5.24, which is almost the same as in my previous ceramic experiments. As the gain medium, we used $Yb^{3+}:Sc_2O_3$ (2.4 mm thickness, C_{Yb}=2. 5 at.%) or $Yb^{3+}:Lu_2O_3$ (1.9 mm thickness, C_{Yb}=3 at.%) single crystals. As the pump source the 5-W fiber-coupled LD or an 8-W broad-stripe LD was used. In case of the

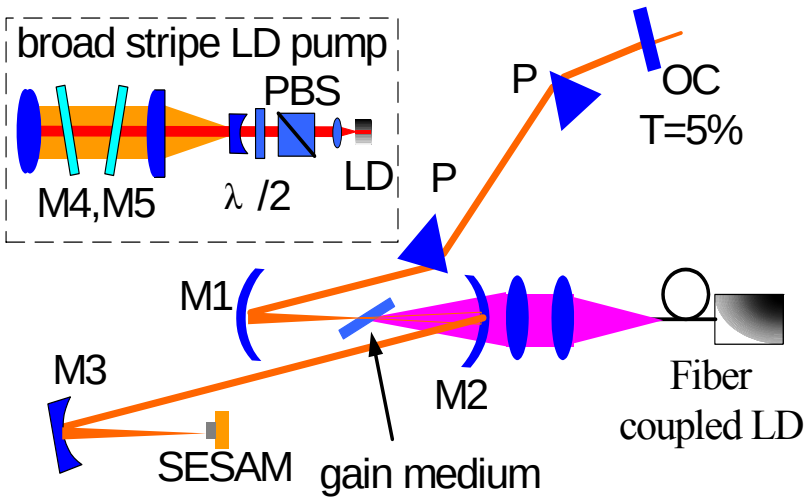

Fig. 5.24. Experimental setup of the mode-locked laser.

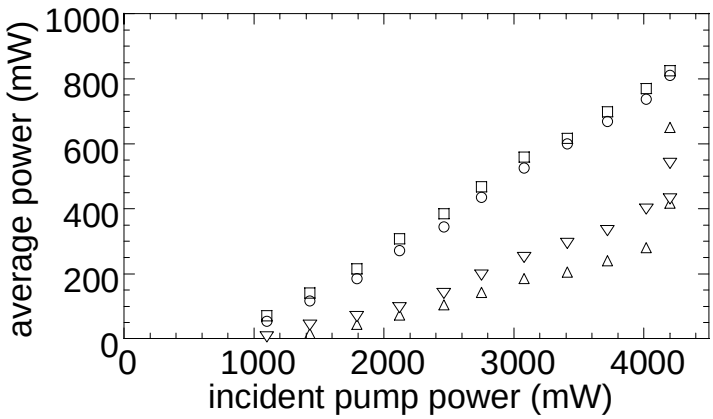

Fig. 5.25. Average power versus the incident pump power. In case of the Yb^{3+}:Sc_2O_3 crystal laser optimized for average power (circles) and optimized for short pulse duration (triangles), and in case of the Yb^{3+}:Lu_2O_3 crystal laser optimized for average power (squares) and optimized for short pulse duration (inverse triangles) are shown.

broad-stripe LD pumping, mirrors M4, M5 having the same coating as M1, a half-wave plate (0th order, λ_{center} of 980 nm) and a broadband polarization beam splitter (PBS, 620~1020 nm) were also used in order to protect the LD from the leaking laser beam through the folding mirror M2. The half-wave plate rotates the polarization of the leaking laser beam including the wavelength below 1020 nm and the PBS reflects it. With this half-wave plate, the pump laser becomes *s*-polarized at the gain medium and therefore it has about 31% reflection loss at the Brewster angle. For stable mode-locked operation a SESAM (BATOP GmbH) was used. A plane mirror with 5% transmission was used as the output coupler (OC).

First we optimized the cavity for high average output powers. An average powers of above 800 mW were obtained by each Yb^{3+}:RE_2O_3 laser (Fig. 5.25) with the 5-W fiber coupled LD pump source and the SESAM with 0.5 % saturable absorption depth (90-μJ/cm^2 saturation fluence, 500-fs recovery time). However, with this setup the pulse durations were limited to be about several hundred fs and multi-sub-pulses were observed in the autocorrelation trace (Fig. 5.26). Next, we optimized the cavity for short pulse durations similar to the aforementioned experiments.. As can be seen in Fig.5.25, the average powers showed large jumping near the maximum pump power. After this jumping, significant change of the laser mode profile (Fig. 5.27) and spectral broadening occurred. At the same time of

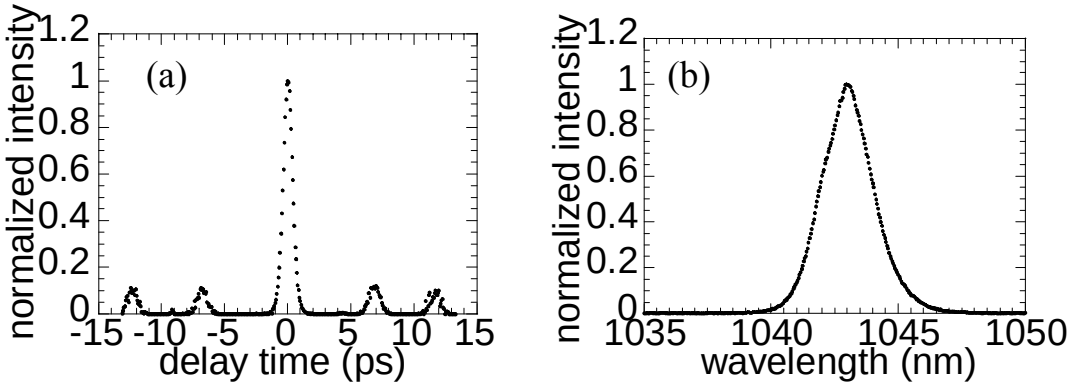

Fig. 5.26 Autocorrelation trace (a) and spectrum (b) of the Yb^{3+}:Sc_2O_3 mode-locked laser with the average power of 830 mW.

the spectral broadening, the center wavelength of the pulses also shifted to longer wavelength side. With the optimizations 64-fs pulses with an average output power of 650 mW at the center wavelength of 1048 nm and a spectral bandwidth of 22 nm were obtained from the Yb^{3+}:Sc_2O_3 single crystal, and 68-fs pulse duration with the average power of 540 mW at the center wavelength of 1037 nm with the spectral bandwidth of 20 nm from the Yb^{3+}:Lu_2O_3 single crystal were obtained (Fig. 5.28). The time-bandwidth products were 0.386 and 0.379. The repetition rate was 100 MHz in each case. The distance between the prism pair was 41 cm and the insertion depth of the prisms were changed in each case to optimize the total amount of dispersion. The proper distance between the folding mirrors (M1, M2) to obtain this pulse shortening had allowance of only several

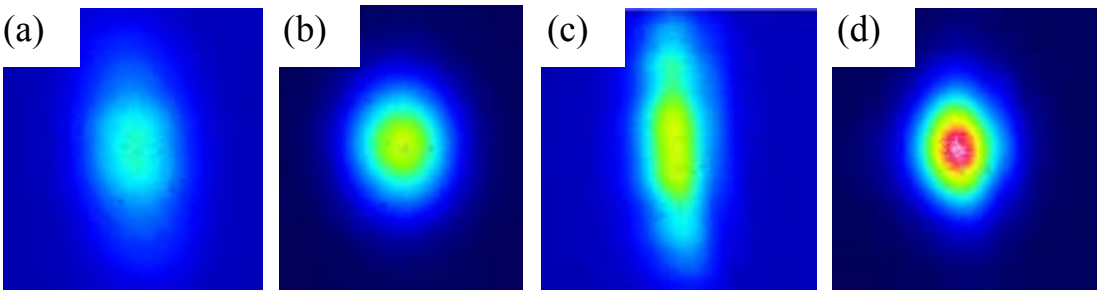

Fig. 5.27. Mode profiles of the laser outputs. In case of the Yb^{3+}:Sc_2O_3 laser (a) before pulse shortening with the mode field diameters of about 2000 × 3800 μm (tangential × sagittal) and (b) after the pulse shortening with the mode field diameters of about 1900 × 2500 μm. In case of the Yb^{3+}:Lu_2O_3 laser (c) before the pulse shortening with the mode field diameters of about 1600 × 4300 μm and (d) after the pulse shortening with the mode field diameters of about 1700 × 2400 μm.

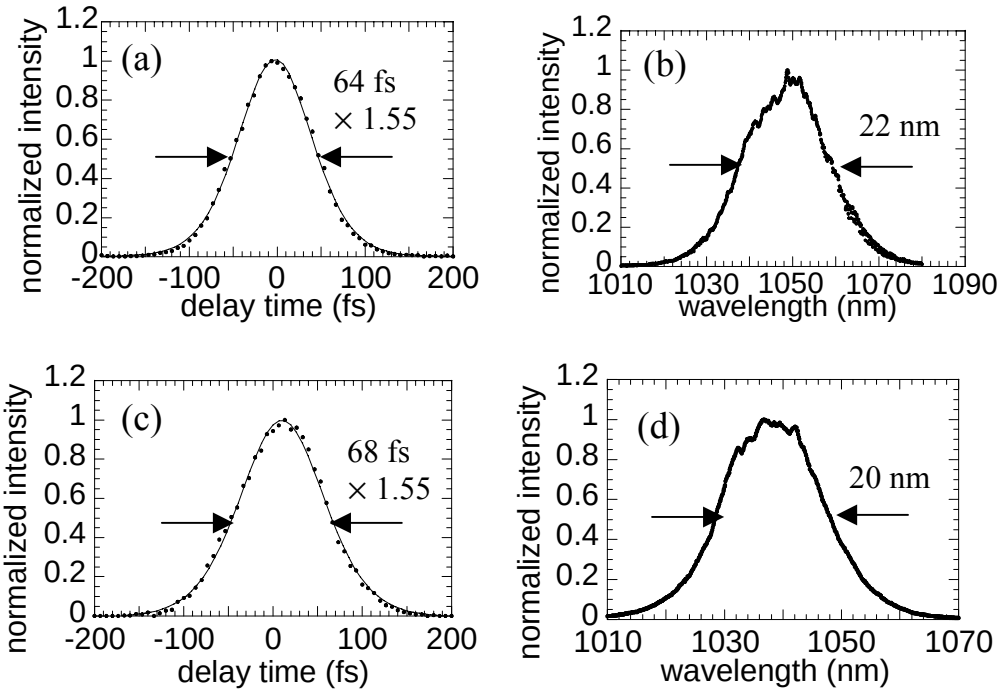

Fig.5.28. Autocorrelation traces and spectra of (a)(b) 64 fs pulses from the Yb^{3+}:Sc_2O_3 crystal and (c)(d) 68 fs pulses from the Yb^{3+}:Lu_2O_3 crystal. The experimental data (points) and $sech^2$-fitting curves (solid curve) are shown.

hundred μm and varied with the pump power.

Next we changed the pump source to the 8-W broad stripe LD (inset of Fig. 5.24) and the SESAM to the 0.4% saturable absorption depth one (120-μJ/cm^2 saturation fluence, 500-fs recovery time). The distance between the prism pair was also changed to 70 cm for the Yb^{3+}:Sc_2O_3 and to 60 cm for the Yb^{3+}:Lu_2O_3. The maximum incident pump power was about 5.2 W (including 31% reflection loss). With this setup 81-fs pulse duration with the average power of 840 mW and the spectral bandwidth of 18.3 nm was obtained from the Yb^{3+}:Sc_2O_3 single crystal and 75-fs pulse duration with the average power of 860 mW and the spectral bandwidth of 19.4 nm was obtained from the Yb^{3+}:Lu_2O_3 single crystal. The optical-to-optical efficiency against the incident pump power was ~16 %. We also observed large jumping of output powers at the same time as mode-locked operation starts (Fig. 5.29). The long-term mode-locking stability was monitored by a 250 kHz photodiode. By shielding the cavity from the airflow, the mode-locked operation was stable for longer than 2

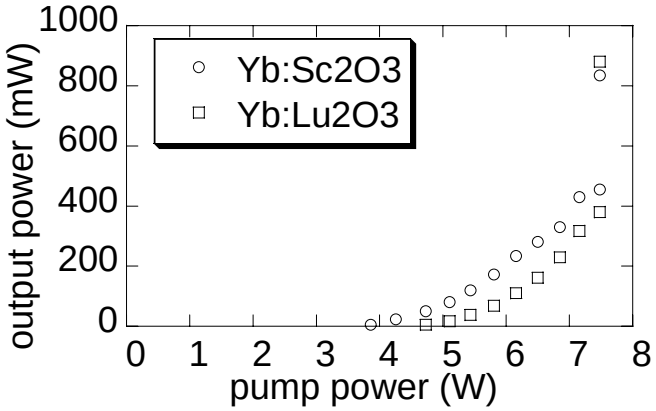

Fig. 5.29. Average power versus the incident pump power.

hours. The small long-term fluctuation seen in Fig.5.30 (a) was caused by temperature change in our laboratory (period of ~90 min.). Without the shielding, instant instability was observed (Fig. 5.30 (b)). The experiment without the half-wave plate was also done. Due to the absence of reflection loss of the pump laser beam, the average power of 1.09 W with the pulse duration of 71 fs and the spectra l bandwidth of 21.3 nm was obtained from the Yb^{3+}:Lu_2O_3 single crystal (Fig.5.31).

While we could obtain the shorter pulse duration and higher average power without the half-wave plate, we suffered destruction of the LD in the experiment. The destruction was observed at the occurrence of the instant instability, which occurred near the threshold pump power level. Even with

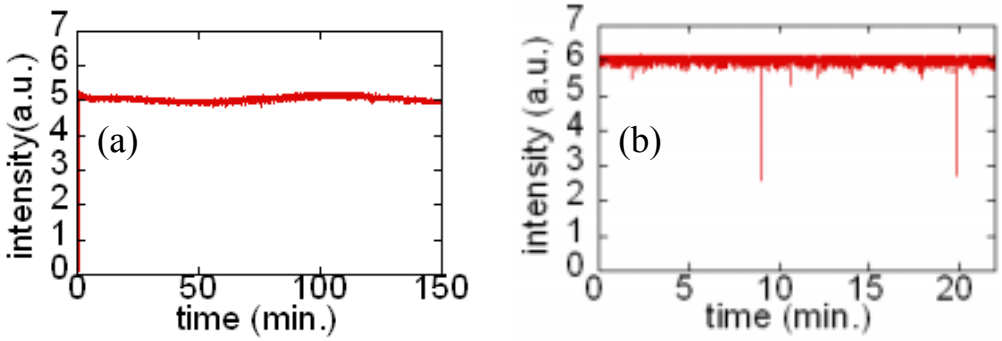

Fig. 5.30. (a)(b) Measured long-term mode-locking stability with the pulse duration of 81 fs and 840 mW average power. (a) With shielding the cavity. (b) Without shielding the cavity.

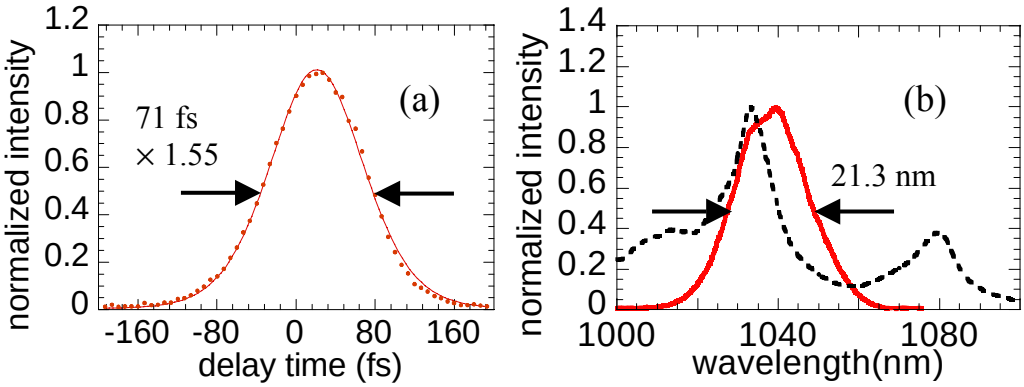

Fig. 5.31. (a) Measured autocorrelation data (dots) and $sech^2$-fitting curves (solid curve) are shown. (b) Fluorescence spectrum of Yb^{3+}:Lu_2O_3 (doted curve) and spectrum of 71 fs pulses (solid curve) are shown.

the sharp short wave pass filters (M4, M5), we have observed such destructions of LD many times. This is the reason why we used the half-wave plate and the PBS to protect the LD in the experiment. The cause of this destruction has not yet been clarified [7].

5.5 Yb^{3+}:$\{YGd_2\}[Sc_2](Al_2Ga)O_{12}$ ceramic laser

The experiments were carried out with a Z-shaped astigmatically compensated cavity as shown in Fig.5.32. As the gain medium, an Yb^{3+}:$\{YGd_2\}[Sc_2](Al_2Ga)O_{12}$ ceramic (C_{Yb} = 10 at.%, 2.2 mm thick) was used. It was put in a copper holder and arranged at the Brewster angle. The pump sources were broad-stripe LD's (emission area of 1 × 90 µm, 9 W, 972 nm, Δλ~4 nm for a cw operation and emission area of 1 × 95 µm, 12 W, 975 nm, Δλ~5 nm for a mode-locked operation). The pump beam was focused into the ceramic to $1/e^2$ diameters of about 25 µm × 190 µm by four beam-shaping lenses. In the cw operation (dashed line in the Fig.5.30), the calculated fundamental laser mode diameters inside the gain medium were about 48 × 91 µm (at the focusing point).
In case of the cw laser operations output couplers of 5% and 10% transmittances (Fig. 5.32. OC 1) were used. With the 10% OC, an average power of 2.8 W at the wavelength of 1031 nm with a 42 % optical-to-optical efficiency was obtained. With the 5% OC, an average power of 2.9 W at the wavelength of 1051 nm with a 44 % efficiency was also obtained (Fig. 5.33). In both cases, the measured laser transverse

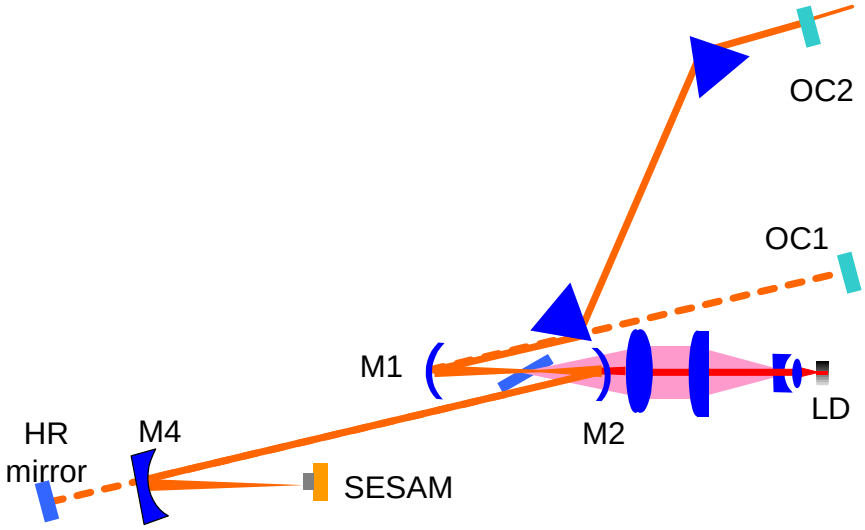

Fig. 5.32. Experimental setup. Solid line shows mode-locked operation. Dashed line shows CW operation.

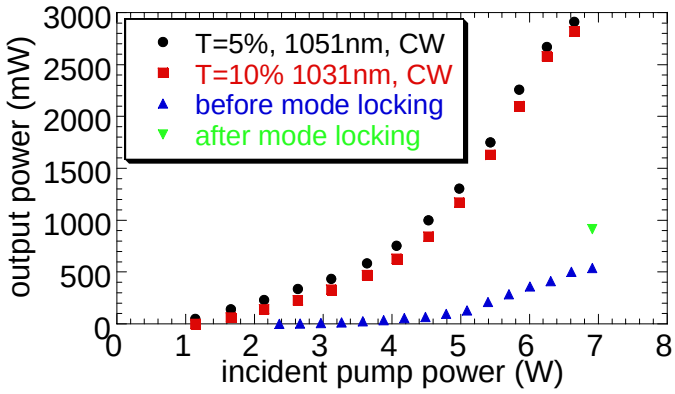

Fig. 5.33. Output power versus incident pump power in the Yb^{3+}:$\{YGd_2\}[Sc_2](Al_2Ga)O_{12}$ ceramic lasers. Continuous-wave operation at 1051 nm wavelength (circle points) and at 1031 nm (square points) as well as mode-locked operation (triangle points: before mode locking, inverse triangle points: after mode locking (86 fs)) are shown.

profiles were multi-moded, which was caused by the large difference between the pump laser profile and cavity's fundamental laser mode profile. Due to the existence of the reabsorption loss around 1030 nm, the peak position of the total gain of the Yb^{3+}:$\{YGd_2\}[Sc_2](Al_2Ga)O_{12}$ depended on the population inversion ratio of Yb^{3+} ions and therefore the dependence of the lasing wavelength on the output coupling efficiency was caused. The center wavelength of the pump source depends on its operating current (temperature) so that the absorption efficiency was also changed with the incident pump power and therefore the output powers in Fig. 5.33 showed nonlinear slopes against the incident pump power. The operation, optical-to-optical efficiency of 44 % was achieved with the Z-shaped cavity, which was used for the purpose of mode-locked operation. By using a simple cavity (as like a cavity consist of flat-concave mirrors [8]), higher efficiency would be available.

To achieve mode-locked operation, a semiconductor saturable absorber mirror (SESAM, BATOP GmbH) of 0.5% saturable absorption depth with a 500-fs recovery time and an SF10 prism pair with the tip-to-tip separation of 50 cm were inserted in the cavity. The laser beam was focused onto the SESAM by a concave mirror (M3, ROC = 400 mm). A 5% transmittance output coupler (OC 2) with a wedge of about 30 minutes was also used. Due to the insertion loss of the SESAM and prism pair, the lasing occurred at the wavelength of 1032 nm before the mode-locked operation started. To achieve short pulse duration, the cavity was carefully aligned. Pulses as short as 69 fs with the average power of 820 mW were obtained. The center wavelength and spectral bandwidth were 1042 nm and 22 nm (Fig.

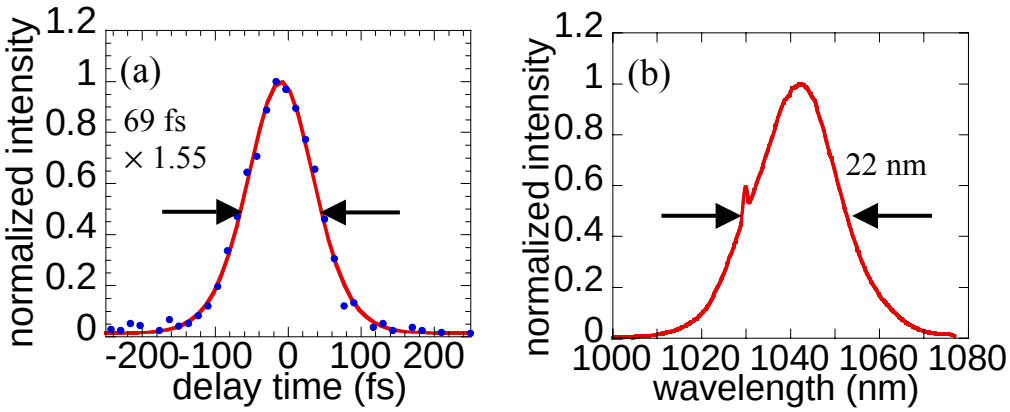

Fig. 5.34. Autocorrelation trace (a) and spectrum (b) of the Yb^{3+}:$(YGd_2)Sc_2(GaAl_2)O_{12}$ mode-locked laser.

5.34). The time bandwidth product was 0.42 and the repetition rate was 99 MHz. At the same time as the mode locking, we have observed the large jumping of output power from ~530 mW to ~850mW (depending on the pulse duration) and large change of the laser mode diameters (Fig. 5.35). The pulse duration could be tuned by modifying the alignment (insertion depth of the prisms, angle and distance between folding mirror (M1, M2), position of gain medium and position of focusing point of pump beam) and the position of center wavelength shifted to longer wavelength side with the pulse shortening (Fig. 5.36).

In case of the mode-locked operation, the short pulse operation (generally shorter than 200 fs) was achieved only with the large change of the laser mode diameters. Without it, we suffered transition to the multi-pulsed operation and pulse duration was limited to be above 200 fs. We mention here again that we suppose that the large jumping of output power and

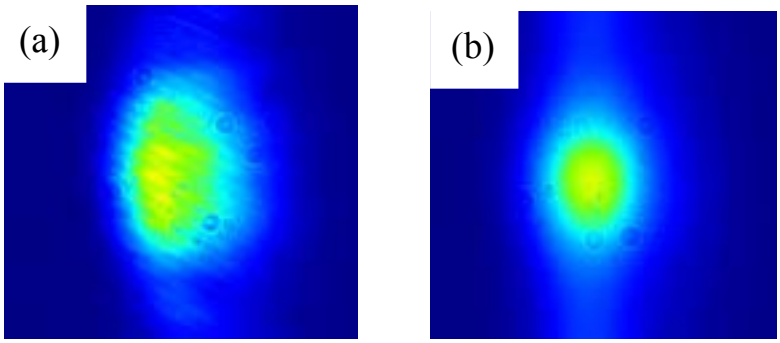

Fig. 5.35. Mode profiles of the laser beam outputs. (a) Before mode locking with the laser mode diameters of about 3100 × 2150 μm (tangential × sagittal) and (b) after the mode locking with the laser mode diameters of about 1900 × 1700 μm.

changes of laser mode diameter were caused by large Kerr-lens effect and the present short pulse operations were sustained by Kerr-lens mode locking as like our previous reports. The available wavelength range in the shorter side of the set-up was limited by the HR coating of mirrors M1, M2 and the reabsorption loss of gain material. Therefore the wavelength shift to a longer wavelength side can be caused as the spectrum broadens. The spectral bandwidth of the 69 fs pulses (22 nm) became about 1.4 times broader than the gain bandwidth of Yb^{3+}:$\{YGd_2\}[Sc_2](Al_2Ga)O_{12}$ (16 nm) and its center wavelength of 1042 nm is 12 nm longer than the peak gain position of the Yb^{3+}:$\{YGd_2\}[Sc_2](Al_2Ga)O_{12}$ (1030 nm), and therefore the gain does not have a completely flat shape across the 69 fs pulse spectrum. The $sech^2$ shape of the pulse spectra, however, was sustained in the operation. It was probably caused by a large nonlinear spectral shaping effect with a fast and large modulation depth of the Kerr-lens effect in soliton-like mode locking [9].

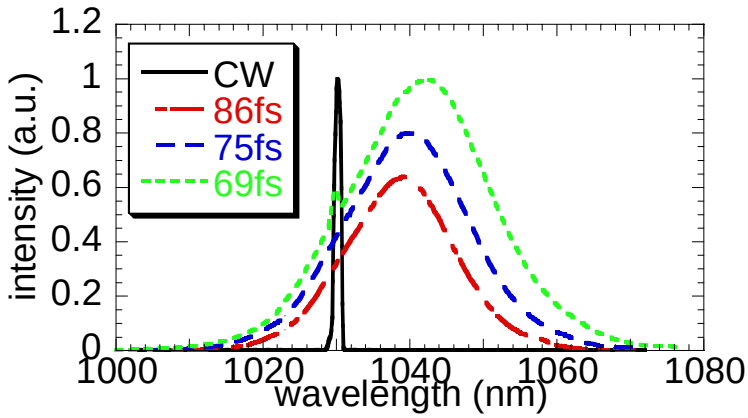

Fig. 5.36. Spectra of mode-locked pulses with several pulse durations. The center wavelength shifted with pulse shortening (spectral broadening).

5.5 Yb^{3+}:$Y_3Al_5O_{12}$ ceramic laser

We also have tried the KLM laser experiment based on Yb:YAG ceramic as a comparative study. The experimental setup is shown in Fig. 5.37 and is almost the same as we used in Yb^{3+}:{YGd_2}[Sc_2](Al_2Ga)O_{12} ceramic laser experiment except for an absence of SESAM. The OC has 5 % output coupling efficiency and the distance between prisms was 71 cm. In case of the SESAM mode-locked Yb:YAG ceramic laser, the pulse duration was limited to be above 300 fs and a transition to multi-pulsed operation was observed. Then, we replaced the SESAM by a high reflection mirror and inserted a knife-edge in output arm as a spectral selective element and hard aperture. As a result, 128 fs pulse duration with 1.35 W average power at the center wavelength of 1052 nm with a spectral bandwidth of 10.3 nm under 5.6 W incident pump power (about 6W pump power from the LD) was obtained (Fig.5. 38). The optical-to-optical efficiency versus incident pump power is about 24 %. The average power increased from 1.23 W to 1.35 W at the same time the mode locked operation started. The change of the laser mode from ~TEM_{01}-mode to ~TEM_{00}-mode was observed (Fig.

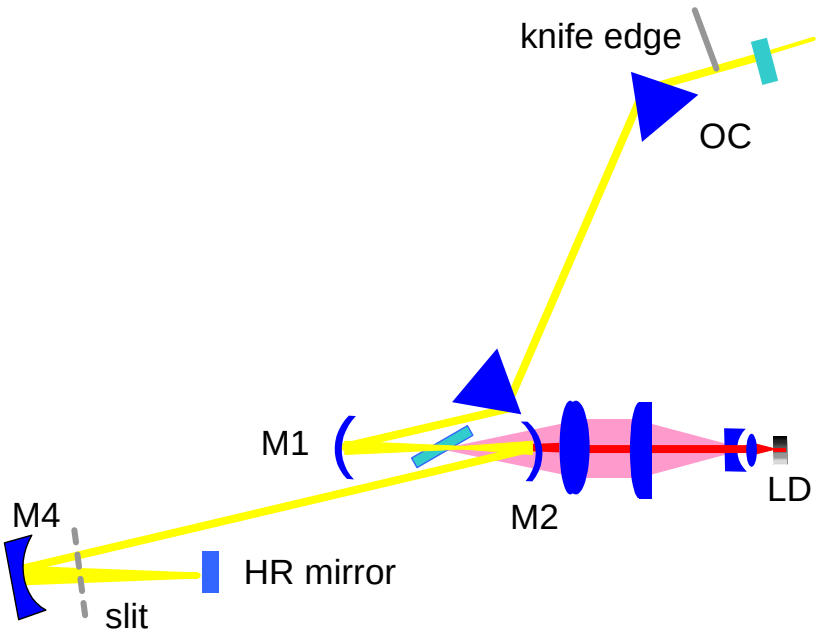

Fig. 5.37. Experimental setup of Yb^{3+}: $Y_3Al_5O_{12}$ Kerr-lens mode locked laser.

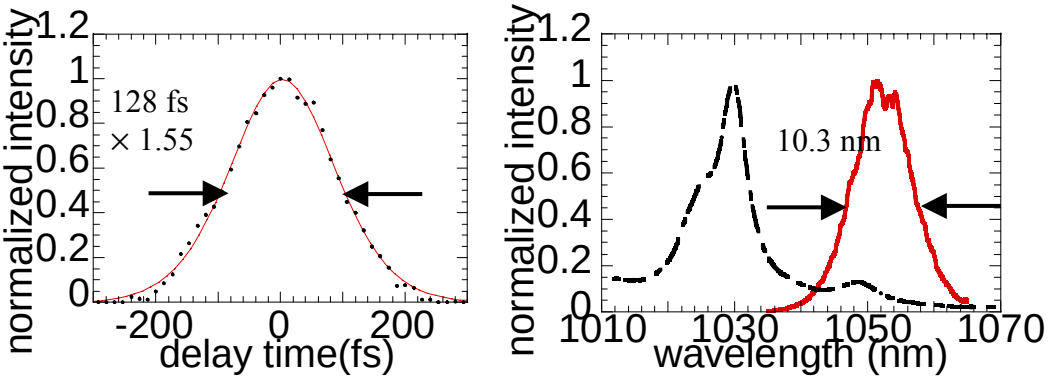

Fig. 5.38. (a) Measured autocorrelation data (dots) and $sech^2$-fitting curves (solid curve) are shown. (b) Fluorescence spectrum of Yb^{3+}:YAG (doted curve) and spectrum of 128 fs pulses are shown.

5.39) as the mode locked operation started. We also have been able to observe KLM without the concave mirror M3, but could not stabilize it. Comparison with ultrashort pulse generation from Yb:YAG reported by other group, the average power of our experiment of 1.35 W is about one order larger. Our ultrashort Kerr-lens mode locked cavity is seems to be suitable to obtain ultrashort pulse duration with high average power.

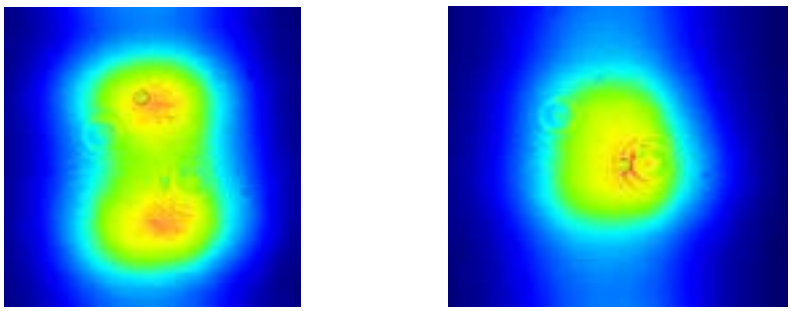

Fig. 5.39. Mode profiles of the laser outputs. (a) TEM_{01} mode appeared in the CW operation (b) TEM_{00} mode appeared in the Kerr lens mode locked operation.

References

[1] M. Tokurakawa, A. Shirakawa, K. Ueda, H. Yagi, T. Yanagitani, and A. A. Kaminskii, "Diode-pumped sub-100 fs Kerr-lens mode-locked Yb^{3+}:Sc_2O_3 ceramic laser," Opt. Lett. **32**, 3382-3384 (2007).
[2] Y. Senatsky, A. Shirakawa, Y. Sato, J. Hagiwara, J. Lu, K. Ueda, H. Yagi, and T. Yanagitani, "Nonlinear refractive index of ceramic laser media and perspectives of their usage in a high-power laser-driver," Laser Phys. Lett. **1**, 500-506 (2004).
[3] P. Wagenblast, R. Ell, U. Morgner, F. Grawert, and F. X. Kärtner, "Diode-pumped 10-fs Cr^{3+}:LiCAF laser,"Opt. Lett. **28**, 1713-1715 (2003).
[4] A. Lagatsky, C. Brown, and W. Sibbett, "Highly efficient and low threshold diode-pumped Kerr-lens mode-locked Yb:KYW laser," Opt. Express **12**, 3928-3933 (2004).
[5] M. Tokurakawa, A. Shirakawa, K. Ueda, H. Yagi, T. Yanagitani, and A. A. Kaminskii, "Diode-pumped 65-fs Kerr-lens mode-locked Yb^{3+}:Lu_2O_3 and non-doped Y_2O_3 combined ceramic laser," Opt. Lett. **33**, 1380-1382 (2008).
[6] M. Tokurakawa, A. Shirakawa, K. Ueda, H. Yagi, M. Noriyuki, T. Yanagitani, and A. A. Kaminskii, "Diode-pumped ultrashort-pulse generation based on Yb^{3+}:Sc_2O_3 and Yb^{3+}:Y_2O_3 ceramic multi-gain-media oscillator," Opt. Express **17**, 3353-3361 (2009).
[7] Will be submitted.
[8] K. Takaichi, H. Yagi, J. Lu, J. F. Bisson, A. Shirakawa, K. Ueda, T. Yanagitani, and A. A. Kaminskii, "Highly efficient continuous-wave operation at 1030 and 1075 nm wavelengths of LD-pumped Yb^{3+}:Y_2O_3 ceramic lasers," Appl. Phys. Lett. **84**, 317-319 (2004).
[9] M. Tokurakawa, H. Kurokawa, A. Shirakawa, K. Ueda, H. Yagi, T. Yanagitani, and A. A. Kaminskii, "Continuous-wave and mode-locked laser operations based on Yb^{3+}:$(YGd_2)Sc_2(GaAl_2)O_{12}$ partially disordered ceramic," Opt. Express. **18**, 4390-4395 (2010).

Chapter 6. Estimation of the gain bandwidth limitation of pulse duration

In this chapter, a gain bandwidth limitation of short pulse duration is estimated by simple rate equations. In general the limitation can be analytically calculated with Maser equation (chapter 2. equation 2.1) introduced by Haus [1,2], which is based on restoration of optical pulses (Fig. 6.1). It also can give us pulse shape and spectral shape. On the other hand, our calculation is based on competition of gain saturation effect between CW operation and mode-locked operation. It is calculated numerically with taking account for three-dimensional pump and laser light distributions, reabsorption effect, and broad spectral bandwidth. The calculation gives us necessary condition for suppressing a parasitic CW component.

$$\left[-j\psi - (L + j\chi) + g\left(1 + \frac{1}{\Omega_g^2}\frac{d^2}{dt^2}\right) + jD\frac{d^2}{dt^2} + (\gamma - j\delta)|a|^2 \right] a = 0 \qquad 2.1$$

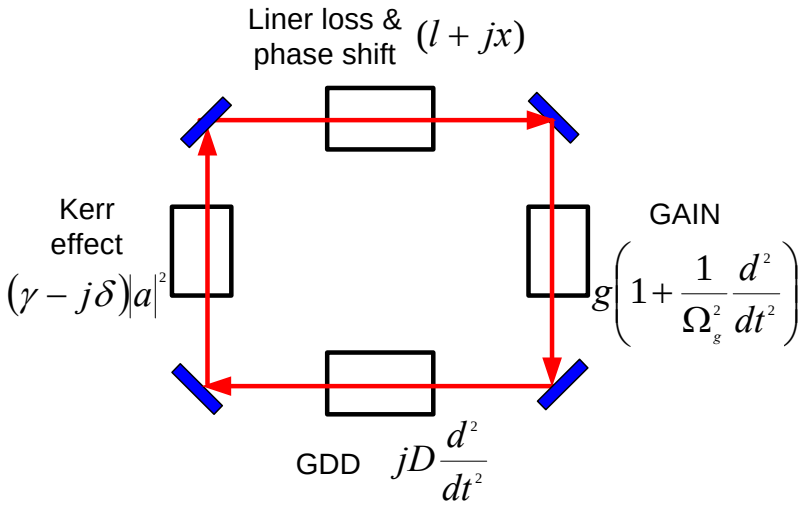

Fig. 6. 1. Schematic picture of a mode-locked ring resonator with the various pulse shaping elements. [2]

6.1 Rate equations for mode-locked laser operation

In a mode-locked laser operation, the shortest pulse duration is limited by growth of the mode-locking instabilities and/or transition to multi-pulsing operations. In general case of our experiments, before the increasing of the instability or transition to the multi-pulsed operation, a narrow spectral component appeared in the spectrum near the peak gain position. In case of the Yb^{3+}:Lu_2O_3 and Yb^{3+}:Sc_2O_3 they appeared at 1033.5 nm and 1041.5 nm, respectively (Fig. 6.2 and Fig. 6.3). We considered that the component was caused by the weaker gain saturation in the ultrashort pulse operation than that in the CW operation. We consider gain saturation effect in ultrashort pulse operation by 3-dimentional rate equations below. In a cw mode-locked operation based on Yb^{3+}-doped laser where the gain saturation effect per pulse is weak so that the gain generally can be assumed to be time independent. We also assumed fast ideal nonlinear gain/loss modulations (SESAM and Kerr-effect) having instant response times (fast saturable absorber). With these assumptions, the 3-dimensional rate equations can be written below

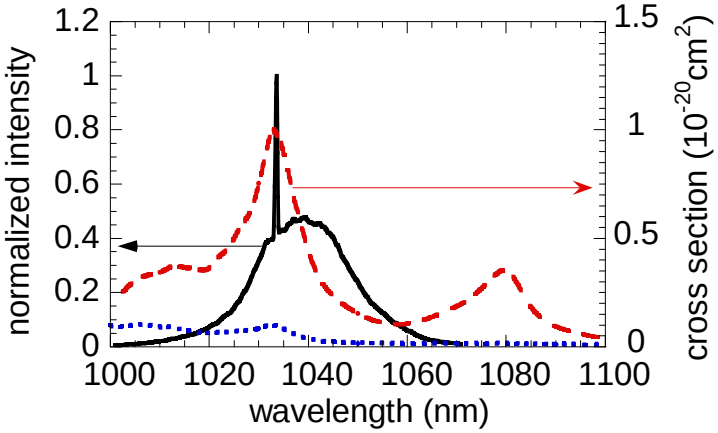

Fig. 6.2. Spectrum of pulses with an additional narrow component (black solid curve) from Yb^{3+}:Lu_2O_3. Emission (red broken curve) and absorption (blue dotted curve) cross-section spectra of Yb^{3+}:Lu_2O_3 are also shown.

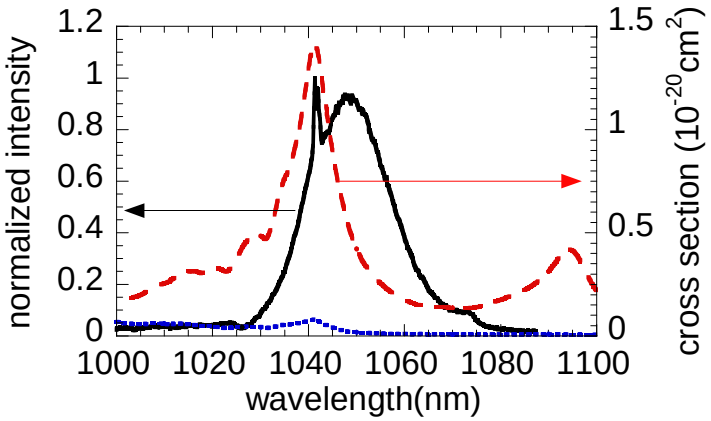

Fig. 6.3. Spectrum of pulses with an additional narrow component (black solid curve) from Yb^{3+}:Sc_2O_3. Emission (red broken curve) and absorption (blue dotted curve) cross-section spectra of Yb^{3+}:Sc_2O_3 are also shown.

$$\frac{I_{total}}{dt} = \int [cS(x,y,z)g(\lambda)\sigma_e(\lambda)N_u(x,y,z) - cS(x,y,z)g(\lambda)\sigma_a(\lambda)N_l(x,y,z)]d\lambda dV - \frac{cLI_{total}}{2l_{cavity}} \qquad 6.1,$$

$$\frac{dN_u(x,y,z)}{dt} = R_p(x,y,z) - \frac{N_u(x,y,z)}{\tau} - S(x,y,z)c\times \int [N_u(x,y,z)g(\lambda)\sigma_e(\lambda) - N_l(x,y,z)g(\lambda)\sigma_a(\lambda)]d\lambda \qquad 6.2,$$

where I_{total} is total photon number in the cavity, c is velocity of light, $S(x,y,z)$ is distribution function of the laser photon density in the cavity, $g(\lambda)$ is normalized spectral shape function of the pulses, $\sigma_e(\lambda)$ and $\sigma_a(\lambda)$ are emission and absorption cross sections of the gain medium, $N_l(x,y,z)$ and $N_u(x,y,z)$ are distribution functions of the lower and upper state Yb^{3+} ion density, l_{cavity} is cavity length, L is round-trip cavity loss and $R_p(x,y,z)$ is pumping rate distribution function. The eqs. 6.1 and 6.2 include the integral part of λ that can be considered as the effective cross section σ^{pulse} written below

$$\sigma_{e(a)}^{pulse} = \int g(\lambda)\times\sigma_{e(a)}(\lambda)d\lambda, \qquad 6.3$$

σ^{pulse} varies with the center wavelength and the spectral bandwidth of the pulses. In case of the Yb^{3+}:Lu_2O_3, the emission and absorption cross-section values at the 1033 nm peak are ~1.34×10^{-20} and 0.66×10^{-21} cm^2, respectively. In case of the our experimental result of 68-fs pulses at the center wavelength of 1038 nm with the spectral bandwidth of 20 nm, the effective emission and absorption cross-section values are calculated to be 0.61×10^{-20} and 0.34×10^{-21} cm^2, respectively. The smaller effective emission cross-section value leads to the weaker gain saturation so that the CW component having a high emission cross-section value cannot be suppressed completely. The necessary condition to suppress the CW component can be written below by threshold upper state Yb^{3+} ion density in pulsed operation $N_u^{th\_pulse}$.

$$\frac{I_{total}^{cw}}{dt} = \int [cS^{cw}(x,y,z)\sigma_e^{cw} N_u^{th\_pulse}(x,y,z) - cS^{cw}(x,y,z)\sigma_a^{cw}(N - N_u^{th\_pulse}(x,y,z))]dV - \frac{cL^{cw} I_{total}}{2l_{cavity}} < 0, \qquad 6.4$$

where N is total Yb^{3+} ion density and superscripts “pulse” and “cw” discriminate between mode-locked operation and cw operation. Assuming the stationary state with the top-hat pumping profile (radius of a in the gain medium) and lasing profile (radius of b in the gain medium, assuming $b \geq a$, shown in Fig. 6.4), from eq. 6.1 the threshold upper state Yb^{3+} ion density in mode-locked operation $N_u^{th\_pulse}$ and cw operation $N_u^{th\_cw}$ can be written below

$$N_u^{th\_pulse} = \frac{b^{pulse^2} N\sigma_a^{pulse}}{a^2\left(\sigma_e^{pulse} + \sigma_a^{pulse}\right)} + \frac{b^{pulse^2} L^{pulse}}{2a^2 l_g\left(\sigma_e^{pulse} + \sigma_a^{pulse}\right)} \qquad 6.5$$

$$N_u^{th\_cw} = \frac{b^{cw^2} N\sigma_a^{cw}}{a^2\left(\sigma_e^{cw} + \sigma_a^{cw}\right)} + \frac{b^{cw^2} L^{cw}}{2a^2 l_g\left(\sigma_e^{cw} + \sigma_a^{cw}\right)} \qquad 6.6$$

where l_g is length of gain medium. The condition 6.4 can be achieved by an additional saturable loss caused by a SESAM or by a hard aperture

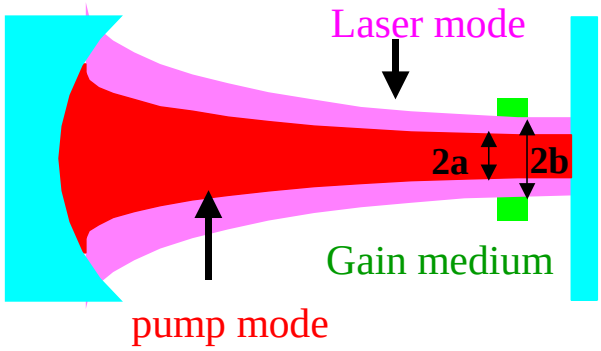

Fig. 6.4. Schematic picture of soft aperture Kerr-lens effect.

Kerr-lens effect. The soft aperture Kerr-lens effect caused by the difference between b^{pulse} and b^{cw} also can influence the N_2^{th} value.

We estimated the required modulation depth for generating 68 fs pulses (FWHM of 20 nm) from the $Yb^{3+}:Lu_2O_3$. We assume linear loss L = 8% (including the 5% output coupling loss) and $b^{pulse} = b^{cw}$. The latter assumption corresponds to absence of soft-aperture effect. In other words, assuming the mode locking is sustained only by loss modulation caused by a SESAM or hard aperture Kerr-lens effect. With this assumption the condition (6.4) can be simplified below

$$N_u^{th\_pulse} - N_u^{th\_cw} = \frac{2l_g N\sigma_a^{pulse} + L^{pulse}}{2l_g\left(\sigma_e^{pulse} + \sigma_a^{pulse}\right)} - \frac{2l_g N\sigma_a^{cw} + L^{cw}}{2l_g\left(\sigma_e^{cw} + \sigma_a^{cw}\right)} < 0 \qquad 6.7.$$

We used the emission and absorption cross-section values at the wavelength of 1033.5 nm in the CW operation. Because of the existence of the reabsorption loss, $N_2^{th\_cw}$ has the lowest value at the wavelength of 1033.5 nm and it agrees experimental result. Under these assumptions, the required modulation depth can be calculated to be ~ about 6 %, more than 15 times bigger than the modulation depth of the SESAM (less than 0.4% modulation depth.) used in the experiment. We conclude that our experimental results of sub-100-fs ultrashort pulse operations were mainly sustained by Kerr-lens effect. As can be shown in eq. 6.7, the necessary condition depends on doping level of Yb^{3+} ion (reabsorption effect). The wavelength of CW component where $N_u^{th\_cw}$ take minimum value also

depend on pulse duration. The required modulation depth shows strong dependence on linear cavity losses (Fig.6.5 (a)).
We have also estimated the required condition with the assumption of the same cavity loss both in the CW and pulsed operations, and the ratios of laser mode and pump mode radius $b^{cw(pulse)}/a$ >1. In other words, assuming the mode locking is sustained only by soft aperture mode locking. With this assumption the condition (4) can be written as below

$$N_u^{th\_pulse} - N_u^{th\_cw} = \frac{b^{pulse^2}\left(2l_g N\sigma_a^{pulse} + L\right)}{l_g\left(\sigma_e^{pulse} + \sigma_a^{pulse}\right)} - \frac{b^{cw^2}\left(2l_g N\sigma_a^{cw} + L\right)}{l_g\left(\sigma_e^{cw} + \sigma_a^{cw}\right)} < 0. \quad 6.8.$$

If we assume no reabsorption effect, the eq. 6.8 becomes

$$N_u^{th\_pulse} - N_u^{th\_cw} = \frac{b^{pulse^2}}{\sigma_e^{pulse}} - \frac{b^{cw^2}}{\sigma_e^{cw}} < 0. \quad 6.9,$$

eq. 6.9 obviously shows that the soft aperture Kerr-lens mode locking is independent from linear cavity loss in case if there is no reabsorption effect. The calculated result of equation 6.8 (including reabsorption effect) is shown in Fig.6.5 (b). To obtain 68 fs pulse duration, the required change of laser mode area is roughly about 35 %, which is lower than the available soft aperture Kerr-lens effect in chapter 4 and therefore the calculated soft aperture Kerr-lens effect of our mode locked laser cavity was enough for generating 68-fs pulses. The required change of the laser mode area In Fig. 6.5 (b) shows smaller dependence on linear cavity losses (Fig. 6.5 (b)) than that of eq. 6.7. The reason easily can be understand from eq. 6.9. On the other hand, The Fig 6.5 (b) shows that the required change of the laser mode area strongly depend of *N* value due to its reabsorption effect. In the estimation we assumed top-hat laser mode and pump mode profiles and they probably make some differences from experiment (Gaussian laser mode profile). However the order of the requirements and physical behavior should be correct. Above calculation also can be expanded to Gaussian laser mode profiles.
These requirements are caused by finite bandwidth of gain material and

therefore the broad gain bandwidth is still very important for suppressing these requirements even though we have succeeded in generating ultrashort pulses overcoming their general gain bandwidth limitation.

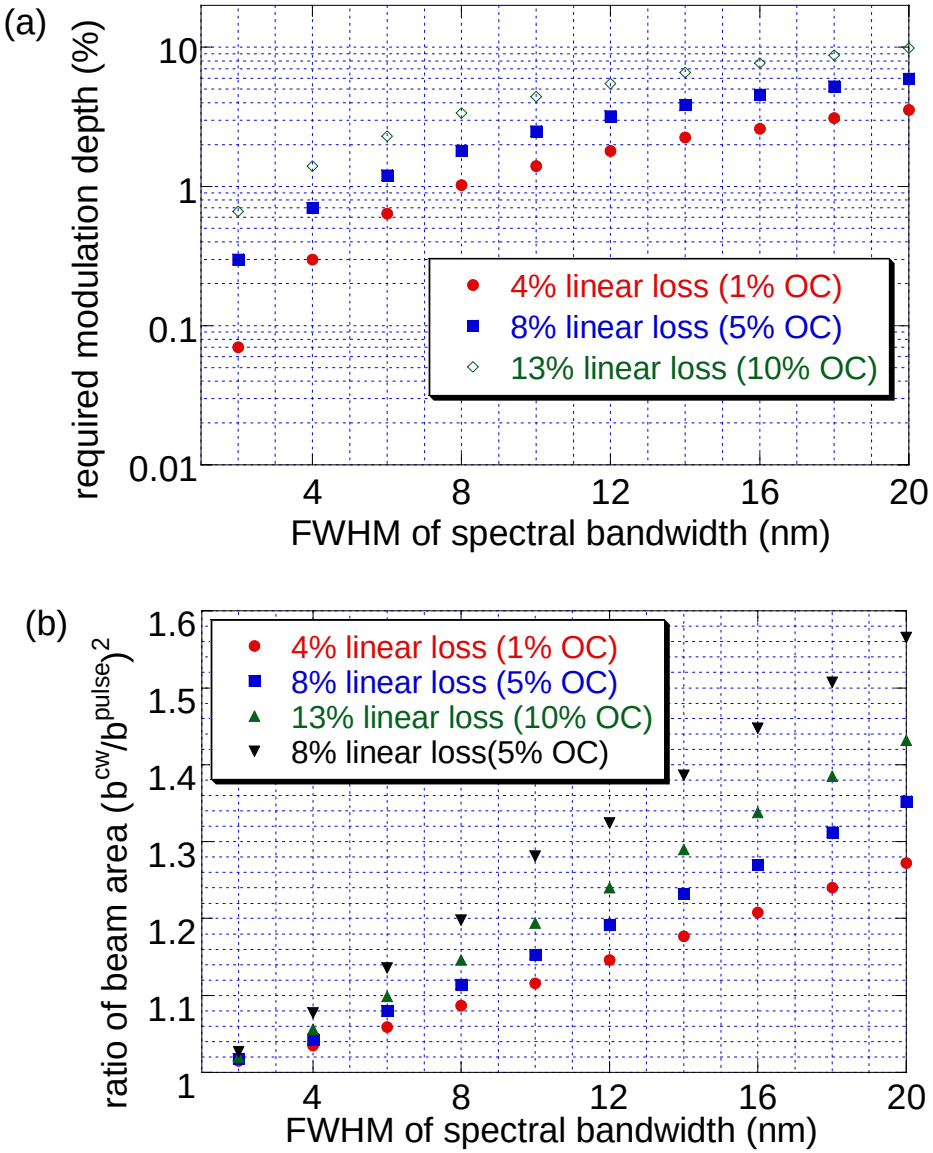

Fig. 6.5. Necessary condition for suppressing parasitic cw oscillation component of (a) Mode locking based on loss modulation and (b) Mode locking based on soft aperture Kerr-lens mode locking are shown. The gain material is 3 at % 1 mm thick Yb^{3+}:Lu_2O_3 except for inverse triangles points in (b) (1.5 at % 0.5 mm thick Yb^{3+}:Lu_2O_3).

6.2 Calculation of output power

We have also calculated the output power property based on 3-dimentional rate equations. In the calculation we used below parameters, linear loss = 9% (5%OC), the effective emission and absorption cross-section values of 0.62×10^{-20} and 0.34×10^{-21} cm^2, in mode-locked operation and 1.17×10^{-20} and 0.67×10^{-21} cm^2 in CW operation. Saturable absorption loss of SESAM = 0.4%. The calculated result and experimental result of 81 fs Yb:Lu_2O_3 are shown in Fig. 6.6. The experimental result and calculated result show some agreement. The nonlinear shape of the experimental output power property was caused by change of the wavelength of pumping light. The pulse duration calculated from soliton equation is about ~70 fs, which also show roughly agreement with the experimental result.

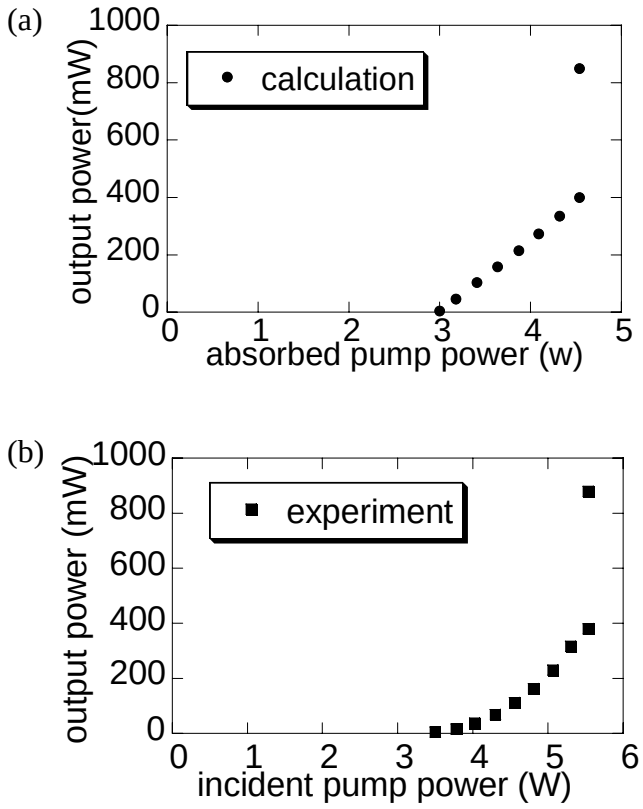

Fig. 6.6. Output power versus absorbed pump power of incident pump power. (a) Calculation result. (b) Experimental result.

References

[1] H. A. Haus, J. G. Fujimoto, and E. P. Ippen, “Structures for additive pulse mode locking,” J. Opt. Soc. Am. B **8**, 2068-2076 (1991).
[2] H. A. Haus, J. G. Fujimoto, “Analytic Theory of Additive Pulse and Kerr Lens Mode Locking,” IEEE J. Quantum Electron. **28**. 2086-2096 (1992).

Chapter 7. Summary and outlook

In this thesis, ultrashort pulse laser operations based on Yb^{3+}-doped materials were described. To obtain power scalability, every experiment was done with direct LD pumping. The gain media having good thermal and mechanical properties were also used for the same purpose. Their properties are shown in chapter 3. However, the available gain bandwidths with such gain media are restricted and narrower than those of other gain media used for ultrashort pulse (<100 fs) laser operation (e.g. glass materials, disordered materials.). In case of the SEASM mode locked laser operation, due to their gain bandwidth limitation, the shortest pulse duration was strongly limited to be ~200 fs by the transition to the multi-pulsed operation and appearance of CW component. The estimation of such gain bandwidth limitation was described in chapter 6. The keys to suppress such phenomenon are to obtain fast and large gain/loss modulation depth, large SPM effect and broad gain bandwidth. In this thesis we have succeeded in overcoming such conventional gain bandwidth limitation by using a large Kerr-lens effect. The modulation depth of the Kerr-lens effect depends on both of the pulse energy and pulse duration, which also make strong suppression effect of multi-pulsed operation. It is big difference from conventional SESAM mode locking. The design of the Kerr-lens mode locked cavity and the calculation of its soft aperture Kerr-lens effect are shown in chapter 4. In general, the available pulse duration tend to be limited by a spectral bandwidth of the gain bandwidth. However, in case of the soliton (solitonlike) mode locking, the pulse and spectral shapes obey solution of nonlinear Schrödinger equation with nonlinear temporal and spectral shaping effect. Combination with large modulation depth, the pulse duration can be shorter than the duration of temporal gain window and the spectral bandwidth can be broader than its gain bandwidth limitation. Such spectral broadening above its gain

bandwidth limitation was also reported in KLM Ti^{3+}:Al_2O_3 laser cases. However, the broad gain bandwidth is still important to generate further ultrashort pulses. To achieve further short pulse duration, Kerr-lens mode-locked operation based on multi-gain media oscillator was demonstrated. The multi-gain media oscillator can broaden the effective gain bandwidth without degrading their thermal and mechanical properties. The information of the multi-gain media used in this thesis is shown in chapter 3. By the combination of the multi-gain media and large soft aperture Kerr-lens effect, as short as 53 fs pulse duration with the average power of 1 W has been obtained by a LD pumping. The properties of Yb^{3+}-doped Kerr-lens mode-locked lasers obtained in this thesis are shown in table 7.1 (chapter 5). Due to their superior thermal and mechanical properties, they will be used in much higher average power laser operation.

Table 7.1. Properties of Yb^{3+}-doped Kerr-lens mode locked lasers.

Host material	P_{out} (mW)	Δt (fs)	Δλ (nm)	Method	Effi. (%)	P_{pump} (W)
Sc_2O_3 ceramic	850	92	13.7	KLM	19	4.5
	515	250	4.7	SESAM	11	4.5
Lu_2O_3 crystal	1090	71	21.3	KLM	15	7.4
	352	357	3.2	SESAM	8.8	4
Sc_2O_3 crystal	840	81	18.3	KLM	16	5.2
Y_2O_3 ceramic	540	68	20	KLM	11	5
	220	188	6.4	SESAM	5.5	4
Lu_2O_3 ceramic	320	65	18.9	KLM	6.4	5
Sc_2O_3 & Y_2O_3	1500	66	19.7	KLM	19	7.4
	1000	53	27.3		14	
$(YGd_2)Sc_2(Al_2Ga)O_{12}$	820	69	22	KLM	12	6.9
YAG	1350	128	10.3	KLM	25	5.3

Future Works

To achieve further high power ultrashort pulse laser operations, we have to overcome some problems: heat loads, excess nonlinearlity and coating damage. The gain materials used in this thesis are suitable for reducing heat loads. On the other hand, the cavity design is also should be optimized for further high average power operation. The one of the promising cavity design for above purpose is thin-disk laser concept [1], which enables highly efficient cooling, low material nonlinearity and reducing coating damage due to its thin gain material length (typically < 400 μm) and large laser mode diameters (typically > 1mm) (Fig.7.1). In case of the sub-ps pulse duration, an average power of above 100 W has been reported. It is very interesting question that how large Kerr-lens effect can be available

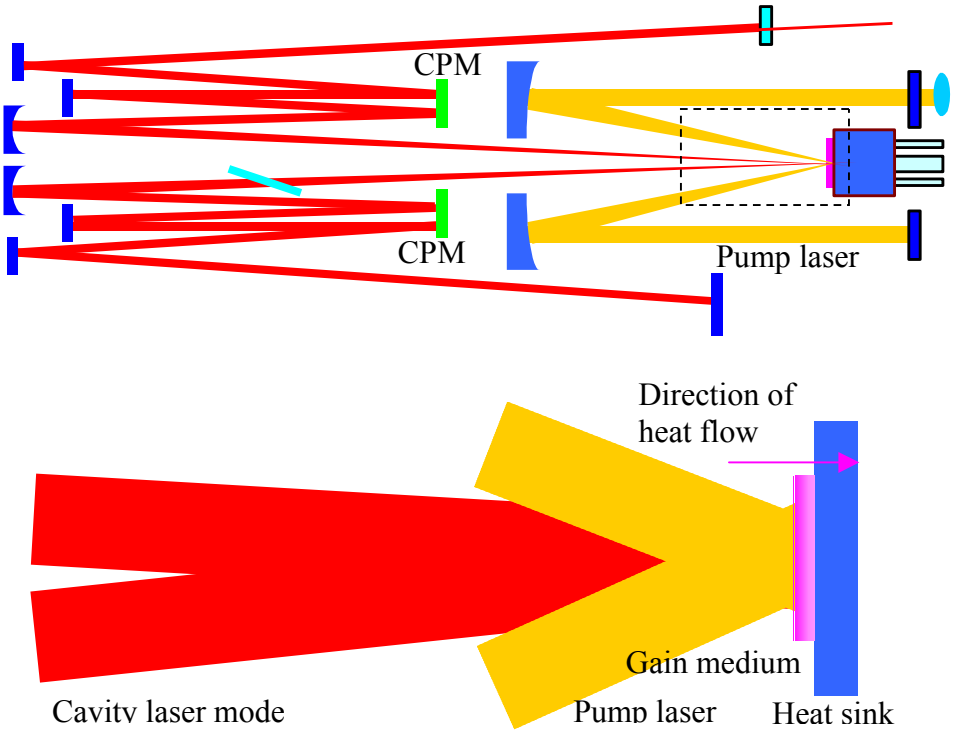

Fig. 7.1. Schematic picture of our thin-disk laser cavity. CPM is chirped mirror. Bottom side shows enlargement of dashed square area in the upside picture.

with a thin-disk cavity. If we could obtain large gain/loss modulation depth by Kerr-lens effect with thin-disk, we might be able to obtain ultrashort pulses with further high average power. The Kerr-lens effect itself is proportional to l/d^4 (l and d are material length and laser mode diameter), and therefore the Kerr-lens effect becomes very small in thin-disk laser cavity. However, the important thing for Kerr-lens mode locking is not the strength of Kerr-lens effect itself. The most important thing is the strength of available change of laser cavity mode by induced Kerr-lens effect, which strongly depends on cavity configurations (laser mode diameters, curvatures of cavity mirrors and so on). The calculated Kerr-lens effect in our thin-disk laser cavity (under preparing) is shown in Fig. 7.2, which obviously shows that large soft (hard) aperture Kerr-lens effect can be obtained even in thin-disk laser cavity. In addition its thin gain material length give us one big advantage in Kerr-lens mode-locked laser operation. It can eliminate the requirement of high beam quality pump source, which is required in conventional Kerr-lens mode-locked lasers to control pump laser mode diameters along gain media. The Kerr-lens mode-locked laser operations with broad-stripe LD pumping in this thesis were also suffered such requirement so that the soft aperture Kerr-lens effect only at sagittal plan could be used. We believe the high average power (>30W, fluence on

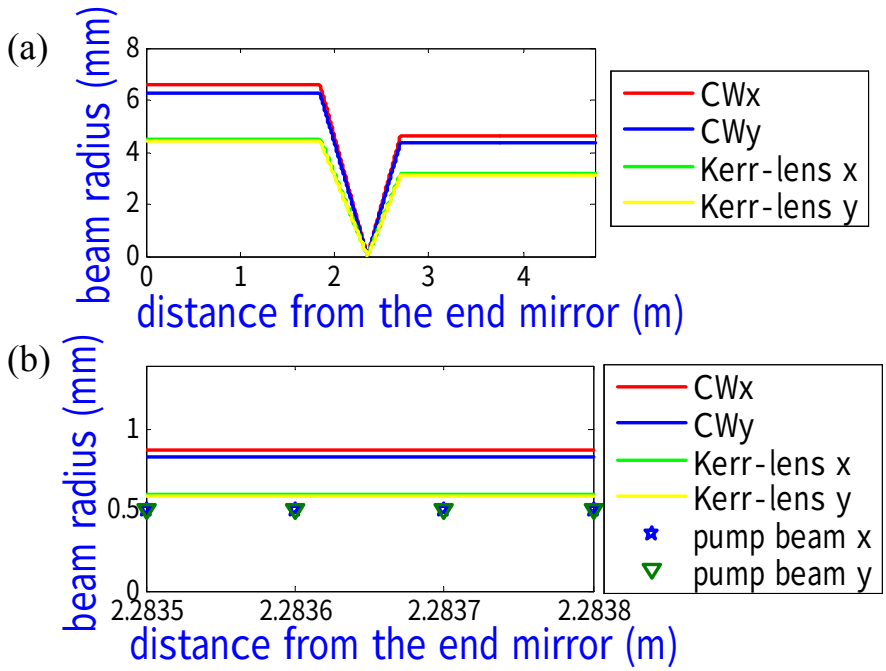

Fig. 7.2. Calculated laser beam radii with thin-disk laser cavity. (a) Laser beam radii inside the cavity and (b) Laser beam radii inside the gain material are shown. We assume pulse energy of 10 μJ and pulse duration of 81 fs inside the cavity.

gain material surface is ~1mJ/cm^2 (one pulse), which is still smaller than coating damage threshold) femtosecond laser operation with sub-100 fs pulse duration at high repetition rate would be available by thin-disk laser cavity in future and we are preparing it. For such a Kerr-lens mode locked thin-disk laser operation, a high precise multi-pass pumping unit is necessary to control pump spot size. In addition, in case of the thin-disk laser, coating damage at material top surface, however, would become problem even in lower laser fluence level than its damage threshold fluence. It is probably caused by its high average power and high temperature at top surface caused by its buck surface cooling constructor. The bonding of nondoped material its top surface might be useful to decrease temperature.

In case of the high pulse energy (> 1 μJ) femtosecond laser operation at low repetition rate, generally large nonlinearlty inside the long cavity including material and air becomes problem which lead to multi-pulsed instability. However, we suppose such multi-pulse instability can be suppressed by large modulation depth based on Kerr-lens effect and or large negative dispersion. Such nonlinearlity would become serious problem in much high pulse energy cavity (> 10 μJ) or extremely long cavity. Vacuum cavity or Helium filled cavity can be used to suppress it. We suppose coating damage at material surface will be more serious problem in high pulse energy ultrashort pulse laser operation as in an ultrashort pulse amplifier system. One of the promising cavities for achieving high pulse energy is multi-pass (laser mode) cavity with extremely high output coupling efficiency [2]. It can significantly reduce the pulse energy inside the cavity. The problem of such cavity is requirement of very large loss/gain modulation depth for short pulse duration. For such large output-coupling cavity, soft aperture Kerr-lens mode locking would be suitable. For a Kerr-lens mode locking, the fluctuation of laser mode size and position at gain material in each pass would be problem. I suppose a combination of soft aperture and hard aperture Kerr-lens mode locking should be used in such multi-pass Kerr-lens mode locked laser cavity.

For further high pulse energy, an amplifier system should be applied. For suppressing gain narrowing effect the concept of multi-gain media could be used in future.

References

[1] A. Giesen and J. Speiser “Fifteen Years of Work on Thin-Disk Lasers: Results and Scaling Laws,” IEEE JSTQE **13**, 598-609 (2007).
[2] J. Neuhaus, D. Bauer, J. Zhang, A. Killi, J. Kleinbauer, M. Kumkar, S. Weiler, M. Guina, D. H. Sutter, and T. Dekorsy, “Subpicosecond thin-disk laser oscillator with pulse energies of up to 25.9 microjoules by use of an active multipass geometry,” Opt. Express **16**, 20530-20539 (2008).

Acknowledgements

I wish to express my sincere appreciation to my supervisor Prof. Ken-ichi Ueda, for guiding me for 7 years since I was undergraduate student. I am so thankful for the guidance, encouragement, and many important advices. His encouragement helped shape the direction of my work. I am also so thankful for his giving me the opportunity to do research work freely in ILS and to join international conferences many times..

At the same time, I also wish to express my sincere appreciation to Dr. Akira Shirakawa, for his personal quality, friendly and great patient supports in my all research works.

I would like to thank Dr. Mitsuru Musha for spending his valuable time for helping me to do the experiments and giving me helpful advises.

I would like to thank Dr. Hideki Yagi, Dr. Takagimi Yanagitani, Mr Noriyuki Meichin and Mr. Syunsuke Hosokawa in Konoshima Chemical Co. Ltd. Their excellent works in fabrication of laser ceramic materials strongly supported all of my research works.

I would like to thank Prof. Alexander. A. Kaminskii for his very interesting advisees and great works especially in spectroscopy and mechanical properties measurements of ceramic materials. His works greatly helped my research. His great passion for the science is very exciting .

I would like to thank Prof. Ken'ichi Nakagawa, Prof. Hitoki Yoneda, Prof. Hajime Nishioka and Dr. Bisson for spending their valuable time for teaching me about ultrashort pulse lasers, experimental knowledge, and interest of physics. I also would like to thank for their important advises and comments about my research works.

I would like to thank Prof. Kohzo Hakuta who was the program leader of the 21st Century COE program on 'Coherent Optical Science'. Thanks to the support from COE, I could concentrate on my research works.

I would like to thank Prof. Günter Huber, Dr. Klaus Petermann, Dr. Rigo Peters, and Ms. Susanne. T. Fredrich-Thornton in Hamburg University. Their single crystals were very helpful for my work. I also wish to express my sincere appreciation for their deep kindness.

I would like to thank Dr. Kazunori Takaichi and Dr. Lu for their preceded research works of ceramic lasers. Their works are helpful for my works.

I also would like to thank my coworkers in ILS for spending delightful life with me in ILS.

I also would like to thank the Japan Science and Technical Agency for supporting my Ph.D.

I also would like to thank my mother for constant and very patient encouragements in my life.

Publications

In Journals

[1] M. Tokurakawa, K. Takaichi, A. Shirakawa, K. Ueda, H. Yagi, S. Hosokawa, T. Yanagitani and A. A. Kaminskii, "Diode-pumped mode-locked Yb^{3+}:Lu_2O_3 ceramic laser," Opt. Express, Vol.**14**, 12832-12838 (2006).

[2] M. Tokurakawa, K. Takaichi, A. Shirakawa, K. Ueda, H. Yagi, T. Yanagitani and A. A. Kaminskii, "Diode-pumped 188-fs mode-locked Yb^{3+}:Y_2O_3 ceramic laser," Appl. Phys. Lett. Vol.**90**, 071101 (2007).

[3] M. Tokurakawa, A. Shirakawa, K. Ueda, H. Yagi, T. Yanagitani, and A. A. Kaminskii, "Diode-pumped sub-100 fs Kerr-lens mode-locked Yb^{3+}:Sc_2O_3 ceramic laser," Opt. Lett. Vol. **32**, 3382-3384 (2007).

[4] M. Tokurakawa, A. Shirakawa, K. Ueda, H. Yagi, T. Yanagitani, and A. A. Kaminskii, "Diode-pumped 65-fs Kerr-lens mode-locked Yb^{3+}:Lu_2O_3 and non-doped Y_2O_3 combined ceramic laser" Opt. Lett. Vol. **33,** 1380-1382 (2008).

[5] M. Tokurakawa, A. Shirakawa, K. Ueda, H. Yagi, M. Noriyuki, T. Yanagitani, and A. A. Kaminskii, "Diode-pumped ultrashort-pulse generation based on Yb^{3+}:Sc_2O_3 and Yb^{3+}:Y_2O_3 ceramic multi-gain-media oscillator," Opt. Express **17**, 3353-3361 (2009)

[6] M. Tokurakawa, H. Kurokawa, Ae. Shirakawa, K. Ueda, H. Yagi, T. Yanagitani, and A. A. Kaminskii, "Continuous-wave and mode-locked lasers on the base of partially disordered crystalline Yb^{3+}:{YGd_2}[Sc_2](Al_2Ga)O_{12} ceramics," Opt. Express **18**, 4390-4395 (2010).

Conference Talks

International

[1] M. Tokurakawa, H. Kurokawa, A. Shirakawa, K. -i. Ueda, H. Yagi, T. Yanagitani, and A. A. Kaminskii, "Diode-Pumped Kerr-Lens Mode-Locked Yb^{3+}:Sc_2O_3 and Yb^{3+}:Y_2O_3 Combined Active Media Ceramic Laser," in *Advanced Solid-State Photonics*, OSA Technical Digest Series (CD) (Optical Society of America, January, 2008, Japan), paper MG2. Oral

[2] M. Tokurakawa, A. Shirakawa, K. -i. Ueda, H. Yagi, T. Yanagitani, and A. A. Kaminskii, "Diode-pumped Kerr-lens mode-locked ceramic laser," The Sixth Asia Pacific Laser Symposium, (Co-organized by: The laser society of Japan, The Chinese Optical Society, Optical Society of Korea, January 2008, Japan), paper 31Bp4, Oral

[3] M. Tokurakawa, A. Shirakawa, K. -i. Ueda, H. Yagi, T. Yanagitani, and A. A. Kaminskii, "Diode-pumped sub 60-fs Kerr-Lens mode-locked Yb-doped sesquioxide combined ceramic laser," in Conference of laser and Electro-Optics, (Optical Society of America, May, 2008, San Jose), paper CFP6, Oral

[4] M. Tokurakawa, A. Shirakawa, K. -i. Ueda, H. Yagi, T. Yanagitani, and A. A. Kaminskii, "Diode-Pumped Sub 100-fs Kerr-Lens Mode-Locked Yb^{3+}:Sc^2O^3Ceramic Laser with High Average Power," in *Advanced Solid-State Photonics*, OSA Technical Digest Series (CD) (Optical Society of America, January, 2008), paper WB9. Poster

[5] M. Tokurakawa, A. Shirakawa, K. -i. Ueda, H. Yagi, T. Yanagitani, and A. A. Kaminskii, "Diode-Pumped 65-fs Kerr-Lens Mode-Locked Combined Yb-Doped

Sesquioxide Ceramic Laser," in *Advanced Solid-State Photonics*, OSA Technical Digest Series (CD) (Optical Society of America, January, 2008), paper WB16. Poster
[6] Masaki Tokurakawa, Akira Shirakawa, Ken-ichi Ueda, Hideki Yagi, Takagimi Yanagitani, and Alexander A. Kaminskii, "Diode-pumped Kerr-lens mode-locked Yb^{3+}:sesquioxide ceramic lasers," 3rd Laser Ceramic Symposium 2007, Paris, 9 October. 2007, Oral
[7] Masaki Tokurakawa, Akira Shirakawa, Ken-ichi Ueda, Hideki Yagi, Takagimi Yanagitani, and Alexander A. Kaminskii, **"**Diode-pumped Kerr-lens mode-locked Yb^{3+}:sesquioxide ceramic lasers," COE Inter national symposium December 2007, invited Oral
[8] M. Tokurakawa, A. Shirakawa, K. Ueda, R. Peters, S. Fredrich-Thornton, K. Petermann, G. Huber, H. Yagi, T. Yanagitani, and A. A. Kaminskii, "Ultra-Short Pulses from Diode-Pumped Yb^{3+}-Doped Crystal and Ceramic Lasers with High Average Power," in *Advanced Solid-State Photonics*, OSA Technical Digest Series (CD) (Optical Society of America, 2009), paper MC3
[9] M. Tokurakawa, A. Shirakawa, K. Ueda, H. Yagi, T. Yanagitani, and A. A. Kaminiskii, "Continuous-Wave and Mode-Locked Laser Operations Based on Yb^{3+}:$(YGd_2)Sc_2(GaAl_2)O_{12}$Disordered Ceramic," in *Conference on Lasers and Electro-Optics/International Quantum Electronics Conference*, OSA Technical Digest (CD) (Optical Society of America, 2009), paper CFO3.
[10] M. Tokurakawa, A. Shirakawa, K. Ueda, R. Peters, S. Fredrich-Thornton, K. Petermann, G. Huber, H. Yagi, T. Yanagitani, and A. A. Kaminskii, "Femtosecond Diode-Pumped Yb-Doped Crystal and Ceramic Lasers with High Average Power," Inter national laser physics workshop, 2009 Spain Barcelona, invited talk**"**

Domestic Conferences

[1] ○**戸倉川 正樹**, **高市 和則**, **八木 秀喜**, **白川 晃，植田 憲一**, **細川 俊介**,**柳谷 高公**, Alexander A.Kaminskii**「イッテルビウム添加** Lu_2O_3 **セラミックレーザー」** 2005 **年春季第** 52 **回応用物理学関係連合講演会**, **口頭**
[2] ○**戸倉川 正樹**, **高市 和則**, **八木 秀喜**, **白川 晃，植田 憲一**, **細川 俊介**, **柳谷 高公**, Alexander A.Kaminskii**「**Yb^{3+}**添加希土類酸化物セラミックモード同期レーザー」**2006 **年** 2 **月、レーザー学会学術講演会第** 26 **回年次大会**, **口頭**
[3] ○**戸倉川 正樹**, **高市 和則**, **八木 秀喜**, **白川 晃，植田 憲一**, **細川 俊介**, **柳谷 高公**, Alexander A.Kaminskii**「**Yb^{3+}**添加希土類酸化物セラミックモード同期レーザー」**2006 **年** 3 **月、第** 6 **回レーザー学会東京支部研究会／電気学会光量子デバイス研究会**, **口頭、**
[4] ○**戸倉川 正樹**, **高市 和則**, **八木 秀喜**, **白川 晃，植田 憲一**, **細川 俊介**, **柳谷 高公**, Alexander A.Kaminskii**「**LD **励起** Yb^{3+}**添加希土類酸化物セラミックモード同期レーザー」**2006 **年** 3 **月、春季第** 53 **回応用物理学関係連合講演会**, **口頭**
[5] ○**戸倉川 正樹**, **白川 晃**, **植田 憲一**, **八木 秀喜**, **柳谷 高公**, Alexander A. Kaminskii, **「波長可変** Yb^{3+}:Y_2O_3 **セラミックレーザー」平成** 19 **年秋季第** 68 **回応用物理学会学術講演会**, **口頭**
[6] ○**戸倉川 正樹**, **白川 晃**, **植田 憲一**, **八木 秀喜**, **柳谷 高公**, Alexander A. Kaminskii, **平成１９年度　日本光学会名古屋講演会　「最近の高出力レーザーの開発状況と産業応用」**

「高出力超短パルスセラミックレーザー光源」招待講演
[7] ○戸倉川 正樹, 白川 晃, 植田 憲一, 八木 秀喜, 柳谷 高公, Alexander A. Kaminskii,「カーレンズモード同期 Yb^{3+}:Lu_2O_3:Y_2O_3 複合セラミックレーザー」, 2008 年 2 月,レーザー学会学術講演会第 28 回年次大会,7pF7, 口頭
[8] ○戸倉川 正樹, 白川 晃, 植田 憲一, 八木 秀喜, 柳谷 高公, Alexander A. Kaminskii ,「カーレンズモード同期Ｙｂ添加複合利得媒質セラミックレーザー」,平成 20 年春季第 55 回応用物理学会学術講演会,口頭
[9] ○戸倉川 正樹, 白川 晃, 植田 憲一, 八木 秀喜, 柳谷 高公, Alexander A. Kaminskii ,「カーレンズモード同期Ｙｂ添加複合利得媒質セラミックレーザー」,平成 20 年春季第 69 回応用物理学会学術講演会,講演奨励賞　受賞記念講演
[10] ○戸倉川 正樹, 黒川 裕章, 白川 晃, 植田 憲一, 八木 秀喜, 柳谷 高公, Alexander A. Kaminskii , 「Yb^{3+}:$(YGd_2)Sc_2(GaAl_2)O_{12}$ セラミックレーザー」,平成 21 年秋季第 56 回応用物理学会学術講演会,口頭
[11] ○戸倉川 正樹, 黒川 裕章, 白川 晃, 植田 憲一, 八木 秀喜, 柳谷 高公, Alexander A. Kaminskii , 「カーレンズモード同期 Yb 添加希土類三二酸化物レーザー」,平成 21 年春季第 70 回応用物理学会学術講演会, 口頭
[12] ○戸倉川 正樹,白川 晃, 植田 憲一、「LD 直接励起フェムト秒 Yb 添加セラミックレーザー」、超高速光エレクトロニクス研究会 2009 年 11 月 10 日筑波　招待講演

Award

[1] M. Tokurakawa, H. Kurokawa, A. Shirakawa, K. -i. Ueda, H. Yagi, T. Yanagitani, and A. A. Kaminskii, "Diode-Pumped Kerr-Lens Mode-Locked Yb^{3+}:$Sc_2O_3$and Yb^{3+}:Y_2O_3 Combined Active Media Ceramic Laser," in *Advanced Solid-State Photonics*, OSA Technical Digest Series (CD) (Optical Society of America, January, 2008, Japan), paper MG2. Research promotion Award
[2] 戸倉川 正樹, 白川 晃, 植田 憲一, 八木 秀喜, 柳谷 高公, Alexander A. Kaminskii , 「カーレンズモード同期Ｙｂ添加複合利得媒質セラミックレーザー」,平成20年春季第55回応用物理学会学術講演会,講演奨励賞受賞